A 3D visualization of a prostate cancer cell cluster. The cells are depicted as red, rounded spheres with a textured surface, arranged in a dense, irregular cluster. The background is dark blue with a subtle, wavy pattern, suggesting a biological or fluid environment. The lighting is soft, highlighting the individual cells and their collective structure.

# Spatiotemporal Modeling in Mathematical Oncology

Case Study in Prostate Cancer

Rosalie Althuis

Delft University of Technology

# Spatiotemporal Modeling in Mathematical Oncology

Case Study in Prostate Cancer

by

Rosalie Althuis

to obtain the degree of Master of Science  
at the Delft University of Technology,  
to be defended publicly on Thursday October 10, 2024 at 10:45 AM.

Student number: 5648742

Project duration: January, 2024 - October, 2024

Thesis committee: Dr. A. B. T. Barbaro,  
Dr. K. Staňková,  
Dr. E. Pulvirenti,

Faculty: Electrical Engineering, Mathematics and Computer Science

Department: Delft Institute of Applied Mathematics, TU Delft

Funding: This research is part of a larger project supported by  
European Union's Horizon 2020 research and innovation program  
under the Marie Skłodowska-Curie grant agreement No 955708.

TU Delft, supervisor  
TU Delft, supervisor  
TU Delft

Cover: 3d rendering of Human cell or Embryonic stem cell microscope  
background by Anusorn.

*To my father, for your love and light,  
and for everything you mean to me.  
Your fight against a brain tumor left a lasting mark on my life.  
This work is dedicated to your memory,  
in the hope that it may contribute,  
even in a small way, to a better understanding of this disease.*

# Acknowledgments

There are so many people who have contributed to this thesis, both directly and indirectly, and I want to express my gratitude to everyone of them.

First and foremost, I would like to thank my supervisors, Dr. Alethea Barbaro and Kateřina Staňková, for all the help and guidance they have provided me over the past months. I have learned so much from them, and without our weekly meetings, writing this thesis would not have been possible. I am grateful for their time, enthusiasm, and the delicious cups of hot chocolate we shared. It has been an honor to know them and walk this journey together. They are a true source of inspiration, and I look forward to their future work.

Furthermore, I want to thank TU Delft, particularly Dr. Elena Pulvirenti, for her role on my thesis committee and for the time she dedicated to understanding my work. I am also grateful for the team from the Evolutionary Game Theory lab meetings for their warm welcome. Additionally, I would like to acknowledge Dr. Abdulaziz Alsenafi and Samuel Zegers for their interesting research, which laid the foundation for my own work.

I am deeply grateful to my fellow students, church and friends, for their support and distractions during stressful times. Each of you is fantastic. I especially want to thank Hester, with whom I did this entire master's program. I am endlessly thankful for you!

Above all, I want to thank my family, my mother and sisters, who have always supported me. Thank you for stepping in at home so I could study at the library, and for your motivational talks. I also want to express my gratitude to my father, who inspired my thesis topic. Lastly, I am grateful to God for giving me the peace, trust, and energy I needed throughout this process.

And a special thanks to my dog, Simba, for all the cuddles and love that helped me through this journey.

Thank you all, I could not have done this without you!

*Rosalie Althuis  
Delft, October 2024*

# List of Symbols

In Table 1, the symbols, which are used in this thesis, together with their descriptions are listed. Other notations and abbreviations will be defined upon their first use in the text.

Parameter	Description
$\rho_1$	The density of the $T^+$ tumor cells, which depend on testosterone but do not produce it
$\rho_2$	The density of the $T^P$ tumor cells, which depend on testosterone and produce it
$\rho_3$	The density of the $T^-$ tumor cells, which are independent of testosterone
$\rho_4$	The density of testosterone
$\rho_5$	The density of the healthy cells
$\rho_N$	The sum of the tumor and healthy cells densities
$\alpha_i$	Birth-rates for $i \in \{1, 2, 3, 4, 5\}$
$\beta$	The rate at which the cells are pushed
$C_i$	Movement probability for $i \in \{1, 2, 3, 4, 5\}$
$\gamma_i$	Death-rates for $i \in \{1, 2, 3, 4, 5\}$
$\delta t$	Time-step
$\kappa$	Death-rate due to lack of testosterone
$L$	$L \times L$ is the lattice size
$l$	Spatial-step
$\eta$	Consumption-rate testosterone
$\mu$	Production-rate testosterone
$\chi$	Base level of testosterone in the blood
$(\tilde{x}, \tilde{y})$	The neighbor sites of $(x, y)$ , which are $\{(x + l, y), (x - l, y), (x, y + l), (x, y - l)\}$

**Table 1:** The symbols, which are used in this thesis, together with their descriptions are listed.

# Abstract

Cancer affects a countless number of lives across the world each day. Mathematical oncology develops and studies mathematical models of cancer and its treatment. This thesis focuses on spatiotemporal modeling in mathematical oncology, developing an agent-based model for prostate cancer, with the aim of gaining insights into how the different tumor cells respond to varying testosterone levels and different treatment strategies. We began by analyzing non-spatial population models, the replicator dynamics and Lotka-Volterra dynamics, proving their equivalence under certain conditions. The study then transitioned to spatial agent-based modeling on a discrete lattice, simulating the interactions between testosterone-dependent and testosterone-independent tumor cells. Through this, we identified a possible phase transition in the testosterone level in the bloodstream, which could influence which tumor cells dominates the grid. A continuum limit of the discrete model was derived, leading to partial differential equations that describe the tumor's spatial behavior. We applied mathematical tools like non-dimensionalization and linear stability analysis to gain deeper insights into the dynamics of the model. Additionally, we simulated three treatment strategies: (1) testosterone removal from the blood with Lupron, (2) Lupron combined with Abiraterone to stop the testosterone producing cancer cell to grow, and (3) Lupron and Abiraterone alongside high-dose testosterone injections to simulate extinction therapy. The flexibility of our model allows for its application to other hormonal cancers, and our findings support the promising potential of hormonal manipulation in controlling tumor growth and composition, especially extinction therapy. The mathematical analysis together with simulations provide unique insights into the tumor dynamics. Future research directions include changing assumptions, expanding the model to three dimensions and integrating patient data for more accurate simulations.

# Contents

<b>Dedication</b>	<b>i</b>
<b>Acknowledgments</b>	<b>ii</b>
<b>List of Symbols</b>	<b>iii</b>
<b>Abstract</b>	<b>iv</b>
<b>1 Introduction</b>	<b>1</b>
1.1 Basic Facts about Cancer . . . . .	1
1.2 Mathematical Modeling of Cancer . . . . .	2
1.3 Mathematical Concepts . . . . .	4
1.4 Overview of the Thesis . . . . .	5
<b>2 Equivalence between Classical Non-spatial Population Models for Cancer</b>	<b>7</b>
2.1 Replicator Dynamics and an Example of its Usage in Mathematical Oncology . . . . .	7
2.2 Lotka-Volterra dynamics and an Example of its Utilization in Mathematical Oncology . . . . .	9
2.3 (Non) Correspondence between Replicator and Lotka-Volterra Dynamics and What it Means for Mathematical Oncology . . . . .	10
2.3.1 Derivation . . . . .	10
2.3.2 Simulations . . . . .	11
<b>3 The Discrete Spatial Model of Prostate Cancer</b>	<b>15</b>
3.1 Initialization . . . . .	15
3.2 Dynamics of the Tumor Cells and the Healthy Cells . . . . .	16
3.2.1 Movement . . . . .	16
3.2.2 Death and Birth . . . . .	17
3.3 Dynamics of Testosterone . . . . .	17
3.3.1 Spreading . . . . .	17
3.3.2 Consumption and Production . . . . .	18
3.4 Total System . . . . .	18
3.5 Simulations of Prostate Cancer . . . . .	19
3.5.1 $T^-$ Independent Cell Dominance . . . . .	19
3.5.2 $T^+$ and $T^P$ Dependent Cells Dominance under Testosterone Influence . . . . .	21
3.5.3 Tumor growth . . . . .	23
<b>4 The Continuum Spatial Model of Prostate Cancer</b>	<b>26</b>
4.1 Partial Differential Equations Derivation . . . . .	26
4.1.1 Theoretic Framework . . . . .	26
4.1.2 Continuum System . . . . .	28
4.2 Equilibrium Solutions . . . . .	31
4.3 Simpler System . . . . .	33
<b>5 An Alternative Continuum Spatial Model of Prostate Cancer</b>	<b>35</b>
5.1 The Model with Alternate Assumptions . . . . .	35
5.2 Non-dimensionalization . . . . .	37
5.2.1 Non-dimensionalization of the Equations for the Tumor Cells . . . . .	37
5.2.2 Non-dimensionalization of the Equations for the Healthy Cells . . . . .	38
5.2.3 Non-dimensionalization of the Equation for Testosterone . . . . .	38
5.2.4 Total Non-dimensionalized System . . . . .	39
5.2.5 Equilibrium Solutions . . . . .	39
5.3 Linear Stability Analysis . . . . .	40
5.3.1 Equilibrium 1 . . . . .	43

---

5.3.2	Equilibrium 2 . . . . .	46
<b>6</b>	<b>Treatment Strategies for Prostate Cancer</b>	<b>49</b>
6.1	Parameter Values and Initial Conditions . . . . .	49
6.2	Effect of Testosterone Removal . . . . .	51
6.3	Testosterone Removal and Targeting $T^P$ . . . . .	53
6.4	Innovative Treatment for Prostate Cancer . . . . .	55
<b>7</b>	<b>Discussion and Conclusions</b>	<b>58</b>
	<b>References</b>	<b>61</b>
<b>A</b>	<b>The C++ Code</b>	<b>64</b>

# 1

## Introduction

Cancer affects a countless number of lives across the world each day. According to the World Health Organization [56], cancer was the second leading cause of death worldwide in 2018, responsible for approximately 9.6 million deaths. This is almost one in six of all deaths. In the Netherlands, the cancer center Integraal Kankercentrum Nederland (IKNL) concluded that one in two people will receive a cancer diagnosis during their lifetime [23]. However, the impact of cancer extends beyond those diagnosed, deeply affecting the lives of their relatives and loved ones [18]. These facts underscore the urgent need to advance research in oncology, not only to improve treatment outcomes but also to deepen the understanding of the disease's complexities and develop strategies for its prevention, control, and ultimately, if possible, its extinction.

One class of cancer is hormone-dependent cancer. Hormones are key contributors to the development of many of the most common cancers globally, such as prostate cancer in men as well as endometrial, breast, and ovarian cancers in women [28]. Hormones, like estrogen and androgen, are known to play critical roles in the development and progression of those cancers [34]. According to Key [28], the primary ways hormones influence cancer are likely to involve regulating cell division rates, guiding cell differentiation, and affecting the quantity of vulnerable cells.

Among the many types of cancer, prostate cancer stands out due to its impact among men [24]. As reported by the IKNL, prostate cancer was one of the five most common cancer diagnoses among the whole population in the Netherlands in 2023, reflecting a significant public health problem [23]. Globally, it is the second most frequently diagnosed cancer in men, with big differences in diagnosis rates and mortality rates across various ethnicity's and age groups [42]. All of this shows the importance of research on prostate cancer to improve treatment strategies for this cancer. In this thesis, we contribute to this research by using spatiotemporal modeling in mathematical oncology with a case study in prostate cancer. In this chapter, we will introduce and discuss some basic facts about cancer, mathematical modeling of cancer, and mathematics concepts necessary to understand this thesis, and in Section 1.4 an overview of the thesis is given.

### 1.1. Basic Facts about Cancer

Cancer begins at the cellular level when errors occur during cell division, the process by which a single cell divides into two new cells [39]. These errors are changes to the DNA of the cell, known as *mutations* [25]. Mutated cells may begin to multiply rapidly and uncontrollably, forming a mass of abnormal cells known as a tumor [36]. If the tumor is cancerous, it can invade surrounding tissues and spread to other parts of the body through a process called *metastasis* [20, 19].

In the case of prostate cancer, there can be several different types of mutated cells present in a tumor, each of which interacts with the hormone testosterone in a different way [59, 57, 10, 53]. Some of these mutated cells do not respond to testosterone at all, and these are categorized as  $T^-$  cells. On

the other hand, there are cancerous cells that do depend on testosterone, which we refer to as  $T^+$  cells. Additionally, there is a third group of cells which do require testosterone to live but have the ability to produce it themselves, and we label these as  $T^P$  cells. The  $T^P$  cells not only use the testosterone they create to meet their own biological needs, but they can also share this hormone with nearby cells as a public good [57]. This sharing can have significant effects, as it allows neighboring cells to benefit from the testosterone that is produced.

This complex interaction between different types of cancer cells and testosterone plays a crucial role in the behavior of prostate cancer and its development. Understanding these interactions is important because it helps researchers learn more about how prostate cancer grows and therefore how to better treat it. If the resistant  $T^-$  cancer cells are present, this is known as *castrate-resistant prostate cancer (CRPC)*; when this cancer becomes metastatic, it is called *metastatic castration-resistant prostate cancer (mCRPC)*. There can also be adaptations, such as phenotypic and genetic changes, which complicate the understanding and targeting of the cancer [11, 19].

There is currently no proven method to prevent prostate cancer, but maintaining a healthy diet and exercising regularly may be beneficial [42]. Recently, there have been new therapies as well as various combinations of existing therapies aimed at treating prostate cancer [9]. They are commonly applied at the *maximum tolerated dose (MTD)*, but many studies and papers argue against always administering the MTD until progression because it can lead to treatment-resistant mutations [32, 16, 60, 47]. A major challenge is the problem of resistance to existing treatments. This resistance can make it much more difficult for therapies to work effectively over time, often leading to an uncontrollably growing tumor that can eventually result in death.

One type of treatment designed to combat this issue is *adaptive therapy*, also referred to as evolutionary therapy [53, 59, 15]. It uses the competitive interactions between drug-sensitive and drug-resistant cancer cells to control the tumor burden, by allowing the number of drug-sensitive cells to grow, suppressing the resistant cells. In this way, the number of resistant cells can be controlled due to a lack of space and resources.

Other common cancer treatments include surgery and chemotherapy, as well as a more recent strategy known as extinction therapy. This approach takes inspiration from the theory behind the mass extinction of dinosaurs, where a single catastrophic event likely caused their extinction. Extinction therapy aims to similarly disrupt cancer by delivering a powerful, unexpected intervention, referred to as a “first strike” [14]. This powerful treatment drastically reduces the tumor size. The therapy is then followed by subsequent “second strike” that targets any surviving cancer cells, progressively driving the tumor population below the point where it can sustain itself, ultimately leading to its eventual extinction.

## 1.2. Mathematical Modeling of Cancer

Mathematical oncology is an interdisciplinary field that uses mathematical modeling and optimization techniques to better understand cancer. This can be done by creating models that simulate the behavior of tumors, predict how they will progress and respond to treatments, and optimize personalized therapies. The models can be fitted to real data from patients or to data from *in vitro* studies [43, 27], which are experiments done outside the body, for example in a Petri dish. We can use the models to make recommendations so that oncologists can explain, test or adjust their expectations or treatment strategies, and help them to make more effective, data-driven decisions to optimize patient outcomes.

Mathematical models are also used to optimize the timing and dosage of medicines and other forms of treatments [13, 7, 35]. By taking into account elements such as drug resistance and the different cell types, the models can make patient-specific adaptive treatment predictions. There is no one-size-fits-all treatment. According to Rejniak and McCawley [43], computational cancer models offer researchers powerful tools that can simplify complex systems into coherent frameworks, while also generating testable hypotheses.

Recent studies have demonstrated the growing impact and importance of mathematical oncology. For example, a study by Powathil, Adamson, and Chaplain [40] demonstrates how a mathematical model replicates the outcomes of earlier biological experiments related to cancer treatment, which can be

used to test the most effective combinations of radiotherapy and medicines. Another recent example is a study by Soboleva et al. that presents a mathematical model for cancer dynamics, based on both in vitro and in vivo data from non-small cell lung cancer treatment [46]. Moreover, game theory, a branch of mathematics, can improve cancer treatment by framing the treatment process as a strategic interaction between the physician and the tumor. This approach focuses on understanding resistance dynamics and the relative sizes of different cell populations, rather than solely considering the tumor size [47]. Hence, by creating models that simulate tumor behavior, predict treatment responses, personalize therapies and allow a better understanding of cancer, mathematical oncology is a powerful tool in the fight against cancer.

There are several different classes of mathematical models used in mathematical oncology. Among the various types of models, it is important to distinguish between spatial and non-spatial models. Non-spatial models focus solely on population dynamics over time, without considering the spatial distribution of cells. These models can be easier to analyze and can provide insights into the overall growth of a tumor or its response to a treatment, but they may miss critical aspects related to the tumor's structure and its interaction with its environment. An example of a non-spatial cancer model can be found in the paper by Cunningham et al., which describes strategies for managing metastatic castrate resistant prostate cancer [10].

Another key type of mathematical modeling are population-based models. These models are typically employed to study the dynamics of populations, such as the spread of diseases or the movement of wildlife. For instance, an article by Okuonghae and Omame [37] describes the COVID-19 dynamics by using population models. In mathematical oncology, similar population-based approaches can be used to study cancer, often to predict cancer cells' response to a particular treatment and/or optimize anti-cancer therapies [26, 57, 16, 4, 17, 60].

Two common types of population-based models in mathematical oncology are the Replicator dynamics [33] and Lotka-Volterra models [5]. While these models are related, they have differences. Replicator dynamics track the changing proportions of different tumor cell types over time, offering insights into competition and selection among cells. On the other hand, Lotka-Volterra models, which describe the changing population sizes of each cancer cell type in a tumor, can also show the total size of the tumor. An example of a predator-prey Lotka-Volterra model is shown in Figure 1.1. The plot was made in Matlab with the Lotka-Volterra system:

$$\begin{cases} \dot{x}_1 = x_1 - 0.5x_1x_2, \\ \dot{x}_2 = -0.75x_2 + 0.25x_1x_2. \end{cases} \quad (1.1)$$

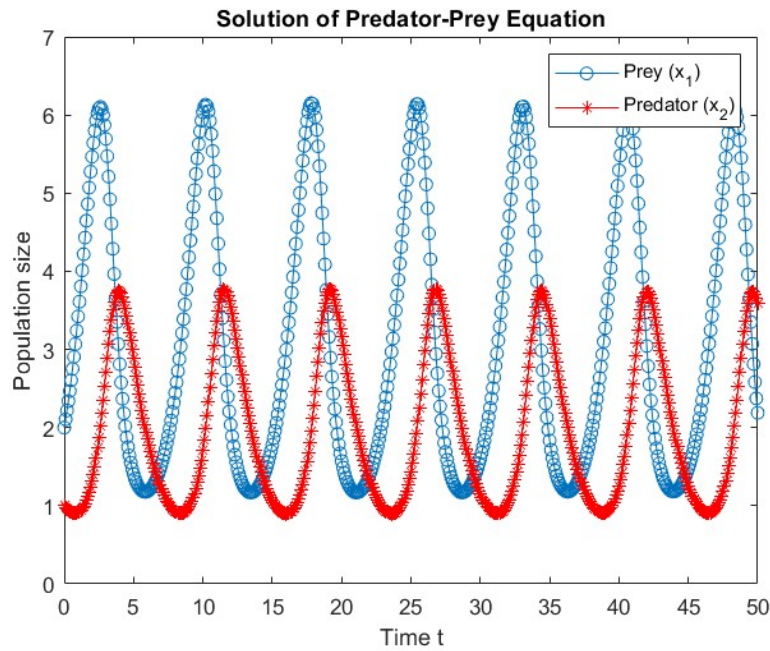


**Figure 1.1:** An example of a population-based model: a predator-prey model, with System (1.1). We see the predators and prey populations alternating.

In the first part of this thesis, we will explore how to relate these two models properly to capture different aspects of cancer dynamics.

In contrast, spatial models incorporate a geographical or positional aspect, for example simulating a population across a two- or three- dimensional lattice [3]. In the context of cancer, spatial models capture the location and movement of cells within the tumor environment, offering insights on how cancer cells interact with each other and their surroundings.

In the second part of the thesis an *agent-based model (ABM)* for prostate cancer will be introduced. Agent-based modeling is a computational modeling method that simulates the interactions of individual agents within a system, typically with discrete, cell-scale space [50]. Agent-based models allow for detailed simulations where individual agents, such as cells or organisms, interact based on predefined rules, in order to understand the behavior of a system and predict the developments. This method can be used to study complex behaviors that emerge from the local interactions of these agents. That is why agent-based modeling is a tool for understanding, predicting, and treating cancer, and it is able to capture multiscale interactions [52]. For example, Alsenafi and Barbaro introduce in their work a lattice-based agent-based model for gang territoriality, where they simulate and analyze the gang dynamics and the graffiti they mark on a two-dimensional discrete lattice [1]. However, many agent-based models lack formal mathematical analysis [48, 38]. In this work, we aim to fill that gap by applying relevant mathematical concepts.

### 1.3. Mathematical Concepts

For this thesis, several key mathematical concepts are needed. We will give a heuristic understanding of these concepts here.

*Diffusion* refers to the process by which particles naturally move from areas of higher concentration to areas of lower concentration. It is typically described by the diffusion equation, a partial differential equation that describes how the concentration of particles or cells changes over time. The diffusion equation is:

$$\frac{\delta y}{\delta t} = D \nabla^2 y,$$

with  $D$  the diffusion constant and  $y(x, t)$  the concentration of the moving object at time  $t$  and position  $x$ . In this process, the probability of a particle moving from one cell to a neighboring cell depends on the concentration differences between the cells. In biological contexts, diffusion often describes how molecules, such as chemicals and cells, spread through tissue. In contrast, an unbiased *random walk* is a stochastic process that models the movement of particles where each step occurs in a random direction, independent of the concentrations. In this case, the probability of moving to any neighboring cell is the same in all directions, meaning that the movement is purely random without being influenced by the surrounding environment. Both diffusion and random walk processes are fundamental in modeling cellular behavior and interactions within tissues.

Another essential distinction to make, is the difference between discrete and continuum models. *Discrete models*, such as agent-based models, treat variables as separate units, often simulating individual agents like cells, and are usually also discrete in time. In contrast, *continuum models* represent the system with smooth variables that change continuously over space and time, typically using differential equations. For example, while agent-based models handle individual cells as separate agents, continuum models can describe densities.

To derive a continuum model from a discrete one, we often assume *smoothness*, which means that the variables change continuously and smoothly over space and time. This allows the formal derivation from discrete models, which consider individual agents, to *partial differential equations (PDEs)*. In mathematical oncology, this transition is useful for studying overall tumor growth or diffusion of treatment effects across the tissue. The continuum limit of an agent-based model can often lead to PDEs [2, 58], such as the reaction-diffusion equations often used in tumor modeling.

After taking the continuum limit of the discrete model and obtaining PDEs, the next step is to analyze the system by examining its equilibria, non-dimensionalizing the equations, and performing a linear stability analysis. This process follows the work of Alsenafi in his PhD thesis [2] and Zegers' bachelor thesis [58]. This analysis is a crucial mathematical tool for determining the stability of equilibrium points in dynamical systems. The method involves introducing a small perturbation to an equilibrium state and observing how the system responds. Specifically, we look at the eigenvalues of the system to find out the stability: if all eigenvalues have negative real parts, the equilibrium is stable, meaning that the system will stay at its equilibrium. If any eigenvalue has a positive real part, the system is unstable, which could correspond to scenarios of uncontrolled tumor growth or tumor extinction. Additionally, it is important to distinguish between real and imaginary eigenvalues. In the context of cancer modeling, this method helps predict whether small changes in the tumor's state will lead to a return to an equilibrium, excessive growth, or other dynamic behaviors.

In the *linear stability analysis*, a small perturbation is added to the equilibrium solutions. This perturbation is of the form  $\delta_i e^{\alpha t + i k \cdot v}$  with  $k$  being the wave numbers, see Chapter 4 for more information. The solutions determine whether the small perturbations will grow in time and, if so, for which wavelengths. They are often interested in the possibility of spatiotemporal oscillations [54].

## 1.4. Overview of the Thesis

The objective of this thesis is to explore modeling techniques in mathematical oncology, with a particular focus on both temporal and spatial dynamics. We aim to mathematically analyze our model, potentially influencing cancer progression and treatment outcomes in the future.

In Chapter 2, we first explore two common non-spatial population models: replicator dynamics and Lotka-Volterra dynamics. The key question we address is whether there is an equivalence between replicator dynamics and the Lotka-Volterra models, and how such an equivalence, if established, can impact the field of mathematical oncology. This analysis will help clarify the challenges of using these models. After that we will switch to spatial models.

Next, in Chapter 3, we design an agent-based model on a discrete lattice to describe prostate cancer with three different cell types. By changing the testosterone level in the blood ( $\chi$ ), we aim to control

which tumor cells, testosterone-dependent or independent, dominate the lattice. We also simulate tumor growth starting from a few mutated cells.

In Chapter 4, we derive the partial differential equations of the continuum system by taking the formal continuum limit of the discrete model. Since this system is challenging to analyze, we propose an alternative continuum spatial model in Chapter 5 and analyze this, through non-dimensionalization and linear stability analysis. Finally, in Chapter 6, we explore three different treatment strategies for prostate cancer, each of which manipulates testosterone levels and therefore affects the evolutions of the tumor. Lupron removes all testosterone from the bloodstream [53], Abiraterone stops the testosterone-producing cancer cells ( $T^P$ ) from dividing [10], and we show further that high-dose testosterone injections could be applied as extinction therapy.

# 2

## Equivalence between Classical Non-spatial Population Models for Cancer

In this chapter, we will examine the equivalence between classical non-spatial population models for cancer. Mathematical oncology develops mathematical models to study cancer, often to predict cancer cells' response to a particular treatment and/or optimize anti-cancer therapies (See [53, 4, 16, 47] for some examples). As highlighted also in recent reviews of game-theoretic models utilized within the mathematical oncology field [55, 8], models based on ordinary differential equations (ODEs) are one of the most prevalent approaches utilized within the mathematical oncology community. In fact, both Replicator dynamics and Lotka-Volterra dynamics are examples of such models and are widely used [26, 57, 16, 4, 17, 60].

Interestingly enough, while the purpose of replicator dynamics in generic game-theoretic modeling is often to track how proportion of individuals of different types change over time and their main focus is not how population size evolves, in mathematical oncology we also see attempts to optimize cancer treatment in replicator dynamics models of cancer [16], while in reality it is the population size which we want to control in cancer. While Hofbauer and Sigmund [22] introduced transformation between Lotka-Volterra dynamics and replicator dynamics preserving both equilibria and the transient dynamics, this transformation utilized  $n + 1$  types in replicator dynamics, which corresponding to  $n$  types in Lotka-Volterra dynamics. Here we demonstrate some of the pitfalls of assuming that optimization in an  $n$ -type replicator dynamics corresponds to an optimization to an  $n$ -type Lotka-Volterra dynamics.

Let us introduce the replicator dynamics and Lotka-Volterra dynamics and examples of their usage in mathematical oncology in Sections 2.1 and 2.2, respectively. This will lead us to Section 2.3 where we explain which dynamics do correspond and which do not in terms of both transient dynamics and equilibria, and illustrate this by simulations.

### 2.1. Replicator Dynamics and an Example of its Usage in Mathematical Oncology

Replicator dynamics were developed by Taylor and Jonker in 1978 [49]. Let us consider a population consisting of  $n$  different types of individuals, where proportion  $y_i$  of these individuals of type  $i$  and  $\mathbf{y} = (y_1, y_2, \dots, y_n)^T$ . Let us assume that  $f_i(\mathbf{y})$  denotes the fitness of individuals of type  $i$  and  $N$  is the total number of individuals. If the population is very large, has overlapping generations and asexual reproduction, we may consider  $N_i = y_i N$  to be a continuous variable, the population growth is given

by the differential equation

$$\frac{d}{dt}N_i = \dot{N}_i = N_i f_i(\mathbf{y}(t)),$$

and we obtain the replicator dynamics [49, 22]

$$\dot{y}_i = y_i (f_i(\mathbf{y}(t)) - \bar{f}(\mathbf{y}(t))), \quad (2.1)$$

where  $\bar{f}(\mathbf{y}(t))$  denotes the average fitness of the population  $\mathbf{y}(t)$  at time  $t$ . If the fitness of the population is given by a fitness matrix  $B = (b_{ij})_{n \times n}$  where  $b_{ij}$  describes the chances for proliferation of type  $i$  when interacting with types  $j$ , we can rewrite (2.1) as

$$\dot{y}_i = y_i \left( (B\mathbf{y}(t))_i - (\mathbf{y}(t))^T B\mathbf{y}(t) \right). \quad (2.2)$$

We can then analyze Nash equilibria and evolutionary stable equilibria of (2.2).

An example of utilizing replicator dynamics in the context of cancer is [57], a paper co-authored by one of the supervisors of this thesis, a game between three cell prostate cancer cell types from the set  $\mathcal{T} = \{1, 2, 3\}$  was studied, where the first type depends on testosterone and is referred to as  $T^+$ , second type is able to produce its own testosterone and is referred to as  $T^P$ , and the third one is independent of testosterone and is referred to as  $T^-$ , refer to Chapter 1 for details. Let  $y_i$ ,  $i \in \mathcal{T}$ , denoting the frequency of the cells of type  $i \in \mathcal{T}$  in the population, it was assumed that the cancer cells interacted with each other as a game. When a focal cell of type  $i \in \mathcal{T}$  interacts with a cell of type  $j \in \mathcal{T}$ , the outcome was the probability that the focal cell divides and creates an offspring of type  $i$ . These division probabilities for interaction between all types form a payoff (fitness) matrix  $B = (b_{ij})_{3 \times 3}$  defined as

$$B = \begin{pmatrix} 0 & b_{12} & b_{13} \\ b_{21} & 0 & b_{23} \\ b_{31} & b_{32} & 0 \end{pmatrix}, \quad (2.3)$$

with  $b_{i,j} \in (0, 1)$  for each  $i, j \in T$ . For each type  $i \in T$ , the replicator dynamics [49] defined the time change  $\dot{y}_i$  of its cell frequency  $y_i$ , thus:

$$\dot{y}_i = y_i \left( (B\mathbf{y})_i - \mathbf{y}^T B\mathbf{y} \right), \quad i \in T \quad (2.4)$$

where  $\mathbf{y} = (y_{T^+}, y_{T^P}, y_{T^-})^T \in \mathbb{R}^3$ . The frequency dynamics (2.4) was studied for different assumptions on elements of  $B$  for which particular inequalities on the relations between the individual elements were satisfied. These assumptions led to 22 cases of the replicator dynamics, with the frequency trajectories and the evolutionarily stable strategies (ESSs) mapped on a simplex. When starting from an all initial frequencies  $\mathbf{y}(0)$  being nonzero, You et al. [57]'s model results in a single ESS, which is the attractor for the dynamics given by (2.4). The interior ESSs can be found independently from the fitness matrix  $B$  utilizing the ESS conditions, or through setting  $(B\mathbf{y})_i - \mathbf{y}^T B\mathbf{y}$  in (2.4). While [57] demonstrated the stability of the interior equilibria, of (2.4), here we can calculate the candidates for these equilibria by setting  $B\mathbf{y} = 0$ , and leading to the following interior equilibrium candidate  $\bar{\mathbf{y}} = (\bar{y}_1, \bar{y}_2, \bar{y}_3)^T$ , satisfying

$$b_{12}\bar{y}_2 + b_{13}\bar{y}_3 = b_{21}\bar{y}_1 + b_{23}\bar{y}_3 = b_{31}\bar{y}_1 + b_{32}\bar{y}_2,$$

where  $\bar{y}_1 + \bar{y}_2 + \bar{y}_3 = 1$ , leading to

$$\begin{aligned} \bar{y}_1 &= -\frac{b_{12}b_{23} + b_{13}b_{32} - b_{23}b_{32}}{b_{12}b_{21} - b_{12}b_{23} - b_{12}b_{31} - b_{13}b_{21} + b_{13}b_{31} - b_{13}b_{32} - b_{21}b_{32} - b_{23}b_{31} + b_{23}b_{32}}, \\ \bar{y}_2 &= -\frac{b_{13}b_{21} - b_{13}b_{31} + b_{23}b_{31}}{b_{12}b_{21} - b_{12}b_{23} - b_{12}b_{31} - b_{13}b_{21} + b_{13}b_{31} - b_{13}b_{32} - b_{21}b_{32} - b_{23}b_{31} + b_{23}b_{32}}, \\ \bar{y}_3 &= \frac{b_{12}b_{21} - b_{12}b_{31} - b_{21}b_{32}}{b_{12}b_{21} - b_{12}b_{23} - b_{12}b_{31} - b_{13}b_{21} + b_{13}b_{31} - b_{13}b_{32} - b_{21}b_{32} - b_{23}b_{31} + b_{23}b_{32}}. \end{aligned} \quad (2.5)$$

For the parametrizations utilized in You et al. [57] the evolutionary stability of the interior equilibria was demonstrated while the main purpose of that paper was to extend the replicator dynamics into a spacial agent-based model and to analyze its spatio-temporal equilibria.

## 2.2. Lotka-Volterra dynamics and an Example of its Utilization in Mathematical Oncology

The Lotka-Volterra dynamics, proposed separately by Lotka [29] and Volterra [51], describe the dynamics of systems in which two or more species interact. While Hofbauer and Sigmund [22] utilized this form of the Lotka-Volterra dynamics

$$\dot{x}_i = x_i \left( a_{i0} + \sum_{j=1}^n a_{ij} x_j \right), \quad i = 1, \dots, n, \quad (2.6)$$

with  $x_i$  the population sizes for  $i = 1, \dots, n$  and  $A = (a_{ij})_{n \times n}$  a  $n$  by  $n$  real matrix, in Mathematical Oncology the following form with a carrying capacity for each type  $i$  is more common [4, 10, 17, 30, 44, 53, 12]:

$$\dot{x}_i = r_i x_i \left( 1 - \frac{\sum_{j=1}^n a_{ij} x_j}{K_i} \right), \quad i = 1, \dots, n, \quad (2.7)$$

with  $r_i$  being the intrinsic growth rates and  $K_i$  the carrying capacity for type  $i$ . This form can also be rewritten into the form (2.6) as

$$\dot{x}_i = x_i \left( r_i + \sum_{j=1}^n \frac{(-r_i) a_{ij}}{K_i} x_j \right), \quad i = 1, \dots, n. \quad (2.8)$$

Even though the Lotka-Volterra dynamics were introduced earlier than evolutionary game theory [31], the dynamical system (2.6) may fit well to describe how interactions between different species impact their population sizes and frequencies. In such games, the individuals of different populations/types interact with each other and through such interactions players influence each other's chances of survival (fitness).

We could calculate the steady points/equilibria of (2.7), which are useful to analyze the dynamic stability of the system in question system.

For an example of usage of Lotka-Volterra dynamics, let us analyze a model utilized by Zhang et al. [60] to design and explain novel therapies in metastatic-castrate resistant prostate cancer. While the goal of this paper was to analyze impact of the so-called adaptive therapy under two different treatments which both were assumed to manipulate carrying capacity of some of the cell types, their basic model was much related to the replicator dynamics model in [57].

More specifically, the model of Zhang et al. [60] assumes a  $3 \times 3$  competition matrix  $A = (a_{ij})_{3 \times 3}$ , where  $i, j \in \mathcal{T}$  and  $a_{ij} = 1 - b_{ij}$  for each  $b_{ij}$  from matrix  $B$  of [57]. The initial dynamics before the treatment was applied was (2.7). If we calculate interior equilibria  $x_1^*$ ,  $x_2^*$ , and  $x_3^*$  of (2.7) by setting

$$1 - \frac{\sum_{j=1}^n a_{ij} x_j}{K_i} = 0 \quad (2.9)$$

for each  $i, j \in \mathcal{T}$  and divide these by the total equilibrium population  $x_1^* + x_2^* + x_3^*$ , and additionally assume that all carrying capacities  $K_i$  are equal, we will obtain exactly the same candidates for interior equilibria.

The key question is: While the paper by Zhang et al. [60] obtained the same interior equilibria as You et al. [57] in terms of population frequencies, will their transient dynamics correspond to that of You et al. [57]? While none of the two papers claimed this, perhaps this was implicitly assumed, as both these models were supposed to capture the frequency dynamics of cancer cells realistically enough, thus answering this question may be important. And, in general, under which conditions the frequencies of Lotka-Volterra dynamics correspond to those of the replicator dynamics?

## 2.3. (Non) Correspondence between Replicator and Lotka-Volterra Dynamics and What it Means for Mathematical Oncology

Hofbauer (1981) [21] demonstrated how from a Lotka-Volterra dynamics of  $n$  types one can derive replicator dynamics with  $n + 1$  types, where the frequency dynamics of the two will coincide [21].

Here we will demonstrate that without conversion of the number of types, the evolutionary stable strategies of the two dynamics may coincide, however it is not meaningful to assume that they have a 1-to-1 relationship. The interior equilibrium  $\bar{\mathbf{y}} = (\bar{y}_1, \bar{y}_2, \bar{y}_3)^T$  of (2.2) coincide with ESS candidates for matrix  $B$ .

### 2.3.1. Derivation

We can transform the Lotka-Volterra Equation (2.7) system of equations into the form of the replicator equations, by following the transformation which is proposed by Hofbauer [21]. We start with Equation (2.7):

$$\dot{x}_i = r_i x_i \left( 1 - \frac{\sum_{j=1}^n a_{ij} x_j}{K_i} \right), \quad i = 1, \dots, n,$$

which can also be written as

$$\dot{x}_i = x_i \left( r_i + \sum_{j=1}^n \frac{-r_i a_{ij}}{K_i} x_j \right), \quad i = 1, \dots, n. \quad (2.10)$$

Set  $x_0 = 1$ , and let  $y_i = \frac{x_i}{\sum_{j=0}^n x_j}$ , for  $i = 0, \dots, n$ . Then by using the quotient rule, we obtain for  $i = 0, \dots, n$ ,

$$\begin{aligned} \dot{y}_i &= \frac{\sum_{j=0}^n x_j \cdot \dot{x}_i - x_i \cdot \sum_{j=0}^n \dot{x}_j}{\left( \sum_{j=0}^n x_j \right)^2} \\ &= \frac{\dot{x}_i}{\sum_{j=0}^n x_j} - \frac{x_i \cdot \sum_{j=0}^n \dot{x}_j}{\left( \sum_{j=0}^n x_j \right)^2} \\ &= \dot{x}_i \cdot y_0 - x_i \left( \sum_{j=0}^n \dot{x}_j \right) y_0^2. \end{aligned}$$

Substituting Equation (2.10) in for  $\dot{x}_i$  results now in

$$\dot{y}_i = x_i \left( r_i + \sum_{j=1}^n \frac{-r_i a_{ij}}{K_i} x_j \right) \cdot y_0 - x_i \left( \sum_{l=0}^n x_l \left( r_l + \sum_{j=1}^n \frac{-r_l a_{lj}}{K_l} x_j \right) \right) y_0^2.$$

We know  $x_i = \frac{y_i}{y_0}$ , using this gives us

$$\begin{aligned} \dot{y}_i &= y_i \left( r_i + \sum_{j=1}^n \frac{-r_i a_{ij}}{K_i} \frac{y_j}{y_0} \right) - y_i \left( \sum_{l=0}^n \frac{y_l}{y_0} \left( r_l + \sum_{j=1}^n \frac{-r_l a_{lj}}{K_l} \frac{y_j}{y_0} \right) \right) y_0 \\ &= y_i \left( r_i + \sum_{j=1}^n \frac{-r_i a_{ij}}{K_i} \frac{y_j}{y_0} - \sum_{l=0}^n y_l \left( r_l + \sum_{j=1}^n \frac{-r_l a_{lj}}{K_l} \frac{y_j}{y_0} \right) \right) \\ &= y_i \left( r_i y_0 + \sum_{j=1}^n \frac{-r_i a_{ij}}{K_i} y_j - \sum_{l=0}^n y_l \left( r_l y_0 + \sum_{j=1}^n \frac{-r_l a_{lj}}{K_l} y_j \right) \right) \frac{1}{y_0} \end{aligned} \quad (2.11)$$

Now assume  $b_{0j} = 0$  for  $j = 0, \dots, n$ ; Note that this is always possible by scaling the columns. Let  $B$  be the matrix with  $b_{i0} = r_i$  and  $b_{ij} = \frac{-r_i a_{ij}}{K_i}$  for  $i = 1, \dots, n$  and  $j = 1, \dots, n$ . For  $n = 2$  this  $B$  is for example

$$\begin{pmatrix} 0 & 0 & 0 \\ r_1 & \frac{-r_1 a_{11}}{K_1} & \frac{-r_1 a_{12}}{K_1} \\ r_2 & \frac{-r_2 a_{21}}{K_2} & \frac{-r_2 a_{22}}{K_2} \end{pmatrix}. \quad (2.12)$$

Now Equation (2.11) is equal to

$$\dot{y}_i = y_i \left( \sum_{j=0}^n b_{ij} y_j - \sum_{k,l=0}^n y_k b_{kl} y_l \right) \frac{1}{y_0}. \quad (2.13)$$

Ignoring the  $\frac{1}{y_0}$  term on the right hand side results in the replicator dynamics from Equation (2.4), which is a system with the same behavior in the  $x_1 - \dots - x_n$  space, but has a different velocity.

$$\begin{aligned} \dot{y}_i &= y_i \left( \sum_{j=0}^n b_{ij} y_j - \sum_{k,l=0}^n y_k b_{kl} y_l \right) \\ &= y_i ((By)_i - y^T B y), \quad i = 0, \dots, n. \end{aligned}$$

Note that we use  $n + 1$  variables here, and only  $n$  variables with Lotka-Volterra.

### 2.3.2. Simulations

In the simulations of this section, we will utilize the parametrization from [60], with focus on one of the 22 matrices studied:  $K_1 = K_2 = K_3 = 10^4$ . In Figure 2.1, we show a simulation of the following Lotka-Volterra system,

$$\begin{cases} \dot{x}_1 = r_1 x_1 \left( 1 - \frac{\sum_{j=1}^3 a_{1j} x_j}{K_1} \right), \\ \dot{x}_2 = r_2 x_2 \left( 1 - \frac{\sum_{j=1}^3 a_{2j} x_j}{K_2} \right), \\ \dot{x}_3 = r_3 x_3 \left( 1 - \frac{\sum_{j=1}^3 a_{3j} x_j}{K_3} \right), \end{cases} \quad (2.14)$$

to demonstrate its behavior, with  $K_i = 10,000$ ,  $r = (0.0278, 0.0355, 0.0665)$  and  $a_{ij}$  are the entries of matrix:

$$\begin{pmatrix} 1 & 0.7 & 0.8 \\ 0.4 & 1 & 0.6 \\ 0.5 & 0.9 & 1 \end{pmatrix}. \quad (2.15)$$

These parameter values are taken from the paper by Zhang et al. [60] and the matrix gives the interior ESSs 10 of Table 2 of the paper by You et al. [57]. For the initial values we take populations below  $K$ , where  $T^-$  has the lowest proportion:  $x_{t=0} = (2000, 2000, 1500)$ ,  $x_0 = 1$ , and  $y_i = \frac{x_i}{1 + 2000 + 2000 + 1500}$ . In Figure 2.1 we see that the population finally stabilizes into the interior equilibrium.

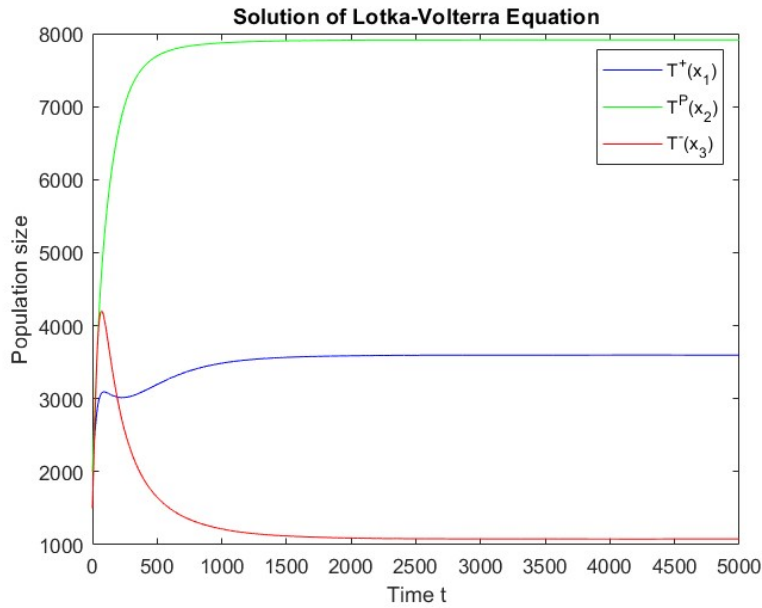


**Figure 2.1:** Time evolution of the three populations using the Lotka-Volterra model for  $n = 3$ , with  $a_{ij}$  as in Equation (2.15).

Now the equivalent Equation (2.13) is equal to

$$\dot{y}_i = y_i \left( \sum_{j=0}^3 b_{ij} y_j - \sum_{k,l=0}^3 y_k b_{kl} y_l \right) \frac{1}{y_0},$$

for  $i = 0, 1, 2, 3$  and  $B$  such as (2.12). If we look at the solution of  $y_i$  in Figure 2.2, we see the same behavior as in Figure 2.1.

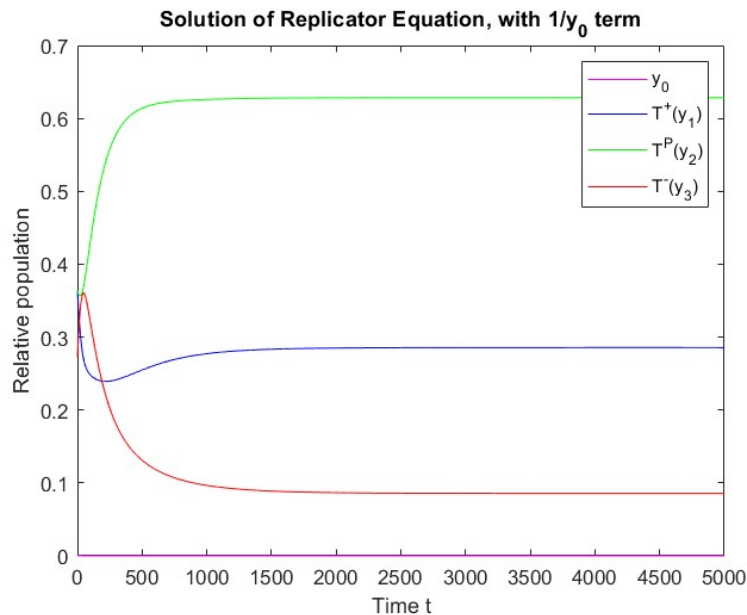


**Figure 2.2:** An example of the equivalent system for  $n = 3$  to the predator-prey model of Figure 2.1, with  $b_{ij}$  as in Equation (2.12). Time evolution of the four ratios.

If we then let go of the  $\frac{1}{y_0}$  term we obtain the replicator dynamics in Figure 2.3, which has the same behavior as illustrated in Figure 2.2, but at a significantly reduced speed.

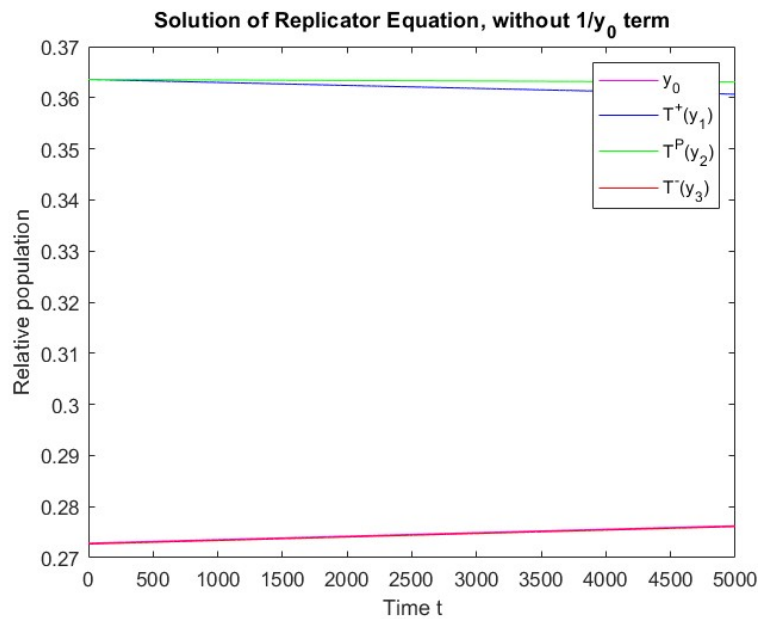


**Figure 2.3:** Time evolution of the four ratios using the replicator dynamics (without the  $\frac{1}{y_0}$  term), which has the same behavior as Figure 2.2 in the  $x_1$ - $x_2$  space, but has a different velocity, with  $b_{ij}$  as in Equation (2.12).

To check this, let the time go to  $8 \cdot 10^7$ , see Figure 2.4, and we see the same behavior back as in Figure 2.2.

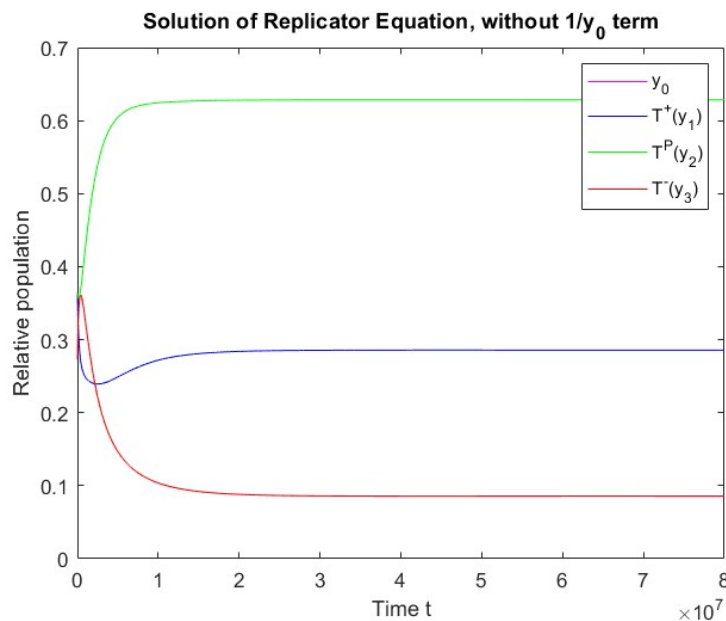


**Figure 2.4:** Time evolution of the four ratios using the replicator dynamics (without the  $\frac{1}{y_0}$  term), which has the same behavior as Figure 2.2 in the  $x_1$ - $x_2$  space, but has a different velocity, with  $b_{ij}$  as in Equation (2.12). Note that the time goes until  $8 \cdot 10^7$ .

Finally, we will show what happens if we totally let go of  $y_0$  and use  $n$  variables instead of  $n + 1$ . If one examines the solution depicted in Figure 2.5, one will observe a totally behavior as illustrated in Figure 2.2. This shows the importance of needing one extra variable in the replicator dynamics, when someone compares it to the Lotka-Volterra dynamics.

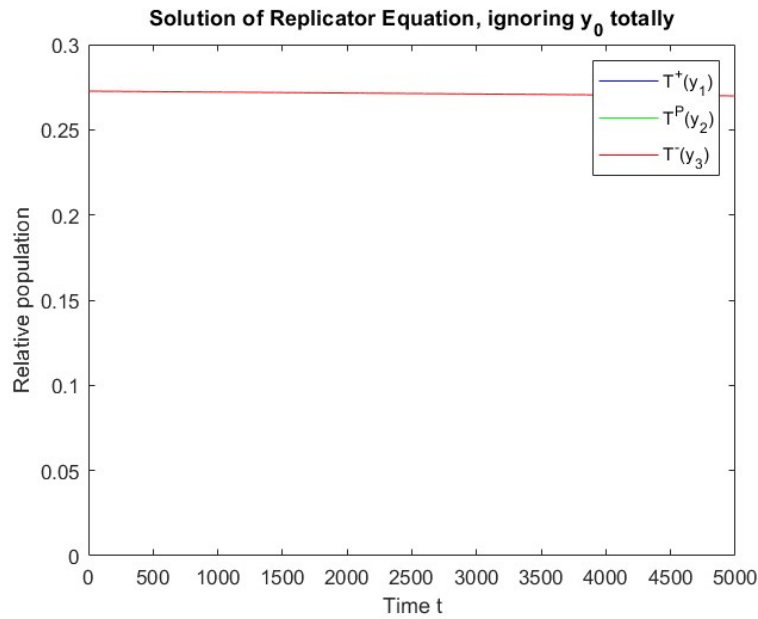


**Figure 2.5:** Time evolution of the three ratios using the replicator dynamics, ignoring the  $y_0$  term totally, which looks totally different than the plots before, with  $b_{i,j}$  as in Equation (2.12).

In conclusion, the number of variables increases by 1 when changing from Lotka-Volterra to replicator dynamics. The variable  $y_0$  is added to track the population.  $y_0$  affects the speed that solutions travel along the trajectories, as well as (if “natural birth” rates  $a_{10}$  and  $a_{20}$  are nonzero) average population fitness calculation. A two-dimensional replicator dynamics system can be used in place of a two-dimensional Lotka-Volterra system with some caveats:

- “Natural birth” rates  $a_{10}$  and  $a_{20}$  must both be zero
- Total population must be tracked and its multiplicative inverse must be used as a factor in the speed.
- If  $y_0$  is not kept track of, then the transformation back to Lotka-Volterra is completely lost, so even the equilibria cannot be compared.

# 3

## The Discrete Spatial Model of Prostate Cancer

In the next chapters, we will focus on the spatial aspect of mathematical oncology models. This process follows the work of Alsenafi in his PhD thesis [2] and Zegers' bachelor thesis [58]. This chapter introduces our spatial discrete agent-based model of prostate cancer. We begin by introducing the lattice in Section 3.1, along with the initialization of the different types of cells. Section 3.2 describes the dynamics of both tumor and healthy cells, focusing on cell movement, cell death, and cell reproduction. In Section 3.3, we address the behavior of testosterone within the cells. The complete discrete system is outlined in Section 3.4. Finally, in Section 3.5, we present simulations of the model.

### 3.1. Initialization

Our model is an agent-based model on a two-dimensional spatial lattice. In the case of prostate cancer, there can be different types of mutated cells present that interact with the hormone testosterone in various ways [59, 57, 10, 53]. A population of cancer cells is a mutation of the healthy cells. This population reproduces and dies at a different rate than the healthy cells do. The tumor cells reproduce faster. We denote this tumor population by  $T^+$ . The  $T^+$  tumor cells and the healthy cells are dependent of testosterone, but do not produce it. One other type of tumor cells, which can be seen as a mutation of the  $T^+$  cells, need testosterone to survive but have evolved to produce testosterone themselves. We refer to that population as  $T^P$  cells. The  $T^-$  tumor cells are independent of testosterone. If the resistant cells are there, we refer to the cancer as *castrate-resistant prostate cancer (cRPC)*; when it becomes metastatic, it is called *metastatic castration-resistant prostate cancer (mCRPC)*. There can be also adaptations, such as phenotypic and genetic changes, which complicate our understanding and targeting of the cancer [11, 19].

We will look at how these cell populations develop into a tumor over a  $L \times L$  square lattice with no-flux boundary conditions, which means that movement across the boundary is not allowed and cells cannot leave the lattice. The spatial step is  $l = \frac{1}{L}$  such that  $x, y \in \{0, l, 2l, \dots, 1 - l\}$ . The time step is  $\delta t$ . The number of  $T^+$  tumor cells at time-step  $t$  at site  $(x, y)$  is denoted by  $n_1(x, y, t)$ , the same for the  $T^P$  tumor cells  $n_2(x, y, t)$ , the  $T^-$  tumor cells  $n_3(x, y, t)$ , the healthy cells  $n_5(x, y, t)$  and the amount of testosterone per lattice point  $n_4(x, y, t)$ . So the total number of tumor and healthy cells at time  $t$  at lattice point  $(x, y)$  is equal to

$$N(x, y, t) = n_1(x, y, t) + n_2(x, y, t) + n_3(x, y, t) + n_5(x, y, t).$$

See List of Symbols for a list of the symbols we use. At each lattice point multiple cells of different types can be present. One can think, for example, that the cells are stacked on top of one another. This is necessary since there are types which depend on each other for the testosterone.

For each simulation, we begin with all the different cells and testosterone uniformly distributed on the lattice. The neighbor sites of  $(x, y)$  are  $\{(x + l, y), (x - l, y), (x, y + l), (x, y - l)\}$  and are denoted by

$(\tilde{x}, \tilde{y})$ . We will first look at the dynamics of the healthy and tumor cells and then we will focus on the dynamics of the testosterone. For every species, we look at three different kind of events: movement, death and production. So the update equations will have the following form:

$$n_i(x, y, t + \delta t) = n_i(x, y, t) + \text{movement-term} - \text{death-term} + \text{birth-term},$$

for  $i \in \{1, 2, 3, 4, 5\}$ .

## 3.2. Dynamics of the Tumor Cells and the Healthy Cells

### 3.2.1. Movement

The first thing which can happen to a cell is that it is pushed to a neighboring site. We assume that this is influenced by the total number of cells at the neighboring sites  $N(\tilde{x}, \tilde{y}, t)$ . The lower the amount of cells at neighbor lattice point  $(\tilde{x}, \tilde{y})$ , the higher the probability that the cell is going to move to that neighbor. At every time-step it can be pushed to a neighboring site or it remains at its current position. This leads us to the following movement probability of a cell at site  $(x_1, y_1)$  to neighbor  $(x_2, y_2)$  at time  $t$ :

$$\mathbb{P}_i((x_1, y_1) \rightarrow (x_2, y_2), t) = C_i \frac{e^{-\frac{\beta}{l^2} N(x_2, y_2, t)}}{\sum_{(\tilde{x}, \tilde{y}) \sim (x_1, y_1)} e^{-\frac{\beta}{l^2} N(\tilde{x}, \tilde{y}, t)}}$$

with  $i \in \{1, 2, 3, 5\}$ . The parameter  $\beta > 0$  ensures that the cells have a preference to not move to a crowded neighboring lattice point and  $C_i \in [0, 1]$  are constants such that

$$\mathbb{P}_i(\text{no movement}, t) = 1 - C_i$$

for  $i \in \{1, 2, 3, 5\}$ . Then we know that for  $i \in \{1, 2, 3, 5\}$  the following holds:

$$\begin{aligned} \sum_{(\tilde{x}, \tilde{y}) \sim (x, y)} \mathbb{P}_i((x, y) \rightarrow (\tilde{x}, \tilde{y}), t) + \mathbb{P}_i(\text{no movement}, t) &= \\ C_i \frac{\sum_{(\tilde{x}, \tilde{y}) \sim (x, y)} e^{-\frac{\beta}{l^2} N(\tilde{x}, \tilde{y}, t)}}{\sum_{(\tilde{x}, \tilde{y}) \sim (x, y)} e^{-\frac{\beta}{l^2} N(\tilde{x}, \tilde{y}, t)}} + 1 - C_i &= \\ C_i + 1 - C_i &= 1. \end{aligned}$$

Furthermore,  $\mathbb{P}_i((x_1, y_1) \rightarrow (x_2, y_2), t)$  and  $\mathbb{P}_i(\text{no movement}, t)$  lie in the interval  $[0, 1]$  making the countable additive  $\mathbb{P}_i$  probability measures.

We now divide each number of cells by  $l^2$  to convert them into densities  $\rho_i$ . We denote  $\frac{N(x, y, t)}{l^2}$  by  $\rho_N(x, y, t)$ . So the movement probability of a cell at site  $(x_1, y_1)$  to neighbor  $(x_2, y_2)$  at time  $t$  is equal to

$$\mathbb{P}_i((x_1, y_1) \rightarrow (x_2, y_2), t) = C_i \frac{e^{-\beta \rho_N(x_2, y_2, t)}}{\sum_{(\tilde{x}, \tilde{y}) \sim (x_1, y_1)} e^{-\beta \rho_N(\tilde{x}, \tilde{y}, t)}}. \quad (3.1)$$

This results in the following movement-term of cells  $i$  at time  $t + \delta t$  at site  $(x, y)$ :

$$\begin{aligned} \sum_{(\tilde{x}, \tilde{y}) \sim (x, y)} \rho_i(\tilde{x}, \tilde{y}, t) \mathbb{P}_i((\tilde{x}, \tilde{y}) \rightarrow (x, y), t) - \rho_i(x, y, t) \sum_{(\tilde{x}, \tilde{y}) \sim (x, y)} \mathbb{P}_i((x, y) \rightarrow (\tilde{x}, \tilde{y}), t) &= \\ \sum_{(\tilde{x}, \tilde{y}) \sim (x, y)} \rho_i(\tilde{x}, \tilde{y}, t) \mathbb{P}_i((\tilde{x}, \tilde{y}) \rightarrow (x, y), t) - C_i \rho_i(x, y, t), & \end{aligned}$$

where the first sum is equal to the cells moving from a neighboring site to site  $(x, y)$  and the second term is equal to all the cells leaving this site.

### 3.2.2. Death and Birth

The next thing which can happen is that a cell can die. We have two types of death: natural death and death due to a lack of testosterone.

Firstly, the higher the population of type  $i \in \{1, 2, 3, 5\}$  in a lattice point, the more dying cells of type  $i$ . Also, we want the death term to be dependent on the total number of cells in a site, so there will be more death due to overcrowding. This results in the death-term of cells  $i$  at time  $t + \delta t$  at site  $(x, y)$ :

$$-\delta t \cdot \gamma_i \rho_i(x, y, t) \cdot \rho_N(x, y, t)$$

with  $i \in \{1, 2, 3, 5\}$  and death-rates  $\gamma_i > 0$ .

The healthy cells and the  $T^P$  and  $T^+$  tumor cells are dependent on testosterone. The less testosterone there is at a site, the more they die. This results in the death-term due to a lack of testosterone at time  $t + \delta t$  at site  $(x, y)$ :

$$-\delta t \cdot \rho_i(x, y, t) \cdot \frac{\kappa}{1 + \rho_4(x, y, t)}$$

with  $i \in \{1, 2, 5\}$  and  $\kappa > 0$ . Note that since  $\rho_4(x, y, t) \geq 0$  for all  $x, y, t$ , we do not divide by zero. Furthermore notice that we do not have this term for the  $T^-$  cells, since they do not depend on testosterone.

We also have a production term, where the cells are being produced by their own type at every time-step. The more cells of type  $i$  on a site, the more cells of type  $i$  will be produced at that site. This results in the following birth-term of cells  $i$  at time  $t + \delta t$  at site  $(x, y)$ :

$$\delta t \cdot \alpha_i \rho_i(x, y, t)$$

with  $i \in \{1, 2, 3, 5\}$  and birth-rates  $\alpha_i > 0$ .

## 3.3. Dynamics of Testosterone

### 3.3.1. Spreading

The testosterone spreads in a different way than the tumor cells and the healthy cells do. We assume that the testosterone diffuses over time. This is modeled by a random walk. The probability to move to a neighboring site at time  $t$  is the same for every neighbor:

$$\mathbb{P}_4((x_1, y_1) \rightarrow (x_2, y_2), t) = \frac{C_4}{4}$$

with  $C_4 \in [0, 1]$  a constant such that

$$\mathbb{P}_4(\text{no spreading}, t) = 1 - C_4.$$

Then we know that the following holds:

$$\begin{aligned} \sum_{(\tilde{x}, \tilde{y}) \sim (x, y)} \mathbb{P}_4((x, y) \rightarrow (\tilde{x}, \tilde{y}), t) + \mathbb{P}_4(\text{no spreading}, t) &= \\ \sum_{(\tilde{x}, \tilde{y}) \sim (x, y)} \left(\frac{C_4}{4}\right) + 1 - C_4 &= \\ C_4 + 1 - C_4 &= 1. \end{aligned}$$

Furthermore,  $\mathbb{P}_4((x_1, y_1) \rightarrow (x_2, y_2), t)$  and  $\mathbb{P}_4(\text{no spreading}, t)$  lie in the interval  $[0, 1]$  making the countable additive  $\mathbb{P}_4$  a probability measure.

This results in the following spreading-term of testosterone at time  $t + \delta t$  at site  $(x, y)$ :

$$\sum_{(\tilde{x}, \tilde{y}) \sim (x, y)} \rho_4(\tilde{x}, \tilde{y}, t) \mathbb{P}_4((\tilde{x}, \tilde{y}) \rightarrow (x, y), t) - \rho_4(x, y, t) \sum_{(\tilde{x}, \tilde{y}) \sim (x, y)} \mathbb{P}_4((x, y) \rightarrow (\tilde{x}, \tilde{y}), t) = \frac{C_4}{4} \sum_{(\tilde{x}, \tilde{y}) \sim (x, y)} \rho_4(\tilde{x}, \tilde{y}, t) - C_4 \rho_4(x, y, t),$$

where the first sum is equal to the testosterone spreading from a neighboring site to site  $(x, y)$  and the second term is equal to all the testosterone leaving this site.

### 3.3.2. Consumption and Production

The next thing which can happen is that the testosterone can be consumed by the  $T^+$  and the  $T^P$  tumor cells and the healthy cells. The more of those cells at a site, the more testosterone will be consumed. This is also dependent of the amount of testosterone at the site. The more testosterone the easier it is to be found and consumed. This results in the death-term at time  $t + \delta t$  at site  $(x, y)$ :

$$-\delta t \cdot \eta (\rho_1(x, y, t) + \rho_2(x, y, t) + \rho_5(x, y, t)) \cdot \rho_4(x, y, t)$$

with the consumption-rate  $\eta > 0$ .

Note that this multiplication by  $\rho_4(x, y, t)$  makes sure that the testosterone cannot go below zero if we take  $\delta t$  small enough.

The testosterone is being produced by the  $T^P$  cells. So the more  $T^P$  cells, the more testosterone is being produced. Furthermore, for the testosterone we start with a base level which is added at every time-step. The body provides this for example through the blood. This results in the production-term at time  $t + \delta t$  at site  $(x, y)$ :

$$\delta t \cdot \mu \rho_2(x, y, t) + \delta t \cdot \chi$$

with the production-rate  $\mu > 0$  and the base-level  $\chi > 0$ .

## 3.4. Total System

Adding all the terms together gives us the total discrete system of prostate cancer:

$$\left\{ \begin{array}{l} \rho_1(x, y, t + \delta t) = \rho_1(x, y, t) + \sum_{(\tilde{x}, \tilde{y}) \sim (x, y)} \rho_1(\tilde{x}, \tilde{y}, t) \mathbb{P}_1((\tilde{x}, \tilde{y}) \rightarrow (x, y), t) - C_1 \rho_1(x, y, t) \\ \quad + \delta t \cdot \rho_1(x, y, t) \left( \alpha_1 - \gamma_1 \rho_N(x, y, t) - \frac{\kappa}{1 + \rho_4(x, y, t)} \right), \\ \rho_2(x, y, t + \delta t) = \rho_2(x, y, t) + \sum_{(\tilde{x}, \tilde{y}) \sim (x, y)} \rho_2(\tilde{x}, \tilde{y}, t) \mathbb{P}_2((\tilde{x}, \tilde{y}) \rightarrow (x, y), t) - C_2 \rho_2(x, y, t) \\ \quad + \delta t \cdot \rho_2(x, y, t) \left( \alpha_2 - \gamma_2 \rho_N(x, y, t) - \frac{\kappa}{1 + \rho_4(x, y, t)} \right), \\ \rho_3(x, y, t + \delta t) = \rho_3(x, y, t) + \sum_{(\tilde{x}, \tilde{y}) \sim (x, y)} \rho_3(\tilde{x}, \tilde{y}, t) \mathbb{P}_3((\tilde{x}, \tilde{y}) \rightarrow (x, y), t) - C_3 \rho_3(x, y, t) \\ \quad + \delta t \cdot \rho_3(x, y, t) (\alpha_3 - \gamma_3 \rho_N(x, y, t)), \\ \rho_4(x, y, t + \delta t) = \rho_4(x, y, t) + \frac{C_4}{4} \sum_{(\tilde{x}, \tilde{y}) \sim (x, y)} \rho_4(\tilde{x}, \tilde{y}, t) - C_4 \rho_4(x, y, t) + \delta t \cdot \chi \\ \quad + \delta t \cdot \mu \rho_2(x, y, t) - \delta t \cdot \eta (\rho_1(x, y, t) + \rho_2(x, y, t) + \rho_5(x, y, t)) \cdot \rho_4(x, y, t). \\ \rho_5(x, y, t + \delta t) = \rho_5(x, y, t) + \sum_{(\tilde{x}, \tilde{y}) \sim (x, y)} \rho_5(\tilde{x}, \tilde{y}, t) \mathbb{P}_5((\tilde{x}, \tilde{y}) \rightarrow (x, y), t) - C_5 \rho_5(x, y, t) \\ \quad + \delta t \cdot \rho_5(x, y, t) \left( \alpha_5 - \gamma_5 \rho_N(x, y, t) - \frac{\kappa}{1 + \rho_4(x, y, t)} \right), \end{array} \right. \quad (3.2)$$

### 3.5. Simulations of Prostate Cancer

In the last section of this chapter, simulations of our discrete model are presented. These simulations are used to confirm how adjusting some of the system parameters influences the behavior of the system. All calculations were performed using C++ in Microsoft Visual Studio. The code can be found in the appendix. For the simulations, we utilized SFML, commonly used in game development, which is freely available for download [45]. We used the parameter values which are portrayed in Table 3.1.

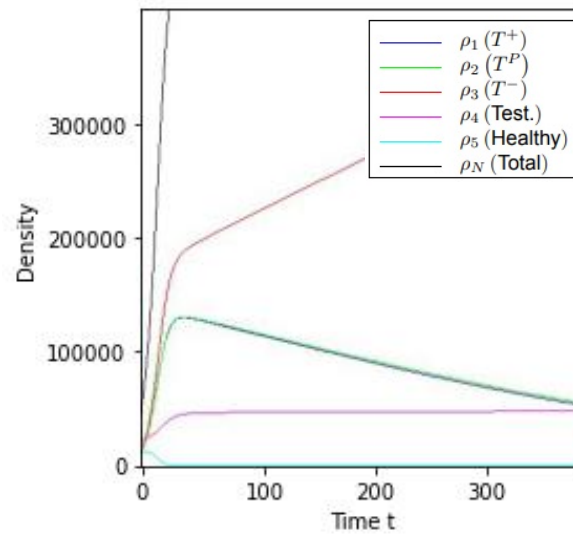
Parameter	Description	Value
$L$	$L \times L$ is the lattice size	50
$l$	Spatial-step	0.02
$\delta t$	Time-step	1
$C_i$	Movement probability	0.1 for all $i$
$\beta$	The rate at which the cells are pushed	$1.0 \cdot 10^{-5}$
$\alpha_i$	Birth-rates	$\alpha_1 = \alpha_2 = 0.21, \alpha_3 = 0.2, \alpha_5 = 0.1$
$\gamma_i$	Death-rates	$\gamma_1 = \gamma_2 = \gamma_3 = 0.001, \gamma_5 = 0.002$
$\kappa$	Death-rate due to lack of testosterone	0.3
$\mu$	Production-rate testosterone	0.04
$\eta$	Consumption-rate testosterone	0.001

**Table 3.1:** The parameter values which are used in the simulations in this chapter.

The initial conditions are set as  $\rho_1 = \rho_2 = \rho_3 = \rho_5 = 5.0$  and  $\rho_4 = 10.0$  in all cells, while the boundaries remain empty. We will adjust the value of  $\chi$ , representing the baseline level of testosterone supplied by the blood. This parameter can be altered by medical intervention, such as through the administration of testosterone. Initially,  $\chi = 0.04$ , and we later simulate the effect of adding testosterone to the blood by increasing  $\chi$  to 10.

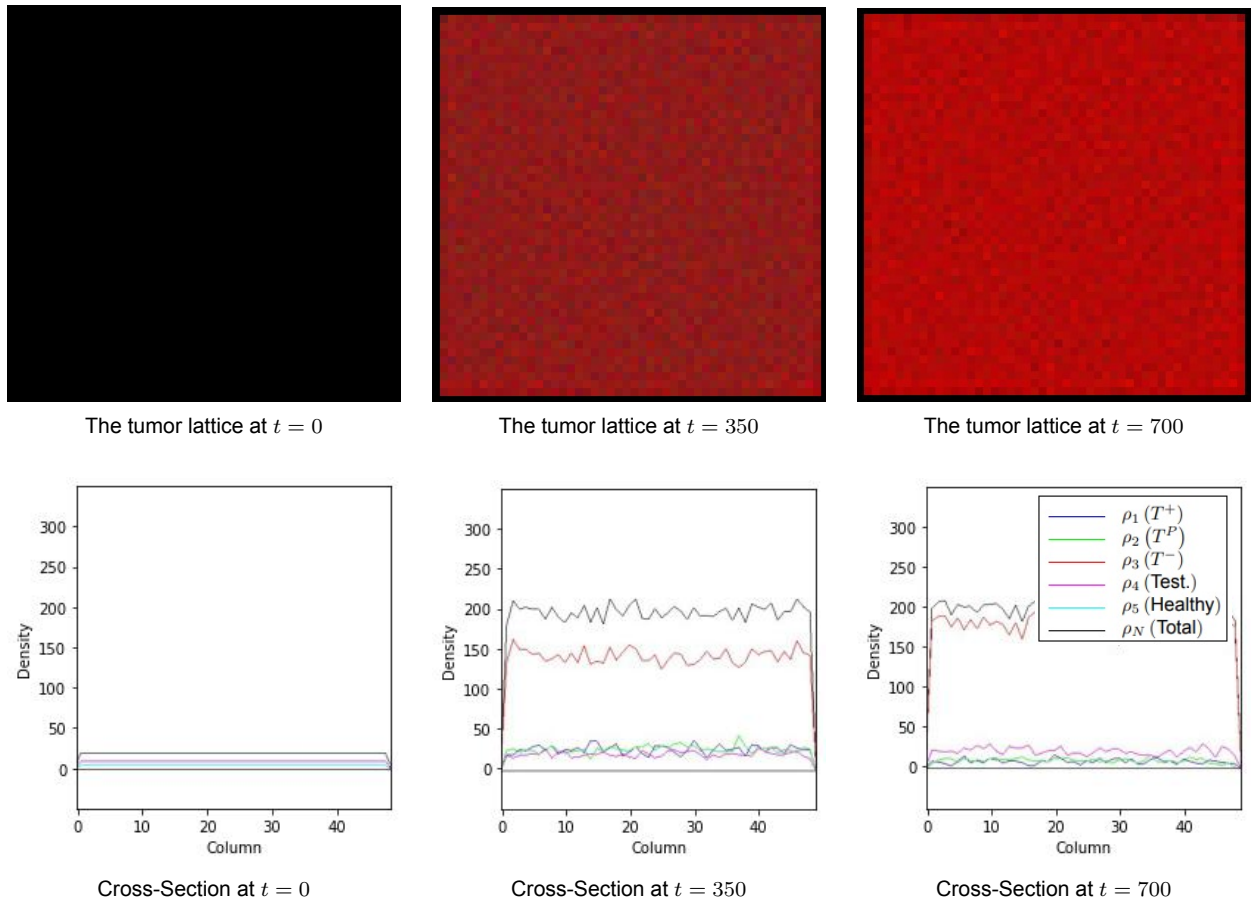
#### 3.5.1. $T^-$ Independent Cell Dominance

We start the simulation with  $\chi = 0.04$ . In Figure 3.1, we observe the tumor dynamics over time at  $\chi = 0.04$ . Initially, all tumor cell populations grow rapidly, leading to a sharp decline in the number of healthy cells. However, as the  $T^-$  cells, which do not rely on testosterone for survival, begin to dominate, the  $T^P$  and  $T^+$  cells start to die off due to insufficient space and low testosterone levels. The  $T^-$  cell population starts rising sharply and by the end of the simulation at  $t = 390$ , the  $T^-$  cells have nearly taken over the tumor environment.

Testosterone and Cell Dynamics Over Time for  $\chi = 0.04$ 

**Figure 3.1:** The total number of cells (black),  $T^-$  cells (red),  $T^P$  cells (green),  $T^+$  cells (blue), testosterone levels (purple), and healthy cells (light blue) are plotted against time from  $t = 0$  to  $t = 390$ . Initially, all tumor cell populations grow rapidly, crushing the healthy cells. Over time,  $T^-$  cells, which are not dependent on testosterone, begin to expand aggressively. The  $T^P$  and  $T^+$  cells, unable to secure enough space and testosterone, gradually die off.

In Figure 3.2, the spatial evolution of the tumor is shown both in lattice form and as cross-sectional views at  $t = 0$ ,  $t = 350$  and  $t = 700$ . The lattice snapshots depict how the tumor grows over time by the color getting brighter, while the cross-sectional views provide a detailed look at the changes in the distribution of all the different cells across the tumor. As the  $T^-$  cells increasingly dominate, the  $T^P$  and  $T^+$  cells struggle to survive, gradually disappearing from the tumor's core. We see this in the tumor pictures by the bright red color at  $t = 700$ .

Tumor Growth and Cross-Section for  $\chi = 0.04$ 

**Figure 3.2:** (a) Lattice representations of the tumor at  $t = 0$ ,  $t = 350$  and  $t = 700$ , showing the evolution of the tumor's spatial distribution of the  $T^+$  (blue),  $T^-$  (red) and  $T^P$  (green) cells. (b) Cross-sectional views of the middle row of the lattice at the same time-points, illustrating changes in the total number of cells (black),  $T^-$  cells (red),  $T^P$  cells (green),  $T^+$  cells (blue), testosterone levels (purple), and healthy cells (light blue).

### 3.5.2. $T^+$ and $T^P$ Dependent Cells Dominance under Testosterone Influence

Next, we 'add testosterone to the blood' at every time step, by running the simulation with  $\chi = 10$ . All the other parameters and initial conditions stay the same. In Figure 3.3, we observe the tumor dynamics over time at  $\chi = 10$ . Initially, the testosterone grows rapidly, leading to an increase in the number of  $T^P$  and  $T^+$  cells. Thereafter, as the  $T^P$  and  $T^+$  cells begin to dominate, the  $T^-$  cells start to die off due to insufficient space and resources. The testosterone and the  $T^P$  and  $T^+$  cell levels start stabilizing by the end of the simulation at  $t = 390$ , while the  $T^-$  cells die out.

In Figure 3.4, the spatial evolution of the tumor is shown both in lattice form and as cross-sectional views at  $t = 0$ ,  $t = 350$  and  $t = 700$ . The lattice snapshots depict how the tumor grows over time by the changing color shade, while the cross-sectional views provide a detailed look at the changes in the distribution of all the different cells across the tumor. As the  $T^P$  and  $T^+$  cells increasingly dominate, the  $T^-$  cells struggle to survive, gradually disappearing from the tumor's core. We see this in the tumor cross section by the red lines being close to zero at  $t = 700$ .

Testosterone and Cell Dynamics Over Time for  $\chi = 10$

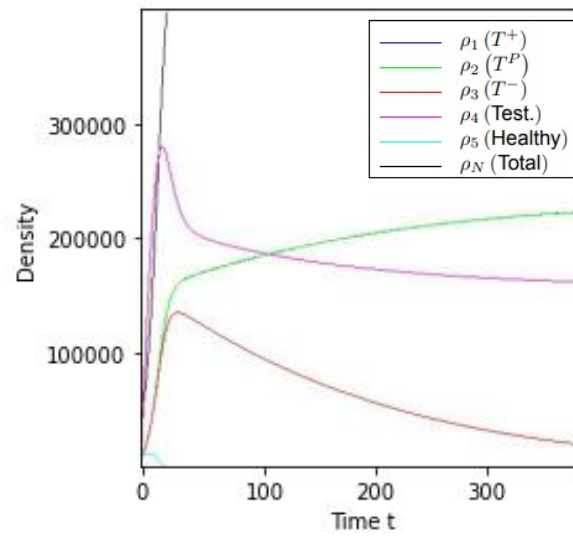


**Figure 3.3:** The total number of cells (black),  $T^-$  cells (red),  $T^P$  cells (green),  $T^+$  cells (blue), testosterone levels (purple), and healthy cells (light blue) are plotted against time from  $t = 0$  to  $t = 390$ . In the beginning, we see a high peak in testosterone after which all tumors grow. Subsequently, the number of  $T^-$  cells start decreasing while the  $T^P$  and  $T^+$  cells keep on growing.

Tumor Growth and Cross-Section for  $\chi = 10$

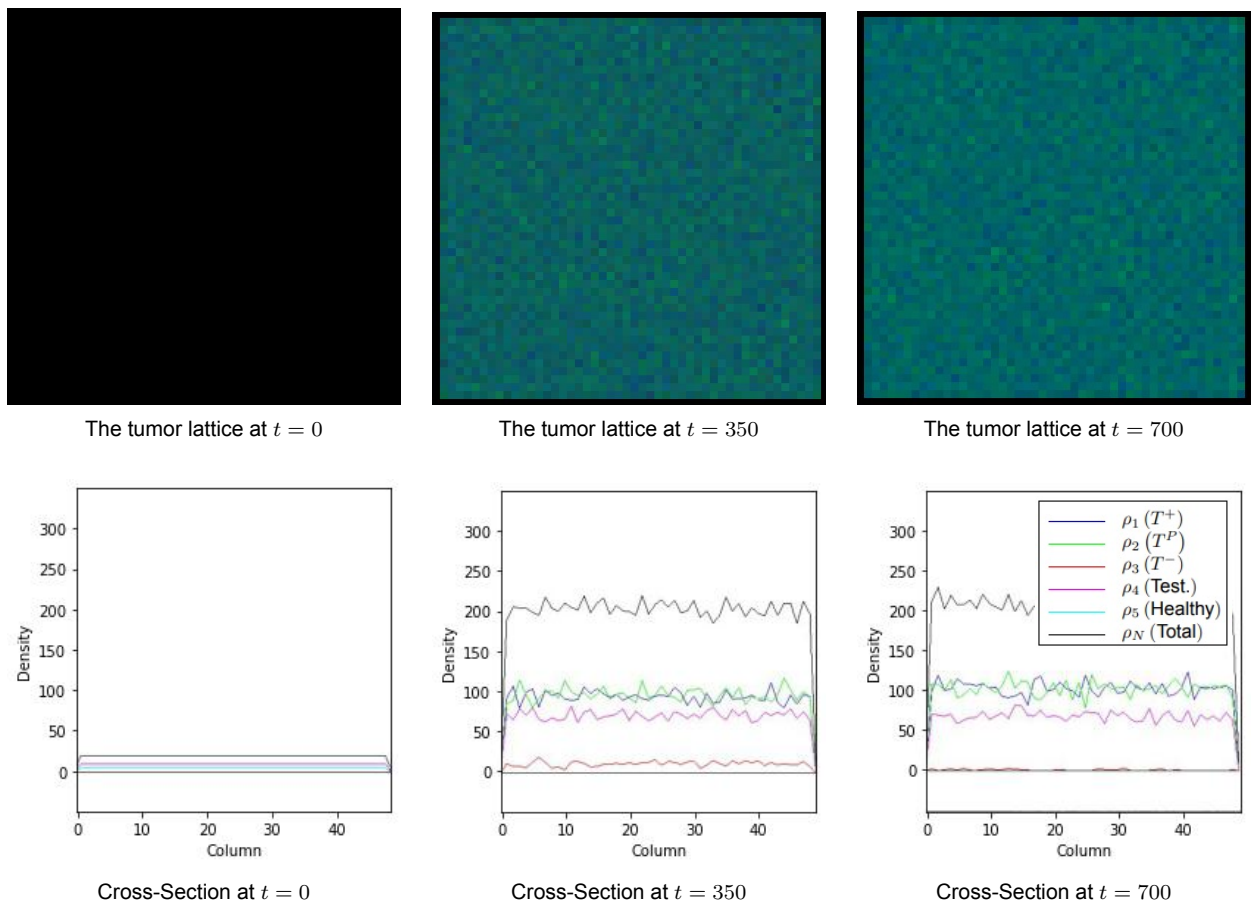


**Figure 3.4:** (a) Lattice representations of the tumor at  $t = 0$ ,  $t = 350$  and  $t = 700$ , showing the evolution of the tumor's spatial distribution of the  $T^+$ ,  $T^-$  and  $T^P$  cells. (b) Cross-sectional views of the middle row of the lattice at the same time-points, illustrating changes in the total number of cells (black),  $T^-$  cells (red),  $T^P$  cells (green),  $T^+$  cells (blue), testosterone levels (purple), and healthy cells (light blue).

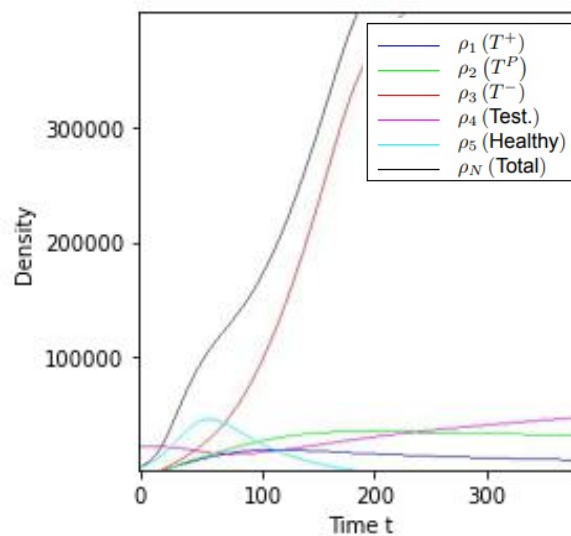
The combining results of Sections 3.5.1 and 3.5.2 indicate that changing  $\chi$  will lead to a phase transition, which we will explore later on in the thesis.

### 3.5.3. Tumor growth

Lastly, we want to try to simulate what the growth of a tumor looks like starting from only a few mutated cells. For this we start with different initial conditions. Every non-boundary cell has  $\rho_5 = 2.0$  and  $\rho_4 = 10.0$ . Furthermore, uniformly distribute 100  $T^-$ , 100  $T^+$ , and 100  $T^P$  cells ( $\rho_i = 1$ ) in a  $10 \times 10$  square in the middle of the lattice. Furthermore, we take  $\chi = 0.04$  and the rest of parameter values from Table 3.1.

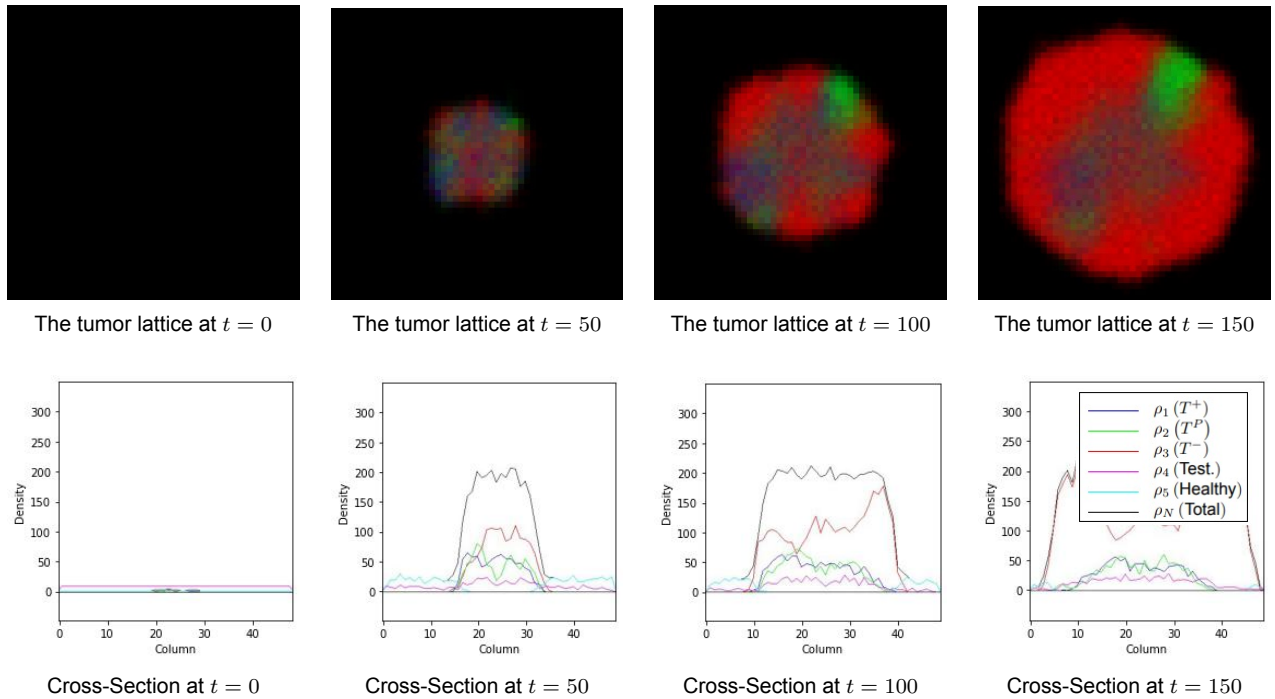
In Figure 3.5, we observe the tumor dynamics over time with  $\chi = 0.04$ . Initially, the healthy cells grow since they are the only ones spread over the whole lattice. However, the tumor cells in the middle start growing and pushing the healthy cells away. Although the  $T^+$  and  $T^P$  cells grow slowly and steady, the  $T^-$  cells grow aggressively causing the tumor to grow very fast.

Testosterone and Cell Dynamics Over Time for  $\chi = 0.04$ , starting from the middle



**Figure 3.5:** The total number of cells (black),  $T^-$  cells (red),  $T^P$  cells (green),  $T^+$  cells (blue), testosterone levels (purple), and healthy cells (light blue) are plotted against time from  $t = 0$  to  $t = 390$ . In the beginning, we see a healthy cells peak, after which the healthy cells are crushed by the tumor cells. The  $T^-$  cells take over and dominate the rest.

In Figure 3.6, the spatial evolution of the tumor is shown both in lattice form and as cross-sectional views at  $t = 0$ ,  $t = 50$ ,  $t = 100$  and  $t = 150$ . The lattice snapshots depict how the tumor grows over time. We can see the tumor expanding in width and becoming more reddish towards the end. The cross-sectional views provide a detailed look at the changes in the distribution of all the different cells across the tumor. We see a few tumor cells starting at the middle of a lattice with healthy cells. Soon it grows into a clump of cells, with the  $T^-$  cells starting to dominate the further time proceeds.

Tumor Growth and Cross-Section for  $\chi = 0.04$ , Starting from the Middle

**Figure 3.6:** (a) Lattice representations of the tumor at  $t = 0$ ,  $t = 50$ ,  $t = 100$  and  $t = 150$ , showing the evolution of the tumor's spatial distribution of the  $T^+$ ,  $T^-$  and  $T^P$  cells. (b) Cross-sectional views of the middle row of the lattice at the same time-points, illustrating changes in the total number of cells (black),  $T^-$  cells (red),  $T^P$  cells (green),  $T^+$  cells (blue), testosterone levels (purple), and healthy cells (light blue).

In Figure 3.7, the spatial evolution of the tumor at  $t = 100$  is depicted through a series of split lattice images. The  $T^-$  cells are shown which dominate the tumor landscape. In areas where  $T^-$  cell density is lower,  $T^P$  and  $T^+$  cells are more prominent. Notably,  $T^+$  cells are mainly found in regions where  $T^P$  cells are also present. This distribution is expected, as these are the areas with higher testosterone levels produced by the  $T^P$  cells. The testosterone distribution map confirms this, showing higher concentrations around the  $T^P$  cells. Additionally, the cross-section of healthy cells reveals a hole in the middle, with most healthy cells being displaced by the growing tumor cells.

Detailed Tumor Growth at  $t = 100$  for  $\chi = 0.04$

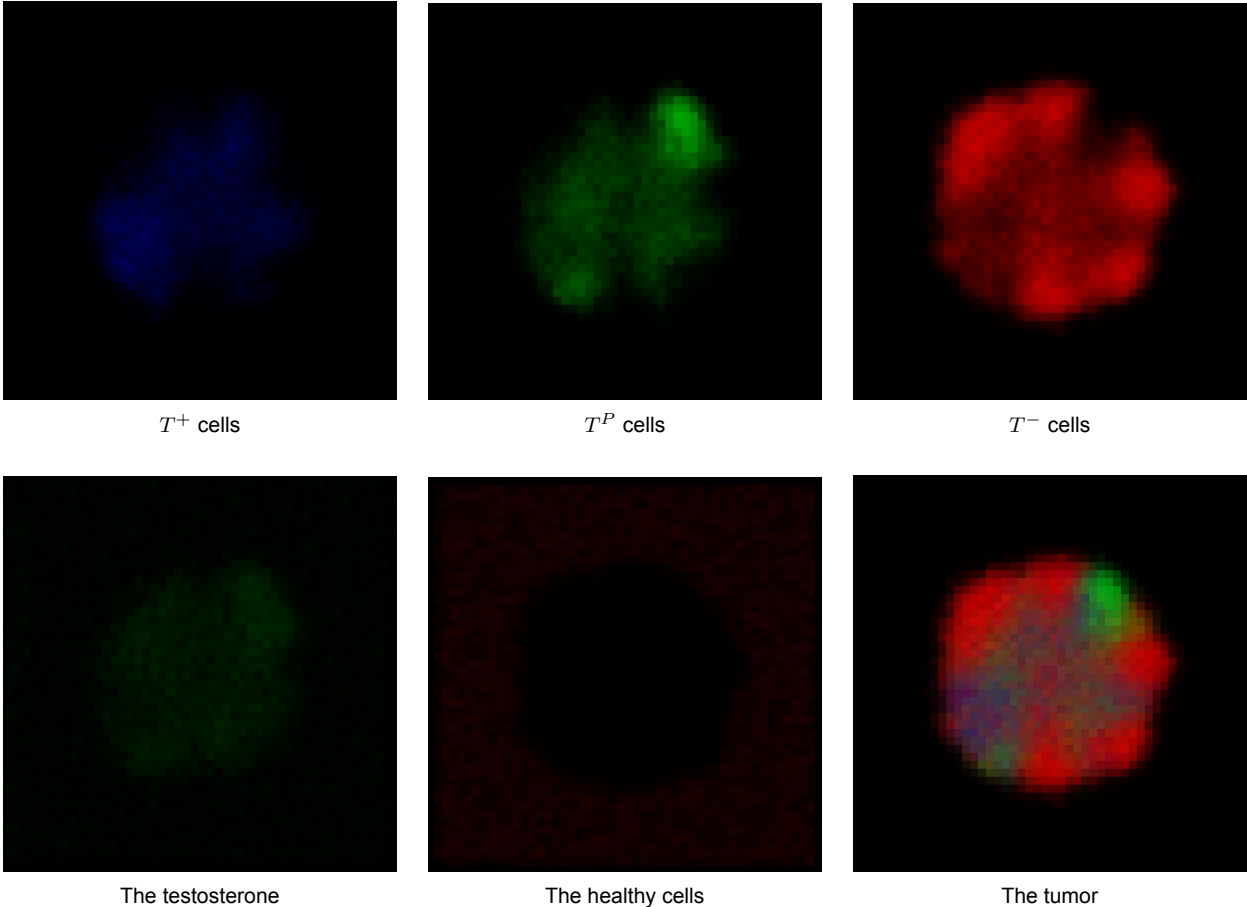


**Figure 3.7:** Lattice representations of the tumor at  $t = 100$ , showing the evolution of the tumor's spatial distribution. It is split into a simulation of the  $T^+$  cells (blue), the  $T^P$  cells (green), the  $T^-$  cells (red), and in the second row we see the testosterone levels (green), the healthy cells (red) and the whole tumor.

# 4

## The Continuum Spatial Model of Prostate Cancer

In this chapter, the partial differential equations of the continuum system will be derived in Section 4.1 by taking the continuum limit of the discrete model of Chapter 3 by a formal derivation using Taylor expansion. After that we will find the equilibria of this system. We will simplify the system in Section 4.2.

### 4.1. Partial Differential Equations Derivation

#### 4.1.1. Theoretic Framework

Before we begin deriving the continuum limit of the discrete system, we need various mathematical tools which will help us. In the model, several terms involve summing over the neighbors of a lattice point. We will use the Laplacian operator to replace this summation. The Laplacian is the divergence of the gradient and it is equal to the sum of the unmixed second partial derivatives:

**Definition 1.** *With  $f$  a twice-differentiable real-valued function and  $v \in \mathbb{R}^2$ , the Laplacian in two dimensions is defined as  $\Delta f(x, y, t) = \sum_{i=1}^2 \frac{\delta^2 f(x, y, t)}{\delta v_i^2} = \frac{\delta^2 f(x, y, t)}{\delta x^2} + \frac{\delta^2 f(x, y, t)}{\delta y^2}$ .*

We will use the backward finite difference scheme to first approximate the first order partial derivative in  $x$ , so that

$$\frac{\delta f(x, y, t)}{\delta x} \approx \frac{f(x, y, t) - f(x - l, y, t)}{l}.$$

For the second derivative approximation in  $x$ , we use the forward finite difference scheme, so that

$$\begin{aligned} \frac{\delta^2 f(x, y, t)}{\delta x^2} &\approx \frac{\frac{f(x + l, y, t) - f(x, y, t)}{l} - \frac{f(x, y, t) - f(x - l, y, t)}{l}}{l} \\ &= \frac{f(x + l, y, t) + f(x - l, y, t) - 2f(x, y, t)}{l^2}. \end{aligned} \quad (4.1)$$

Doing the same for  $y$  and adding them together gives us the following approximation of the Laplacian:

$$\Delta f(x, y, t) \approx \frac{f(x + l, y, t) + f(x - l, y, t) + f(x, y + l, t) + f(x, y - l, t) - 4f(x, y, t)}{l^2}.$$

To determine the order of the error, we use the Taylor series expansion of each term at point  $(x, y, t)$ :

$$\begin{cases} f(x + l, y, t) = f(x, y, t) + lf_x(x, y, t) + \frac{l^2}{2}f_{xx}(x, y, t) + \frac{l^3}{6}f_{xxx}(x, y, t) + O(l^4), \\ f(x - l, y, t) = f(x, y, t) - lf_x(x, y, t) + \frac{l^2}{2}f_{xx}(x, y, t) - \frac{l^3}{6}f_{xxx}(x, y, t) + O(l^4), \\ f(x, y + l, t) = f(x, y, t) + lf_y(x, y, t) + \frac{l^2}{2}f_{yy}(x, y, t) + \frac{l^3}{6}f_{yyy}(x, y, t) + O(l^4), \\ f(x, y - l, t) = f(x, y, t) - lf_y(x, y, t) + \frac{l^2}{2}f_{yy}(x, y, t) - \frac{l^3}{6}f_{yyy}(x, y, t) + O(l^4) \\ -4f(x, y, t) = -4f(x, y, t). \end{cases}$$

Adding these all together results in:

$$f(x+l, y, t) + f(x-l, y, t) + f(x, y+l, t) + f(x, y-l, t) - 4f(x, y, t) = l^2 \Delta f(x, y, t) + O(l^4).$$

Dividing by  $l^2$  and rearranging the terms gives us:

$$\Delta f(x, y, t) = \frac{f(x+l, y, t) + f(x-l, y, t) + f(x, y+l, t) + f(x, y-l, t) - 4f(x, y, t)}{l^2} + O(l^2).$$

Recall that we define the neighbors of lattice point  $(x, y)$  equal to  $\{(x+l, y), (x-l, y), (x, y+l), (x, y-l)\}$ . So the Laplacian is equal to

$$\Delta f(x, y, t) = \frac{\sum_{(\tilde{x}, \tilde{y}) \sim (x, y)} f(\tilde{x}, \tilde{y}, t) - 4f(x, y, t)}{l^2} + O(l^2). \quad (4.2)$$

Finally we can rewrite the summation over the neighbors of a lattice point using this Laplacian operator:

$$\sum_{(\tilde{x}, \tilde{y}) \sim (x, y)} f(\tilde{x}, \tilde{y}, t) = l^2 \Delta f(x, y, t) + 4f(x, y, t) + O(l^4). \quad (4.3)$$

Furthermore, following Alsenafi [2] and Zegers [58], we define  $F$  to simplify the notation later. This  $F$  is defined as followed:

$$F(v, t) = e^{\beta \rho_N(v, t)} \left( \frac{1}{4} - \frac{l^2}{16} \left( \Delta(-\beta \rho_N(v, t)) + \nabla(\beta \rho_N(v, t))^2 \right) \right). \quad (4.4)$$

In the derivation of the partial differential equations, we will need the Laplacian of  $F$ . To do this, we must first calculate the gradient. For readability, we will omit  $(x, t)$  in the notation.

$$\begin{aligned} \nabla F &= \nabla \left[ \frac{e^{\beta \rho_N}}{4} \left( 1 - \frac{l^2}{4} \left( \Delta(-\beta \rho_N) + \nabla(\beta \rho_N^2) \right) \right) \right] \\ &= \frac{e^{\beta \rho_N}}{4} \left( \nabla(\beta \rho_N) - \frac{l^2}{4} \nabla \beta \rho_N \left( \Delta(-\beta \rho_N) + \nabla(\beta \rho_N^2) \right) - \frac{l^2}{4} \nabla \left( \Delta(-\beta \rho_N) + \nabla(\beta \rho_N^2) \right) \right) \\ &= \frac{e^{\beta \rho_N}}{4} \nabla(\beta \rho_N) + O(l^2). \end{aligned} \quad (4.5)$$

Now let us calculate the Laplacian of  $F$ :

$$\Delta F = \nabla \cdot \nabla F = \frac{e^{\beta \rho_N}}{4} \left( \nabla(\beta \rho_N)^2 + \Delta(\beta \rho_N) \right) + O(l^2). \quad (4.6)$$

The final tool we will use for the derivation is that we can rewrite  $f(x) = \frac{1}{x}$  using its Taylor expansion at point  $a$ , which is

$$\frac{1}{x} = \frac{1}{a} - \frac{x-a}{a^2} + O(l^2),$$

since  $f'(x) = -\frac{1}{x^2}$  and substitute  $x = a+l$ :

$$\frac{1}{a+l} = \frac{1}{a} - \frac{l}{a^2} + O(l^2), \quad (4.7)$$

since  $x-a = a+l-a = l$ .

### 4.1.2. Continuum System

Now we are ready to derive the continuum system by taking a formal limit of the discrete model of Equation (3.2). We will start with the densities of the tumor cells and the healthy cells. We will organize the derivation into two claims.

**Claim 1.** *If  $\delta t \rightarrow 0$  and  $l \rightarrow 0$  in such a way that  $\frac{l^2}{\delta t} \rightarrow D$  for some constant  $D \in \mathbb{R}$ , then the formal limit of evolution equation for density of the cancerous and healthy cells given by Equation (3.2) is*

$$\frac{\delta \rho_i(v, t)}{\delta t} = \frac{DC_i}{4} \nabla (\nabla \rho_i(v, t) + 2\rho_i(v, t) \nabla (\beta \rho_N(v, t))) + \rho_i(v, t) \left( \alpha_i - \gamma_i \rho_N(v, t) - \frac{\kappa}{1 + \rho_4(v, t)} \right)$$

for  $i \in \{1, 2, 3, 5\}$ .

*Proof.* Recall, from Equation (3.2), that the discrete model is:

$$\left\{ \begin{array}{l} \rho_1(x, y, t + \delta t) = \rho_1(x, y, t) + \sum_{(\tilde{x}, \tilde{y}) \sim (x, y)} \rho_1(\tilde{x}, \tilde{y}, t) \mathbb{P}_1((\tilde{x}, \tilde{y}) \rightarrow (x, y), t) - C_1 \rho_1(x, y, t) \\ \quad + \delta t \cdot \rho_1(x, y, t) \left( \alpha_1 - \gamma_1 \cdot \rho_N(x, y, t) - \frac{\kappa}{1 + \rho_4(x, y, t)} \right), \\ \rho_2(x, y, t + \delta t) = \rho_2(x, y, t) + \sum_{(\tilde{x}, \tilde{y}) \sim (x, y)} \rho_2(\tilde{x}, \tilde{y}, t) \mathbb{P}_2((\tilde{x}, \tilde{y}) \rightarrow (x, y), t) - C_2 \rho_2(x, y, t) \\ \quad + \delta t \cdot \rho_2(x, y, t) \left( \alpha_2 - \gamma_2 \cdot \rho_N(x, y, t) - \frac{\kappa}{1 + \rho_4(x, y, t)} \right), \\ \rho_3(x, y, t + \delta t) = \rho_3(x, y, t) + \sum_{(\tilde{x}, \tilde{y}) \sim (x, y)} \rho_3(\tilde{x}, \tilde{y}, t) \mathbb{P}_3((\tilde{x}, \tilde{y}) \rightarrow (x, y), t) - C_3 \rho_3(x, y, t) \\ \quad + \delta t \cdot \rho_3(x, y, t) (\alpha_3 - \gamma_3 \cdot \rho_N(x, y, t)), \\ \rho_5(x, y, t + \delta t) = \rho_5(x, y, t) + \sum_{(\tilde{x}, \tilde{y}) \sim (x, y)} \rho_5(\tilde{x}, \tilde{y}, t) \mathbb{P}_5((\tilde{x}, \tilde{y}) \rightarrow (x, y), t) - C_5 \rho_5(x, y, t) \\ \quad + \delta t \cdot \rho_5(x, y, t) \left( \alpha_5 - \gamma_5 \cdot \rho_N(x, y, t) - \frac{\kappa}{1 + \rho_4(x, y, t)} \right). \end{array} \right.$$

We can write this as

$$\begin{aligned} \rho_i(x, y, t + \delta t) = & \rho_i(x, y, t) + \sum_{(\tilde{x}, \tilde{y}) \sim (x, y)} \rho_i(\tilde{x}, \tilde{y}, t) \mathbb{P}_i((\tilde{x}, \tilde{y}) \rightarrow (x, y), t) - C_i \rho_i(x, y, t) \\ & + \delta t \cdot \rho_i(x, y, t) \left( \alpha_i - \gamma_i \cdot \rho_N(x, y, t) - \frac{\kappa}{1 + \rho_4(x, y, t)} \right), \end{aligned} \quad (4.8)$$

where  $i \in \{1, 2, 3, 5\}$ , letting  $\kappa_i = \kappa$  generally and  $\kappa_i = 0$  if and only if  $i = 3$ . Recall from Equation (3.1) that the movement probability of a cell at site  $v_1 = (x_1, y_1)$  to neighbor  $v_2 = (x_2, y_2)$  at time  $t$  is equal to

$$\mathbb{P}_i(v_1 \rightarrow v_2, t) = C_i \frac{e^{-\beta \rho_N(v_2, t)}}{\sum_{\tilde{v} \sim (v_1)} e^{-\beta \rho_N(\tilde{v}, t)}}.$$

Using Equation (4.3) produces

$$\mathbb{P}_i(v_1 \rightarrow v_2, t) = C_i \frac{e^{-\beta \rho_N(v_2, t)}}{l^2 \Delta e^{-\beta \rho_N(v_1, t)} + 4e^{-\beta \rho_N(v_1, t)}} + O(l^4).$$

Using that

$$\Delta e^{f(x)} = e^{f(x)} \left( \Delta f(x) + \nabla f(x)^2 \right),$$

we obtain the following expression for the movement probability

$$\begin{aligned} \mathbb{P}_i(v_1 \rightarrow v_2, t) &= C_i \frac{e^{-\beta\rho_N(v_2, t)}}{l^2 e^{-\beta\rho_N(v_1, t)} \left( \Delta(-\beta\rho_N(v_1, t)) + \nabla(\beta\rho_N(v_1, t))^2 \right) + 4e^{-\beta\rho_N(v_1, t)}} + O(l^4) \\ &= C_i e^{-\beta\rho_N(v_2, t)} \frac{e^{\beta\rho_N(v_1, t)}}{l^2 \left( \Delta(-\beta\rho_N(v_1, t)) + \nabla(\beta\rho_N(v_1, t))^2 \right) + 4} + O(l^4). \end{aligned}$$

Using Equations (4.7) and (4.4) gives us

$$\begin{aligned} \mathbb{P}_i(v_1 \rightarrow v_2, t) &= C_i e^{-\beta\rho_N(v_2, t)} \left( e^{\beta\rho_N(v_1, t)} \left( \frac{1}{4} - \frac{l^2}{16} \left( \Delta(-\beta\rho_N(v_1, t)) + \nabla(\beta\rho_N(v_1, t))^2 \right) \right) \right) + O(l^2) \\ &= C_i e^{-\beta\rho_N(v_2, t)} F(v_1, t) + O(l^2). \end{aligned} \quad (4.9)$$

Substituting Equation (4.9) into (4.8), dividing by  $\delta t$  and rearranging the terms results in

$$\begin{aligned} \frac{\rho_i(v, t + \delta t) - \rho_i(v, t)}{\delta t} &= \frac{1}{\delta t} \left( C_i e^{-\beta\rho_N(v, t)} \sum_{\tilde{v} \sim v} \rho_i(\tilde{v}, t) F(\tilde{v}, t) - C_i \rho_i(v, t) \right) \\ &\quad + \rho_i(v, t) \left( \alpha_i - \gamma_i \cdot \rho_N(v, t) - \frac{\kappa}{1 + \rho_4(v, t)} \right) + O(l^2). \end{aligned} \quad (4.10)$$

To simplify the sum, first use Equation (4.3), and after that substitute  $F$  with (4.4):

$$\begin{aligned} \sum_{\tilde{v} \sim v} \rho_i(\tilde{v}, t) F(\tilde{v}, t) &= l^2 \Delta(\rho_i(v, t) F(v, t)) + 4\rho_i(v, t) F(v, t) + O(l^4) \\ &= l^2 \Delta(\rho_i(v, t) F(v, t)) + 4\rho_i(v, t) e^{\beta\rho_N(v, t)}. \\ &\quad \left( \frac{1}{4} - \frac{l^2}{16} \left( \Delta(-\beta\rho_N(v, t)) + \nabla(\beta\rho_N(v, t))^2 \right) \right) + O(l^4). \end{aligned} \quad (4.11)$$

With the product rule, (4.4), (4.5) and (4.6) we obtain:

$$\begin{aligned} \Delta(\rho_i F) &= 2 \nabla F \nabla \rho_i + F \Delta \rho_i + \rho_i \Delta F \\ &= \frac{2e^{\beta\rho_N}}{4} \nabla \beta\rho_N \nabla \rho_i + e^{\beta\rho_N} \frac{1}{4} \Delta \rho_i + \frac{\rho_i e^{\beta\rho_N}}{4} \left( \nabla(\beta\rho_N)^2 + \Delta(\beta\rho_N) \right) + O(l^2) \\ &= \frac{e^{\beta\rho_N}}{4} \left( 2 \nabla \beta\rho_N \nabla \rho_i + \Delta \rho_i + \rho_i \left( \nabla(\beta\rho_N)^2 + \Delta(\beta\rho_N) \right) \right) + O(l^2). \end{aligned}$$

Substituting this into Equation (4.11) and multiplying it by  $e^{-\beta\rho_N(v, t)}$  results in

$$\begin{aligned} e^{-\beta\rho_N(v, t)} \sum_{\tilde{v} \sim v} \rho_i(\tilde{v}, t) F(\tilde{v}, t) &= \frac{l^2}{4} \left( 2 \nabla \beta\rho_N(v, t) \nabla \rho_i(v, t) + \Delta \rho_i(v, t) + \rho_i(v, t) \left( \nabla(\beta\rho_N(v, t))^2 \right. \right. \\ &\quad \left. \left. + \Delta(\beta\rho_N(v, t)) \right) \right) + \rho_i(v, t) \left( 1 - \frac{l^2}{4} \left( \Delta(-\beta\rho_N(v, t)) + \nabla(\beta\rho_N(v, t))^2 \right) \right) + O(l^4), \end{aligned}$$

which can be rearranged to

$$e^{-\beta\rho_N(v, t)} \sum_{\tilde{v} \sim v} \rho_i(\tilde{v}, t) F(\tilde{v}, t) = \frac{l^2}{4} \left( \nabla(\nabla \rho_i + 2\rho_i \nabla(\beta\rho_N)) \right) + \rho_i(v, t) + O(l^4).$$

Substituting this into (4.10) results in

$$\begin{aligned} \frac{\rho_i(v, t + \delta t) - \rho_i(v, t)}{\delta t} &= \frac{l^2 C_i}{4\delta t} \nabla (\nabla \rho_i(v, t) + 2\rho_i(v, t) \nabla (\beta \rho_N(v, t))) \\ &\quad + \rho_i(v, t) \left( \alpha_i - \gamma_i \cdot \rho_N(v, t) - \frac{\kappa}{1 + \rho_4(v, t)} \right) + O\left(\frac{l^4}{\delta t}\right). \end{aligned}$$

Now let  $\delta t \rightarrow 0$  and  $l \rightarrow 0$ , and define  $D$  such that  $\frac{l^2}{\delta t} \rightarrow D$ .

Then we finally obtain the following partial differential equation for the density of the tumor cells and the healthy cells:

$$\begin{aligned} \frac{\delta \rho_i(v, t)}{\delta t} &= \frac{DC_i}{4} \nabla (\nabla \rho_i(v, t) + 2\rho_i(v, t) \nabla (\beta \rho_N(v, t))) \\ &\quad + \rho_i(v, t) \left( \alpha_i - \gamma_i \rho_N(v, t) - \frac{\kappa}{1 + \rho_4(v, t)} \right). \end{aligned}$$

□

Now that we have derived the continuum limit of the discrete evolution equations for the cell populations, we will, in the next claim, derive the partial differential equation for the density of testosterone.

**Claim 2.** *If  $\delta t \rightarrow 0$  and  $l \rightarrow 0$  in such a way that  $\frac{l^2}{\delta t} \rightarrow D$  for some constant  $D \in \mathbb{R}$ , then the formal limit of evolution equation for density of testosterone given by Equation (3.2) is*

$$\frac{\delta \rho_4(v, t)}{\delta t} = \frac{DC_4}{4} \Delta \rho_4(v, t) + \chi + \mu \cdot \rho_2(v, t) - \eta (\rho_1(v, t) + \rho_2(v, t) + \rho_5(v, t)) \cdot \rho_4(v, t)$$

for  $i \in \{1, 2, 3, 5\}$ .

*Proof.* Recall that the change in the amount of testosterone can be written as

$$\begin{aligned} \rho_4(v, t + \delta t) &= \rho_4(v, t) + \frac{C_4}{4} \sum_{\tilde{v} \sim v} \rho_4(\tilde{v}, t) - C_4 \rho_4(v, t) + \delta t \cdot \chi \\ &\quad + \delta t \cdot \mu \cdot \rho_2(v, t) - \delta t \cdot \eta (\rho_1(v, t) + \rho_2(v, t) + \rho_5(v, t)) \cdot \rho_4(v, t). \end{aligned}$$

Dividing by  $\delta t$  and rearranging terms produces:

$$\begin{aligned} \frac{\rho_4(v, t + \delta t) - \rho_4(v, t)}{\delta t} &= \frac{C_4}{4\delta t} \sum_{\tilde{v} \sim v} \rho_4(\tilde{v}, t) - \frac{C_4}{\delta t} \rho_4(v, t) + \chi \\ &\quad + \mu \cdot \rho_2(v, t) - \eta (\rho_1(v, t) + \rho_2(v, t) + \rho_5(v, t)) \cdot \rho_4(v, t). \end{aligned}$$

Rewriting the sum and combining with (4.3), gives:

$$\begin{aligned} \frac{\rho_4(v, t + \delta t) - \rho_4(v, t)}{\delta t} &= \frac{l^2 C_4}{4\delta t} \Delta \rho_4(v, t) + \chi + \mu \cdot \rho_2(v, t) \\ &\quad - \eta (\rho_1(v, t) + \rho_2(v, t) + \rho_5(v, t)) \cdot \rho_4(v, t) + O\left(\frac{l^4}{\delta t}\right). \end{aligned}$$

Now let  $\delta t \rightarrow 0$  and  $l \rightarrow 0$ , such that  $\frac{l^2}{\delta t} \rightarrow D$ .

Then we finally obtain the following partial differential equation for the density of testosterone:

$$\frac{\delta \rho_4(v, t)}{\delta t} = \frac{DC_4}{4} \Delta \rho_4(v, t) + \chi + \mu \cdot \rho_2(v, t) - \eta (\rho_1(v, t) + \rho_2(v, t) + \rho_5(v, t)) \cdot \rho_4(v, t).$$

□

Finally, it follows from Claims 1 and 2 that the full continuum limit of the discrete model described by Equation (3.2) is:

$$\begin{cases} \frac{\delta \rho_1}{\delta t} = \frac{DC_1}{4} \nabla \cdot [\nabla \rho_1 + 2\beta \rho_1 \nabla \rho_N] + \rho_1 \left( \alpha_1 - \gamma_1 \rho_N - \frac{\kappa}{1+\rho_4} \right), \\ \frac{\delta \rho_2}{\delta t} = \frac{DC_2}{4} \nabla \cdot [\nabla \rho_2 + 2\beta \rho_2 \nabla \rho_N] + \rho_2 \left( \alpha_2 - \gamma_2 \rho_N - \frac{\kappa}{1+\rho_4} \right), \\ \frac{\delta \rho_3}{\delta t} = \frac{DC_3}{4} \nabla \cdot [\nabla \rho_3 + 2\beta \rho_3 \nabla \rho_N] + \rho_3 (\alpha_3 - \gamma_3 \rho_N), \\ \frac{\delta \rho_4}{\delta t} = \frac{DC_4}{4} \Delta \rho_4 + \mu \rho_2 - \eta (\rho_1 + \rho_2 + \rho_5) \rho_4 + \chi, \\ \frac{\delta \rho_5}{\delta t} = \frac{DC_5}{4} \nabla \cdot [\nabla \rho_5 + 2\beta \rho_5 \nabla \rho_N] + \rho_5 \left( \alpha_5 - \gamma_5 \rho_N - \frac{\kappa}{1+\rho_4} \right). \end{cases}$$

## 4.2. Equilibrium Solutions

To determine the steady-state solutions, assume each  $\rho_i$  is a constant, denoted  $\bar{\rho}_i$ . We assume all densities are non-negative and all parameters are greater than zero. To calculate the equilibrium solutions, we set  $\frac{\delta \bar{\rho}_i}{\delta t} = 0$  for all  $i$ , ensuring that the solution remains constant. For the  $T^-$  tumor density, this results in:

$$\bar{\rho}_3 = 0 \text{ or } \bar{\rho}_N = \frac{\alpha_3}{\gamma_3}.$$

For the other tumor cells and the healthy cells we obtain the equations:

$$\bar{\rho}_i = 0 \text{ or } \bar{\rho}_N = \frac{\alpha_i}{\gamma_i} - \frac{\kappa}{\gamma_i (1 + \bar{\rho}_4)},$$

where  $i \in \{1, 2, 5\}$ . Finally, for testosterone the equilibrium density must be:

$$\bar{\rho}_4 = \frac{\mu \bar{\rho}_2 + \chi}{\eta (\bar{\rho}_1 + \bar{\rho}_5 + \bar{\rho}_2)},$$

with  $\bar{\rho}_1 + \bar{\rho}_5 + \bar{\rho}_2 \neq 0$ . By using Wolfram Mathematica, the 7 equilibria  $(\bar{\rho}_1, \bar{\rho}_2, \bar{\rho}_3, \bar{\rho}_4, \bar{\rho}_5)$  where  $\bar{\rho}_1 = 0$  are:

- Equilibrium 1:

$$\begin{aligned} & [0, (-\gamma_3 \alpha_2 \chi + \alpha_3 \gamma_2 \chi) / (\gamma_3 \alpha_2 \mu - \alpha_3 \gamma_2 \mu - \kappa \gamma_3 \eta + \gamma_3 \alpha_2 \eta - \alpha_3 \gamma_2 \eta), (\alpha_3 \gamma_3 \alpha_2 \mu - \alpha_3^2 \gamma_2 \mu \\ & - \kappa \alpha_3 \gamma_3 \eta + \alpha_3 \gamma_3 \alpha_2 \eta - \alpha_3^2 \gamma_2 \eta + \gamma_3^2 \alpha_2 \chi - \alpha_3 \gamma_3 \gamma_2 \chi) / (\gamma_3 (\gamma_3 \alpha_2 \mu - \alpha_3 \gamma_2 \mu \\ & - \kappa \gamma_3 \eta + \gamma_3 \alpha_2 \eta - \alpha_3 \gamma_2 \eta)), (\kappa \gamma_3 - \gamma_3 \alpha_2 + \alpha_3 \gamma_2) / (\gamma_3 \alpha_2 - \alpha_3 \gamma_2), 0], \end{aligned}$$

- Equilibrium 2:

$$\begin{aligned} & [0, 0, (\kappa \alpha_3 \gamma_3 \eta - \alpha_3 \gamma_3 \alpha_5 \eta + \alpha_3^2 \gamma_5 \eta - \gamma_3^2 \alpha_5 \chi + \alpha_3 \gamma_3 \gamma_5 \chi) / (\gamma_3 (\kappa \gamma_3 - \gamma_3 \alpha_5 + \alpha_3 \gamma_5) \eta), \\ & (\kappa \gamma_3 - \gamma_3 \alpha_5 + \alpha_3 \gamma_5) / (\gamma_3 \alpha_5 - \alpha_3 \gamma_5), (\gamma_3 \alpha_5 \chi - \alpha_3 \gamma_5 \chi) / ((\kappa \gamma_3 - \gamma_3 \alpha_5 + \alpha_3 \gamma_5) \eta)], \end{aligned}$$

- Equilibrium 3:

$$\begin{aligned} & [0, (\kappa \alpha_2 \gamma_2 \eta - \kappa \gamma_2 \alpha_5 \eta - \alpha_2 \gamma_2 \alpha_5 \eta + \gamma_2 \alpha_5^2 \eta - \kappa \alpha_2 \gamma_5 \eta + \alpha_2^2 \gamma_5 \eta + \kappa \alpha_5 \gamma_5 \eta - \alpha_2 \alpha_5 \gamma_5 \eta \\ & - \gamma_2^2 \alpha_5 \chi + \alpha_2 \gamma_2 \gamma_5 \chi + \gamma_2 \alpha_5 \gamma_5 \chi - \alpha_2 \gamma_5^2 \chi) / ((\gamma_2 - \gamma_5) (\gamma_2 \alpha_5 - \alpha_2 \gamma_5) \mu), 0, \\ & (\kappa \gamma_2 - \gamma_2 \alpha_5 - \kappa \gamma_5 + \alpha_2 \gamma_5) / (\gamma_2 \alpha_5 - \alpha_2 \gamma_5), (\alpha_2 \gamma_2 \alpha_5 \mu - \gamma_2 \alpha_5^2 \mu - \alpha_2^2 \gamma_5 \mu \\ & + \alpha_2 \alpha_5 \gamma_5 \mu - \kappa \alpha_2 \gamma_2 \eta + \kappa \gamma_2 \alpha_5 \eta + \alpha_2 \gamma_2 \alpha_5 \eta - \gamma_2 \alpha_5^2 \eta + \kappa \alpha_2 \gamma_5 \eta - \alpha_2^2 \gamma_5 \eta \\ & - \kappa \alpha_5 \gamma_5 \eta + \alpha_2 \alpha_5 \gamma_5 \eta + \gamma_2^2 \alpha_5 \chi - \alpha_2 \gamma_2 \gamma_5 \chi - \gamma_2 \alpha_5 \gamma_5 \chi + \alpha_2 \gamma_5^2 \chi) / \\ & ((\gamma_2 - \gamma_5) (\gamma_2 \alpha_5 - \alpha_2 \gamma_5) \mu)], \end{aligned}$$

- Equilibrium 4:

$$\begin{aligned} & [0, (1 / (2(\gamma_2 \mu + \gamma_2 \eta))) (\alpha_2 \mu - \kappa \eta + \alpha_2 \eta - \gamma_2 \chi - (-4\alpha_2 \eta (\kappa \mu - \alpha_2 \mu - \gamma_2 \chi) + (-\alpha_2 \mu - \kappa \eta \\ & + \alpha_2 \eta - \gamma_2 \chi)^2)^{\frac{1}{2}}), 0, (1 / (2\alpha_2 \eta)) (\alpha_2 \mu + \kappa \eta - \alpha_2 \eta + \gamma_2 \chi \\ & - (-4\alpha_2 \eta (\kappa \mu - \alpha_2 \mu - \gamma_2 \chi) + (-\alpha_2 \mu - \kappa \eta + \alpha_2 \eta - \gamma_2 \chi)^2)^{\frac{1}{2}}), 0], \end{aligned}$$

- **Equilibrium 5:**

$$\left[0, (1/(2(\gamma_2\mu + \gamma_2\eta)))(\alpha_2\mu - \kappa\eta + \alpha_2\eta - \gamma_2\chi + (-4\alpha_2\eta(\kappa\mu - \alpha_2\mu - \gamma_2\chi) + (-\alpha_2\mu - \kappa\eta + \alpha_2\eta - \gamma_2\chi)^2)^{\frac{1}{2}}), 0, (1/(2\alpha_2\eta))(\alpha_2\mu + \kappa\eta - \alpha_2\eta + \gamma_2\chi + (-4\alpha_2\eta(\kappa\mu - \alpha_2\mu - \gamma_2\chi) + (-\alpha_2\mu - \kappa\eta + \alpha_2\eta - \gamma_2\chi)^2)^{\frac{1}{2}}), 0\right],$$

- **Equilibrium 6:**

$$\left[0, 0, 0, (\kappa\eta - \alpha_5\eta + \gamma_5\chi - \sqrt{4\alpha_5\gamma_5\eta\chi + (-\kappa\eta + \alpha_5\eta - \gamma_5\chi)^2})/(2\alpha_5\eta), (-\kappa\eta + \alpha_5\eta - \gamma_5\chi - \sqrt{4\alpha_5\gamma_5\eta\chi + (-\kappa\eta + \alpha_5\eta - \gamma_5\chi)^2})/(2\gamma_5\eta)\right],$$

- **Equilibrium 7:**

$$\left[0, 0, 0, (\kappa\eta - \alpha_5\eta + \gamma_5\chi + \sqrt{4\alpha_5\gamma_5\eta\chi + (-\kappa\eta + \alpha_5\eta - \gamma_5\chi)^2})/(2\alpha_5\eta), (-\kappa\eta + \alpha_5\eta - \gamma_5\chi + \sqrt{4\alpha_5\gamma_5\eta\chi + (-\kappa\eta + \alpha_5\eta - \gamma_5\chi)^2})/(2\gamma_5\eta)\right].$$

The remaining 4 equilibria  $(\bar{\rho}_1, \bar{\rho}_2, \bar{\rho}_3, \bar{\rho}_4, \bar{\rho}_5)$  where  $\bar{\rho}_1 \neq 0$  are:

- **Equilibrium 8:**

$$\left[(\gamma_3\alpha_1\chi - \alpha_3\gamma_1\chi)/((\kappa\gamma_3 - \gamma_3\alpha_1 + \alpha_3\gamma_1)\eta), 0, (\kappa\alpha_3\gamma_3\eta - \alpha_3\gamma_3\alpha_1\eta + \alpha_3^2\gamma_1\eta - \gamma_3^2\alpha_1\chi + \alpha_3\gamma_3\gamma_1\chi)/(\gamma_3(\kappa\gamma_3 - \gamma_3\alpha_1 + \alpha_3\gamma_1)\eta), (\kappa\gamma_3 - \gamma_3\alpha_1 + \alpha_3\gamma_1)/(\gamma_3\alpha_1 - \alpha_3\gamma_1), 0\right],$$

- **Equilibrium 9:**

$$\left[(\alpha_1\gamma_1\alpha_2\mu - \gamma_1\alpha_2^2\mu - \alpha_1^2\gamma_2\mu + \alpha_1\alpha_2\gamma_2\mu - \kappa\alpha_1\gamma_1\eta + \kappa\gamma_1\alpha_2\eta + \alpha_1\gamma_1\alpha_2\eta - \gamma_1\alpha_2^2\eta + \kappa\alpha_1\gamma_2\eta - \alpha_1^2\gamma_2\eta - \kappa\alpha_2\gamma_2\eta + \alpha_1\alpha_2\gamma_2\eta + \gamma_1^2\alpha_2\chi - \alpha_1\gamma_1\gamma_2\chi - \gamma_1\alpha_2\gamma_2\chi + \alpha_1\gamma_2^2\chi) / ((\gamma_1 - \gamma_2)(\gamma_1\alpha_2 - \alpha_1\gamma_2)\mu), (\kappa\alpha_1\gamma_1\eta - \kappa\gamma_1\alpha_2\eta - \alpha_1\gamma_1\alpha_2\eta + \gamma_1\alpha_2^2\eta - \kappa\alpha_1\gamma_2\eta + \alpha_1^2\gamma_2\eta + \kappa\alpha_2\gamma_2\eta - \alpha_1\alpha_2\gamma_2\eta - \gamma_1^2\alpha_2\chi + \alpha_1\gamma_1\gamma_2\chi + \gamma_1\alpha_2\gamma_2\chi - \alpha_1\gamma_2^2\chi) / ((\gamma_1 - \gamma_2)(\gamma_1\alpha_2 - \alpha_1\gamma_2)\mu), 0, (\kappa\gamma_1 - \gamma_1\alpha_2 - \kappa\gamma_2 + \alpha_1\gamma_2)/(\gamma_1\alpha_2 - \alpha_1\gamma_2), 0\right],$$

- **Equilibrium 10:**

$$\left[(-\kappa\eta + \alpha_1\eta - \gamma_1\chi - \sqrt{4\alpha_1\gamma_1\eta\chi + (-\kappa\eta + \alpha_1\eta - \gamma_1\chi)^2})/(2\gamma_1\eta), 0, 0, (\kappa\eta - \alpha_1\eta + \gamma_1\chi - \sqrt{4\alpha_1\gamma_1\eta\chi + (-\kappa\eta + \alpha_1\eta - \gamma_1\chi)^2})/(2\alpha_1\eta), 0\right],$$

- **Equilibrium 11:**

$$\left[(-\kappa\eta + \alpha_1\eta - \gamma_1\chi + \sqrt{4\alpha_1\gamma_1\eta\chi + (-\kappa\eta + \alpha_1\eta - \gamma_1\chi)^2})/(2\gamma_1\eta), 0, 0, (\kappa\eta - \alpha_1\eta + \gamma_1\chi + \sqrt{4\alpha_1\gamma_1\eta\chi + (-\kappa\eta + \alpha_1\eta - \gamma_1\chi)^2})/(2\alpha_1\eta), 0\right].$$

By adjusting the values of the parameters, we can also obtain an equilibrium where all the types are present. For this to be the case, the following must hold:

$$\begin{aligned} \bar{\rho}_N &= \frac{\alpha_3}{\gamma_3} \\ &= \frac{\alpha_1}{\gamma_1} - \frac{\kappa}{\gamma_1(1 + \bar{\rho}_4)} \\ &= \frac{\alpha_2}{\gamma_2} - \frac{\kappa}{\gamma_2(1 + \bar{\rho}_4)} \\ &= \frac{\alpha_5}{\gamma_5} - \frac{\kappa}{\gamma_5(1 + \bar{\rho}_4)} \end{aligned}$$

and

$$\bar{\rho}_4 = \frac{\mu \cdot \bar{\rho}_2 + \chi}{\eta(\bar{\rho}_1 + \bar{\rho}_5 + \bar{\rho}_2)}.$$

The equilibrium is then

$$\left(c_1, c_2, c_3, \frac{\mu \cdot c_2 + \chi}{\eta(c_1 + c_5 + c_2)}, c_5\right),$$

with constants  $c_i > 0$  and  $c_1 + c_2 + c_3 + c_5 = \bar{\rho}_N$ .

### 4.3. Simpler System

Since these equilibria are too hard to work with for a master thesis, we will make additional assumptions to obtain a simpler system. Assuming there is no difference in the movement dynamics of different types of cells, we let  $C : C_1 = C_2 = C_3 = C_5$ . This is reasonable because, while different cells may have biological differences, they might behave similarly in terms of movement when modeled mathematically, especially under certain environmental conditions. Let us further define  $\tilde{D} = DC$ . Furthermore we assume that the three different cancer cells are three different mutations which mutated from each other, such that  $\alpha_c := \alpha_1 = \alpha_2 = \alpha_3$  and  $\gamma_c := \gamma_1 = \gamma_2 = \gamma_3$ . For notation define  $\tilde{C} = DC_4$ .

The total simplified continuum system of prostate cancer is therefore:

$$\begin{cases} \frac{\delta \rho_1}{\delta t} = \frac{\tilde{D}}{4} \nabla \cdot [\nabla \rho_1 + 2\beta \rho_1 \nabla \rho_N] + \rho_1 \left( \alpha_c - \gamma_c \rho_N - \frac{\kappa}{1+\rho_4} \right), \\ \frac{\delta \rho_2}{\delta t} = \frac{\tilde{D}}{4} \nabla \cdot [\nabla \rho_2 + 2\beta \rho_2 \nabla \rho_N] + \rho_2 \left( \alpha_c - \gamma_c \rho_N - \frac{\kappa}{1+\rho_4} \right), \\ \frac{\delta \rho_3}{\delta t} = \frac{\tilde{D}}{4} \nabla \cdot [\nabla \rho_3 + 2\beta \rho_3 \nabla \rho_N] + \rho_3 (\alpha_c - \gamma_c \rho_N), \\ \frac{\delta \rho_4}{\delta t} = \frac{\tilde{C}}{4} \Delta \rho_4 + \mu \rho_2 - \eta (\rho_1 + \rho_2 + \rho_5) \rho_4 + \chi, \\ \frac{\delta \rho_5}{\delta t} = \frac{\tilde{D}}{4} \nabla \cdot [\nabla \rho_5 + 2\beta \rho_5 \nabla \rho_N] + \rho_5 \left( \alpha_5 - \gamma_5 \rho_N - \frac{\kappa}{1+\rho_4} \right), \end{cases}$$

reducing the number of parameters from 18 to 11.

To determine the steady-state solutions, assume each  $\rho_i$  is a constant, denoted  $\bar{\rho}_i$ . We assume all densities are non-negative and all parameters are greater than zero. To calculate the equilibrium solutions, we set  $\frac{\delta \bar{\rho}_i}{\delta t} = 0$  for all  $i$ , ensuring that the solution remains constant. For the  $T^-$  tumor density, this results in:

$$\bar{\rho}_3 = 0 \text{ or } \bar{\rho}_N = \frac{\alpha_c}{\gamma_c}.$$

For the  $T^+$  and  $T^P$  tumor cells the following must be true:

$$\bar{\rho}_i = 0 \text{ or } \bar{\rho}_N = \frac{\alpha_c}{\gamma_c} - \frac{\kappa}{\gamma_c(1 + \bar{\rho}_4)},$$

where  $i \in \{1, 2\}$ . For the healthy cells we obtain:

$$\bar{\rho}_5 = 0 \text{ or } \bar{\rho}_N = \frac{\alpha_5}{\gamma_5} - \frac{\kappa}{\gamma_5(1 + \bar{\rho}_4)},$$

Finally, for testosterone the equilibrium density must be:

$$\bar{\rho}_4 = \frac{\mu \bar{\rho}_2 + \chi}{\eta (\bar{\rho}_1 + \bar{\rho}_5 + \bar{\rho}_2)},$$

with  $\bar{\rho}_1 + \bar{\rho}_5 + \bar{\rho}_2 \neq 0$ .

By using Wolfram Mathematica, the 3 equilibria  $(\bar{\rho}_1, \bar{\rho}_2, \bar{\rho}_3, \bar{\rho}_4, \bar{\rho}_5)$  with  $\bar{\rho}_1 = 0$  are:

- Equilibrium 1:

$$\left[ 0, 0, - \left( (-\alpha_c \gamma_c \alpha_5 \eta + \alpha_c^2 \gamma_5 \eta - \gamma_c^2 \alpha_5 \chi + \alpha_c \gamma_c \gamma_5 \chi + \alpha_c \gamma_c \eta \kappa) / (\gamma_c \eta (\gamma_c \alpha_5 - \alpha_c \gamma_5 - \gamma_c \kappa)) \right), \right. \\ \left. (-\gamma_c \alpha_5 + \alpha_c \gamma_5 + \gamma_c \kappa) / (\gamma_c \alpha_5 - \alpha_c \gamma_5), (-\gamma_c \alpha_5 \chi + \alpha_c \gamma_5 \chi) / (\eta (\gamma_c \alpha_5 - \alpha_c \gamma_5 - \gamma_c \kappa)) \right],$$

- Equilibrium 2:

$$\left[ 0, 0, 0, \left( -\alpha_5 \eta + \gamma_5 \chi + \eta \kappa - \sqrt{4\alpha_5 \gamma_5 \eta \chi + (\alpha_5 \eta - \gamma_5 \chi - \eta \kappa)^2} \right) / (2\alpha_5 \eta), \right. \\ \left. \left( \alpha_5 \eta - \gamma_5 \chi - \eta \kappa - \sqrt{4\alpha_5 \gamma_5 \eta \chi + (\alpha_5 \eta - \gamma_5 \chi - \eta \kappa)^2} \right) / (2\gamma_5 \eta) \right],$$

- Equilibrium 3:

$$\left[0, 0, 0, \left(-\alpha_5\eta + \gamma_5\chi + \eta\kappa + \sqrt{4\alpha_5\gamma_5\eta\chi + (\alpha_5\eta - \gamma_5\chi - \eta\kappa)^2}\right) / (2\alpha_5\eta), \right. \\ \left. \left(\alpha_5\eta - \gamma_5\chi - \eta\kappa + \sqrt{4\alpha_5\gamma_5\eta\chi + (\alpha_5\eta - \gamma_5\chi - \eta\kappa)^2}\right) / (2\gamma_5\eta)\right].$$

The remaining 2 equilibria  $(\bar{\rho}_1, \bar{\rho}_2, \bar{\rho}_3, \bar{\rho}_4, \bar{\rho}_5)$  with  $\bar{\rho}_1 \neq 0$  are:

- Equilibrium 4:

$$\left[(\alpha_c\mu + \bar{\rho}_4\alpha_c\mu - \bar{\rho}_4\alpha_c\eta - \bar{\rho}_4^2\alpha_c\eta + \gamma_c\chi + \bar{\rho}_4\gamma_c\chi - \mu\kappa + \bar{\rho}_4\eta\kappa) / ((1 + \bar{\rho}_4)\gamma_c\mu), \right. \\ \left. (\bar{\rho}_4\alpha_c\eta + \bar{\rho}_4^2\alpha_c\eta - \gamma_c\chi - \bar{\rho}_4\gamma_c\chi - \bar{\rho}_4\eta\kappa) / ((1 + \bar{\rho}_4)\gamma_c\mu), 0, \bar{\rho}_4, 0\right],$$

- Equilibrium 5:

$$\left[\bar{\rho}_1, \left(-\alpha_c\gamma_c\alpha_5\eta + \gamma_c\alpha_5^2\eta + \alpha_c^2\gamma_5\eta - \alpha_c\alpha_5\gamma_5\eta - \gamma_c^2\alpha_5\chi + \alpha_c\gamma_c\gamma_5\chi + \gamma_c\alpha_5\gamma_5\chi - \alpha_c\gamma_5^2\chi + \alpha_c\gamma_c\eta\kappa \right. \right. \\ \left. \left. - \gamma_c\alpha_5\eta\kappa - \alpha_c\gamma_5\eta\kappa + \alpha_5\gamma_5\eta\kappa\right) / ((\gamma_c - \gamma_5)(\gamma_c\alpha_5 - \alpha_c\gamma_5)\mu), 0, (-\gamma_c\alpha_5 + \alpha_c\gamma_5 + \gamma_c\kappa - \gamma_5\kappa) / \right. \\ \left. (\gamma_c\alpha_5 - \alpha_c\gamma_5), (\alpha_c\gamma_c\alpha_5\mu - \bar{\rho}_1\gamma_c^2\alpha_5\mu - \gamma_c\alpha_5^2\mu - \alpha_c^2\gamma_5\mu + \bar{\rho}_1\alpha_c\gamma_c\gamma_5\mu + \alpha_c\alpha_5\gamma_5\mu + \bar{\rho}_1\gamma_c\alpha_5\gamma_5\mu \right. \\ \left. - \bar{\rho}_1\alpha_c\gamma_5^2\mu + \alpha_c\gamma_c\alpha_5\eta - \gamma_c\alpha_5^2\eta - \alpha_c^2\gamma_5\eta + \alpha_c\alpha_5\gamma_5\eta + \gamma_c^2\alpha_5\chi - \alpha_c\gamma_c\gamma_5\chi - \gamma_c\alpha_5\gamma_5\chi + \alpha_c\gamma_5^2\chi \right. \\ \left. - \alpha_c\gamma_c\eta\kappa + \gamma_c\alpha_5\eta\kappa + \alpha_c\gamma_5\eta\kappa - \alpha_5\gamma_5\eta\kappa) / ((\gamma_c - \gamma_5)(\gamma_c\alpha_5 - \alpha_c\gamma_5)\mu)\right].$$

With this simplified system, by adjusting the values of the parameters, we cannot obtain an equilibrium where all the types are present. For this to be the case, the following must hold:

$$\bar{\rho}_N = \frac{\alpha_c}{\gamma_c} \\ = \frac{\alpha_c}{\gamma_c} - \frac{\kappa}{\gamma_c(1 + \bar{\rho}_4)}.$$

However,  $\frac{\kappa}{\gamma_c(1 + \bar{\rho}_4)}$  is never equal to zero, since  $\kappa > 0$ . Since there is no coexisting equilibrium solution, we consider an alteration of our model in Chapter 5.1.

# 5

## An Alternative Continuum Spatial Model of Prostate Cancer

In the last chapter, we derived a system of partial differential equations from our discrete model. However, the equilibria we found were unsatisfactory, as none of them included all three cancer cell populations simultaneously. Moreover, the detailed analysis of these equilibria is beyond the scope of a master's thesis due to their complexity. To solve this, we propose an alternative continuum spatial model for prostate cancer, assuming that testosterone levels influence cell birth rather than cell death. This modification allows us to perform a linear stability analysis and gain deeper insights into the system's dynamics. In Section 5.1, the model is given with its equilibrium solutions. In Section 5.2, We will non-dimensionalize the system and the equilibrium solutions of this non-dimensional system are given. Finally, in Section 5.3 to analyze the system even further we will perform a linear stability analysis and check this using simulations.

### 5.1. The Model with Alternate Assumptions

If we instead assume that the birth of the  $T^+$ ,  $T^P$  and healthy cells is influenced by testosterone instead of the death of those cells, we obtain a different system. This time we split  $\alpha_c$  into  $\alpha_d$  for the tumor cells which depend on testosterone and  $\alpha_3$  for the  $T^-$  tumor cells which are independent of testosterone, to make the dimensions fit. The alternate system becomes:

$$\begin{cases} \frac{\delta \rho_1}{\delta t} = \frac{\tilde{D}}{4} \nabla \cdot [\nabla \rho_1 + 2\beta \rho_1 \nabla \rho_N] + \rho_1 (\alpha_d \rho_4 - \gamma_c \rho_N), \\ \frac{\delta \rho_2}{\delta t} = \frac{\tilde{D}}{4} \nabla \cdot [\nabla \rho_2 + 2\beta \rho_2 \nabla \rho_N] + \rho_2 (\alpha_d \rho_4 - \gamma_c \rho_N), \\ \frac{\delta \rho_3}{\delta t} = \frac{\tilde{D}}{4} \nabla \cdot [\nabla \rho_3 + 2\beta \rho_3 \nabla \rho_N] + \rho_3 (\alpha_3 - \gamma_c \rho_N), \\ \frac{\delta \rho_4}{\delta t} = \frac{\tilde{C}}{4} \Delta \rho_4 + \mu \rho_2 - \eta (\rho_1 + \rho_5 + \rho_2) \rho_4 + \chi, \\ \frac{\delta \rho_5}{\delta t} = \frac{\tilde{D}}{4} \nabla \cdot [\nabla \rho_5 + 2\beta \rho_5 \nabla \rho_N] + \rho_5 (\alpha_5 \rho_4 - \gamma_5 \rho_N). \end{cases} \quad (5.1)$$

The more testosterone there is in a cell, the more new tumor and healthy cells are born. This system has 11 parameters. The system can be derived from the following discrete system:

$$\left\{ \begin{array}{l} \rho_1(x, y, t + \delta t) = \rho_1(x, y, t) + \sum_{(\tilde{x}, \tilde{y}) \sim (x, y)} \rho_1(\tilde{x}, \tilde{y}, t) \mathbb{P}_1((\tilde{x}, \tilde{y}) \rightarrow (x, y), t) - C\rho_1(x, y, t) \\ \quad + \delta t \cdot \rho_1(x, y, t) (\alpha_d \rho_4(x, y, t) - \gamma_c \rho_N(x, y, t)), \\ \rho_2(x, y, t + \delta t) = \rho_2(x, y, t) + \sum_{(\tilde{x}, \tilde{y}) \sim (x, y)} \rho_2(\tilde{x}, \tilde{y}, t) \mathbb{P}_2((\tilde{x}, \tilde{y}) \rightarrow (x, y), t) - C\rho_2(x, y, t) \\ \quad + \delta t \cdot \rho_2(x, y, t) (\alpha_d \rho_4(x, y, t) - \gamma_c \rho_N(x, y, t)), \\ \rho_3(x, y, t + \delta t) = \rho_3(x, y, t) + \sum_{(\tilde{x}, \tilde{y}) \sim (x, y)} \rho_3(\tilde{x}, \tilde{y}, t) \mathbb{P}_3((\tilde{x}, \tilde{y}) \rightarrow (x, y), t) - C\rho_3(x, y, t) \\ \quad + \delta t \cdot \rho_3(x, y, t) (\alpha_3 - \gamma_c \rho_N(x, y, t)), \\ \rho_4(x, y, t + \delta t) = \rho_4(x, y, t) + \frac{C_4}{4} \sum_{(\tilde{x}, \tilde{y}) \sim (x, y)} \rho_4(\tilde{x}, \tilde{y}, t) - C_4 \rho_4(x, y, t) + \delta t \cdot \chi \\ \quad + \delta t \cdot \mu \rho_2(x, y, t) - \delta t \cdot \eta (\rho_1(x, y, t) + \rho_2(x, y, t) + \rho_5(x, y, t)) \cdot \rho_4(x, y, t). \\ \rho_5(x, y, t + \delta t) = \rho_5(x, y, t) + \sum_{(\tilde{x}, \tilde{y}) \sim (x, y)} \rho_5(\tilde{x}, \tilde{y}, t) \mathbb{P}_5((\tilde{x}, \tilde{y}) \rightarrow (x, y), t) - C\rho_5(x, y, t) \\ \quad + \delta t \cdot \rho_5(x, y, t) (\alpha_5 \rho_4(x, y, t) - \gamma_5 \rho_N(x, y, t)), \end{array} \right.$$

by the same derivation as in Chapter 4.

To determine the steady-state solutions, again assume each  $\rho_i$  is a constant, denoted  $\bar{\rho}_i$ . We assume all densities are non-negative and all parameters are greater than zero. To calculate the equilibrium solutions, we set  $\frac{\delta \bar{\rho}_i}{\delta t} = 0$  for all  $i$ , ensuring that the solution remains constant. For the  $T^-$  tumor density, this results in:

$$\bar{\rho}_3 = 0 \text{ or } \bar{\rho}_N = \frac{\alpha_3}{\gamma_c}.$$

For the  $T^+$  and  $T^P$  tumor cells the following must be true:

$$\bar{\rho}_i = 0 \text{ or } \bar{\rho}_N = \frac{\alpha_d \bar{\rho}_4}{\gamma_c},$$

where  $i \in \{1, 2\}$ . For the healthy cells we obtain:

$$\bar{\rho}_5 = 0 \text{ or } \bar{\rho}_N = \frac{\alpha_5 \bar{\rho}_4}{\gamma_5}.$$

Finally, for testosterone the equilibrium density must be:

$$\bar{\rho}_4 = \frac{\mu \bar{\rho}_2 + \chi}{\eta (\bar{\rho}_1 + \bar{\rho}_5 + \bar{\rho}_2)},$$

with  $\bar{\rho}_1 + \bar{\rho}_5 + \bar{\rho}_2 \neq 0$ . By using Wolfram Mathematica, the 6 equilibria  $(\bar{\rho}_1, \bar{\rho}_2, \bar{\rho}_3, \bar{\rho}_4, \bar{\rho}_5)$  are:

- Equilibrium 1:  $[(\bar{\rho}_4 \alpha_d \mu - \bar{\rho}_4^2 \alpha_d \eta + \gamma_c \chi) / (\gamma_c \mu), (\bar{\rho}_4^2 \alpha_d \eta - \gamma_c \chi) / (\gamma_c \mu), 0, \bar{\rho}_4, 0]$ ,
- Equilibrium 2:  $[\bar{\rho}_1, -\chi / \mu, 0, 0, (-\bar{\rho}_1 \mu + \chi) / \mu]$ ,
- Equilibrium 3:  $[(\bar{\rho}_2 \alpha_d \mu + \alpha_d \chi - \bar{\rho}_2 \eta \alpha_3) / (\eta \alpha_3), \bar{\rho}_2, (-\bar{\rho}_2 \alpha_d \gamma_c \mu - \alpha_d \gamma_c \chi + \eta \alpha_3^2) / (\gamma_c \eta \alpha_3), \alpha_3 / \alpha_d, 0]$ ,
- Equilibrium 4:  $[0, 0, 0, -\sqrt{\gamma_5 \chi} / \sqrt{\alpha_5 \eta}, -\sqrt{\alpha_5 \chi} / \sqrt{\gamma_5 \eta}]$ ,
- Equilibrium 5:  $[0, 0, 0, \sqrt{\gamma_5 \chi} / \sqrt{\alpha_5 \eta}, \sqrt{\alpha_5 \chi} / \sqrt{\gamma_5 \eta}]$ ,
- Equilibrium 6:  $[0, 0, (-\gamma_c^2 \alpha_5 \chi + \gamma_5 \eta \alpha_3^2) / (\gamma_c \gamma_5 \eta \alpha_3), (\gamma_5 \alpha_3) / (\gamma_c \alpha_5), (\gamma_c \alpha_5 \chi) / (\gamma_5 \eta \alpha_3)]$ .

By adjusting the values of the parameters, we can also obtain an equilibrium where all the types are present. For this to be the case, the following must hold:

$$\begin{aligned}\bar{\rho}_N &= \frac{\alpha_3}{\gamma_c} \\ &= \frac{\alpha_d \bar{\rho}_4}{\gamma_c} \\ &= \frac{\alpha_5 \bar{\rho}_4}{\gamma_5},\end{aligned}$$

and

$$\bar{\rho}_4 = \frac{\mu \bar{\rho}_2 + \chi}{\eta (\bar{\rho}_1 + \bar{\rho}_5 + \bar{\rho}_2)}.$$

The equilibrium is then

$$\left( c_1, c_2, c_3, \frac{\mu c_2 + \chi}{\eta (c_1 + c_5 + c_2)}, c_5 \right),$$

with constants  $c_i > 0$  and  $c_1 + c_2 + c_3 + c_5 = \bar{\rho}_N$ . We will now analyze our model more by non-dimensionalizing the system.

## 5.2. Non-dimensionalization

Parameter	Dimension
$\rho_1, \rho_2, \rho_3, \rho_5, \rho_4, \rho_N$	$cells/space^2$
$\tilde{D}, \tilde{C}$	$space^2/time$
$\beta$	$space^2/cells$
$\alpha_3, \mu$	$1/time$
$\alpha_d, \alpha_5, \gamma_c, \gamma_5, \eta$	$space^2/(time \cdot cells)$
$\chi$	$cells/(time \cdot space^2)$

**Table 5.1:** The dimensions of the parameters of the alternate system of prostate cancer.

In this section, we will non-dimensionalize the system using alternative assumptions to reduce the number of parameters, making the system easier to analyze. The dimensions/units for each variable are given in Table 5.1. Start by defining the non-dimensional time  $t^* = \alpha_3 \cdot t$ , so  $t = \frac{t^*}{\alpha_3}$ . Also, define the non-dimensional space  $X^* = \sqrt{\frac{\alpha_3}{\tilde{D}}} X$  with  $X = (x, y)$ , so  $X = \sqrt{\frac{\tilde{D}}{\alpha_3}} X^*$ . Lastly, we define the non-dimensional densities  $\rho_i^* = \frac{\gamma_c}{\alpha_3} \rho_i$  with  $i \in \{1, 2, 3, 4, 5\}$ , so  $\rho_i = \frac{\alpha_3}{\gamma_c} \rho_i^*$ .

### 5.2.1. Non-dimensionalization of the Equations for the Tumor Cells

Let us first focus on the  $T^+$  cells density partial differential equation:

$$\frac{\delta \rho_1}{\delta t} = \frac{\tilde{D}}{4} \nabla \cdot [\nabla \rho_1 + 2\beta \rho_1 \nabla \rho_N] + \rho_1 (\alpha_d \rho_4 - \gamma_c \rho_N).$$

Note that  $\frac{\delta}{\delta t} = \alpha_3 \frac{\delta}{\delta t^*}$  and  $\nabla_X = \sqrt{\frac{\alpha_3}{\tilde{D}}} \nabla_{X^*}$ , which gives us:

$$\alpha_3 \frac{\delta \rho_1}{\delta t^*} = \frac{\tilde{D}}{4} \sqrt{\frac{\alpha_3}{\tilde{D}}} \nabla_{X^*} \cdot \left[ \sqrt{\frac{\alpha_3}{\tilde{D}}} \nabla_{X^*} \rho_1 + 2\beta \rho_1 \sqrt{\frac{\alpha_3}{\tilde{D}}} \nabla_{X^*} \rho_N \right] + \rho_1 (\alpha_d \rho_4 - \gamma_c \rho_N).$$

By substituting  $\rho_i$  by  $\frac{\alpha_3}{\gamma_c} \rho_i^*$  and simplifying terms we obtain

$$\frac{\alpha_3^2}{\gamma_c} \frac{\delta \rho_1^*}{\delta t^*} = \frac{\tilde{D}}{4} \frac{\alpha_3}{\tilde{D}} \nabla_{X^*} \cdot \left[ \nabla_{X^*} \frac{\alpha_3}{\gamma_c} \rho_1^* + 2\beta \frac{\alpha_3}{\gamma_c} \rho_1^* \nabla_{X^*} \frac{\alpha_3}{\gamma_c} \rho_N^* \right] + \frac{\alpha_3^2}{\gamma_c} \rho_1^* (\alpha_d \rho_4^* - \gamma_c \rho_N^*).$$

Diving everything by  $\alpha_3^2$  and multiplying by  $\gamma_c$  results in:

$$\frac{\delta \rho_1^*}{\delta t^*} = \frac{1}{4} \nabla_{X^*} \cdot \left[ \nabla_{X^*} \rho_1^* + \frac{2\beta \alpha_3}{\gamma_c} \rho_1^* \nabla_{X^*} \rho_N^* \right] + \rho_1^* \left( \frac{\alpha_d}{\gamma_c} \rho_4^* - \rho_N^* \right).$$

Note that we can do exactly the same for the  $T^P$  cells, giving:

$$\frac{\delta \rho_2^*}{\delta t^*} = \frac{1}{4} \nabla_{X^*} \cdot \left[ \nabla_{X^*} \rho_2^* + \frac{2\beta\alpha_3}{\gamma_c} \rho_2^* \nabla_{X^*} \rho_N^* \right] + \rho_2^* \left( \frac{\alpha_d}{\gamma_c} \rho_4^* - \rho_N^* \right).$$

Since the  $T^-$  cells are independent of testosterone, we have to consider its density separately.

$$\frac{\delta \rho_3}{\delta t} = \frac{\tilde{D}}{4} \nabla \cdot [\nabla \rho_3 + 2\beta \rho_3 \nabla \rho_N] + \rho_3 (\alpha_3 - \gamma_c \rho_N).$$

Substitute the dimensional  $\rho_i$ ,  $t$  and  $X$  in the same way as we did before, giving:

$$\frac{\alpha_3^2}{\gamma_c} \frac{\delta \rho_3^*}{\delta t^*} = \frac{\tilde{D}}{4} \frac{\alpha_3}{\tilde{D}} \nabla_{X^*} \cdot \left[ \nabla_{X^*} \frac{\alpha_3}{\gamma_c} \rho_3^* + 2\beta \frac{\alpha_3}{\gamma_c} \rho_3^* \nabla_{X^*} \frac{\alpha_3}{\gamma_c} \rho_N^* \right] + \frac{\alpha_3}{\gamma_c} \rho_3^* \left( \alpha_3 - \gamma_c \frac{\alpha_3}{\gamma_c} \rho_N^* \right).$$

We find the final expression by diving everything by  $\alpha_3^2$  and multiplying by  $\gamma_c$ :

$$\frac{\delta \rho_3^*}{\delta t^*} = \frac{1}{4} \nabla_{X^*} \cdot \left[ \nabla_{X^*} \rho_3^* + \frac{2\beta\alpha_3}{\gamma_c} \rho_3^* \nabla_{X^*} \rho_N^* \right] + \rho_3^* (1 - \rho_N^*).$$

### 5.2.2. Non-dimensionalization of the Equations for the Healthy Cells

Secondly, we focus on the healthy cells density partial differential equation. The non-dimensionalization goes exactly the same as with the  $T^+$  tumor cells. However, note that various parameters are different.

$$\frac{\delta \rho_5}{\delta t} = \frac{\tilde{D}}{4} \nabla \cdot [\nabla \rho_5 + 2\beta \rho_5 \nabla \rho_N] + \rho_5 (\alpha_5 \rho_4 - \gamma_5 \rho_N).$$

Substitute the dimensional  $\rho_i$ ,  $t$  and  $X$  in the same way as we did before, giving:

$$\frac{\alpha_3^2}{\gamma_c} \frac{\delta \rho_5^*}{\delta t^*} = \frac{\tilde{D}}{4} \frac{\alpha_3}{\tilde{D}} \nabla_{X^*} \cdot \left[ \nabla_{X^*} \frac{\alpha_3}{\gamma_c} \rho_5^* + 2\beta \frac{\alpha_3}{\gamma_c} \rho_5^* \nabla_{X^*} \frac{\alpha_3}{\gamma_c} \rho_N^* \right] + \frac{\alpha_3^2}{\gamma_c^2} \rho_5^* (\alpha_5 \rho_4^* - \gamma_5 \rho_N^*).$$

Diving everything by  $\alpha_3^2$  and multiplying by  $\gamma_c$  results in:

$$\frac{\delta \rho_5^*}{\delta t^*} = \frac{1}{4} \nabla_{X^*} \cdot \left[ \nabla_{X^*} \rho_5^* + \frac{2\beta\alpha_3}{\gamma_c} \rho_5^* \nabla_{X^*} \rho_N^* \right] + \rho_5^* \left( \frac{\alpha_5}{\gamma_c} \rho_4^* - \frac{\gamma_5}{\gamma_c} \rho_N^* \right).$$

### 5.2.3. Non-dimensionalization of the Equation for Testosterone

Lastly, we non-dimensionalize the testosterone partial differential equation:

$$\frac{\delta \rho_4}{\delta t} = \frac{\tilde{C}}{4} \Delta \rho_4 + \mu \rho_2 - \eta (\rho_1 + \rho_5 + \rho_2) \rho_4 + \chi.$$

Note that  $\frac{\delta}{\delta t} = \alpha_3 \frac{\delta}{\delta t^*}$ , which gives us:

$$\alpha_3 \frac{\delta \rho_4}{\delta t^*} = \frac{\tilde{C}}{4} \Delta \rho_4 + \mu \rho_2 - \eta (\rho_1 + \rho_5 + \rho_2) \rho_4 + \chi.$$

Now substitute  $\rho_i = \frac{\alpha_3}{\gamma_c} \rho_i^*$  and divide everything by  $\alpha_3$ :

$$\frac{\alpha_3}{\gamma_c} \frac{\delta \rho_4^*}{\delta t^*} = \frac{\tilde{C}}{4\alpha_3} \Delta \left( \frac{\alpha_3}{\gamma_c} \rho_{\text{test}^*} \right) + \frac{\mu}{\gamma_c} \rho_2^* - \frac{\eta}{\gamma_c} (\rho_1^* + \rho_5^* + \rho_2^*) \left( \rho_4^* \frac{\alpha_3}{\gamma_c} \right) + \frac{\chi}{\alpha_3}.$$

Next write  $\nabla_X$  as  $\nabla_{X^*} = \sqrt{\frac{\alpha_3}{\tilde{D}}} \nabla_{X^*}$  and simplify terms,

$$\frac{\alpha_3}{\gamma_c} \frac{\delta \rho_4^*}{\delta t^*} = \frac{\tilde{C}}{4\alpha_3} \frac{\alpha_3}{\gamma_c} \frac{\alpha_3}{\tilde{D}} \Delta_{X^*} \rho_{\text{test}^*} + \frac{\mu}{\gamma_c} \rho_2^* - \frac{\eta \alpha_3}{\gamma_c^2} (\rho_1^* + \rho_5^* + \rho_2^*) \rho_4^* + \frac{\chi}{\alpha_3}.$$

Diving everything by  $\alpha_3$  and multiplying with  $\gamma_c$ , results in the final equation:

$$\frac{\delta \rho_4^*}{\delta t^*} = \frac{\tilde{C}}{4\tilde{D}} \Delta_{X^*} \rho_{\text{test}^*} + \frac{\mu}{\alpha_3} \rho_2^* - \frac{\eta}{\gamma_c} (\rho_1^* + \rho_5^* + \rho_2^*) \rho_4^* + \frac{\chi \gamma_c}{\alpha_3^2}.$$

### 5.2.4. Total Non-dimensionalized System

In conclusion, the total non-dimensionalized alternate system for prostate cancer is presented below. For readability, the asterisks are omitted.

$$\begin{cases} \frac{\delta \rho_1}{\delta t} = \frac{1}{4} \nabla \cdot \left[ \nabla \rho_1 + \frac{2\beta\alpha_3}{\gamma_c} \rho_1 \nabla \rho_N \right] + \rho_1 \left( \frac{\alpha_d}{\gamma_c} \rho_4 - \rho_N \right), \\ \frac{\delta \rho_2}{\delta t} = \frac{1}{4} \nabla \cdot \left[ \nabla \rho_2 + \frac{2\beta\alpha_3}{\gamma_c} \rho_2 \nabla \rho_N \right] + \rho_2 \left( \frac{\alpha_d}{\gamma_c} \rho_4 - \rho_N \right), \\ \frac{\delta \rho_3}{\delta t} = \frac{1}{4} \nabla \cdot \left[ \nabla \rho_3 + \frac{2\beta\alpha_3}{\gamma_c} \rho_3 \nabla \rho_N \right] + \rho_3 (1 - \rho_N), \\ \frac{\delta \rho_4}{\delta t} = \frac{\tilde{C}}{4D} \Delta \rho_4 + \frac{\mu}{\alpha_3} \rho_2 - \frac{\eta}{\gamma_c} (\rho_1 + \rho_2 + \rho_5) \rho_4 + \frac{\chi\gamma_c}{\alpha_3^2}, \\ \frac{\delta \rho_5}{\delta t} = \frac{1}{4} \nabla \cdot \left[ \nabla \rho_5 + \frac{2\beta\alpha_3}{\gamma_c} \rho_5 \nabla \rho_N \right] + \rho_5 \left( \frac{\alpha_5}{\gamma_c} \rho_4 - \frac{\gamma_5}{\gamma_c} \rho_N \right). \end{cases}$$

To reduce the number of parameters such that we can analyze the system, we will do two things. Firstly, we introduce new parameters:  $a = \frac{2\beta\alpha_3}{\gamma_c}$ ,  $b = \frac{\alpha_d}{\gamma_c}$ ,  $c = \frac{\alpha_5}{\gamma_c}$ ,  $d = \frac{\gamma_5}{\gamma_c}$ ,  $f = \frac{\tilde{C}}{4D}$ ,  $g = \frac{\mu}{\alpha_3}$ ,  $h = \frac{\eta}{\gamma_c}$  and  $l = \frac{\chi\gamma_c}{\alpha_3^2}$ . With these symbols the non-dimensionalized system can be written as

$$\begin{cases} \frac{\delta \rho_1}{\delta t} = \frac{1}{4} \nabla \cdot \left[ \nabla \rho_1 + a \rho_1 \nabla \rho_N \right] + \rho_1 (b \rho_4 - \rho_N), \\ \frac{\delta \rho_2}{\delta t} = \frac{1}{4} \nabla \cdot \left[ \nabla \rho_2 + a \rho_2 \nabla \rho_N \right] + \rho_2 (b \rho_4 - \rho_N), \\ \frac{\delta \rho_3}{\delta t} = \frac{1}{4} \nabla \cdot \left[ \nabla \rho_3 + a \rho_3 \nabla \rho_N \right] + \rho_3 (1 - \rho_N), \\ \frac{\delta \rho_4}{\delta t} = f \Delta \rho_4 + g \rho_2 - h (\rho_1 + \rho_2 + \rho_5) \rho_4 + l, \\ \frac{\delta \rho_5}{\delta t} = \frac{1}{4} \nabla \cdot \left[ \nabla \rho_5 + a \rho_5 \nabla \rho_N \right] + \rho_5 (c \rho_4 - d \rho_N). \end{cases}$$

Secondly, we assume that at this stage in the tumor progression there are no healthy cells left. So  $\rho_5 = 0$  at every lattice point and we can then omit the evolution equation of the density of the healthy cells. We end up with the system that we will analyze, which has only 6 parameters and 4 evolution equations left.

$$\begin{cases} \frac{\delta \rho_1}{\delta t} = \frac{1}{4} \nabla \cdot \left[ \nabla \rho_1 + a \rho_1 \nabla \rho_N \right] + \rho_1 (b \rho_4 - \rho_N), \\ \frac{\delta \rho_2}{\delta t} = \frac{1}{4} \nabla \cdot \left[ \nabla \rho_2 + a \rho_2 \nabla \rho_N \right] + \rho_2 (b \rho_4 - \rho_N), \\ \frac{\delta \rho_3}{\delta t} = \frac{1}{4} \nabla \cdot \left[ \nabla \rho_3 + a \rho_3 \nabla \rho_N \right] + \rho_3 (1 - \rho_N), \\ \frac{\delta \rho_4}{\delta t} = f \Delta \rho_4 + g \rho_2 - h (\rho_1 + \rho_2) \rho_4 + l, \end{cases} \quad (5.2)$$

with  $\rho_N = \rho_1 + \rho_2 + \rho_3$ . Furthermore, note that if we want to go back to the original dimensional system (5.1), we will have to, besides going back to the old parameters, transform the densities back by multiplying them  $\rho_i = \frac{\alpha_3}{\gamma_c} \rho_i^*$ .

### 5.2.5. Equilibrium Solutions

To determine the steady-state solutions, again assume each  $\rho_i$  is a constant, denoted  $\bar{\rho}_i$ . By using Maple, the four equilibria  $(\bar{\rho}_1, \bar{\rho}_2, \bar{\rho}_3, \bar{\rho}_4)$  are:

- Equilibrium 1:  $\left( \frac{-bh\bar{\rho}_4^2 + bg\bar{\rho}_4 + l}{g}, \frac{bh\bar{\rho}_4^2 - l}{g}, 0, \bar{\rho}_4 \right)$ ,
- Equilibrium 2:  $\left( -\frac{\bar{\rho}_3 bg - bg - lb - h\bar{\rho}_3 + h}{bg}, -\frac{lb + h\bar{\rho}_3 - h}{bg}, \bar{\rho}_3, \frac{1}{b} \right)$ ,
- Equilibrium 3:  $\left( b\sqrt{\frac{l}{hb}}, 0, 0, \sqrt{\frac{l}{hb}} \right)$ ,
- Equilibrium 4:  $\left( -b\sqrt{\frac{l}{hb}}, 0, 0, -\sqrt{\frac{l}{hb}} \right)$ .

We only have to consider the first three equilibria, since the last one is negative and therefore unphysical. Note that at the second equilibrium, all types can be present.

### 5.3. Linear Stability Analysis

In this section, we will perform a linear stability analysis of the non-dimensional system by adding a perturbation to an equilibrium solution  $\bar{\rho}_i$ , so that:

$$\rho_j = \bar{\rho}_j + \delta_j e^{\alpha t} e^{i\vec{k}\cdot\vec{v}},$$

with  $\delta_j \ll 0$  and  $\vec{k} \in \mathbb{R}_{\geq 0}^2$  called wave numbers. Furthermore, denote the following sum by  $\delta_N := \delta_1 + \delta_2 + \delta_3$ . Substituting all of this in the  $T^+$  cells equation of System 5.2, we find

$$\begin{aligned} \frac{\delta}{\delta t} (\bar{\rho}_1 + \delta_1 e^{\alpha t} e^{i\vec{k}\cdot\vec{v}}) &= \frac{1}{4} \nabla \cdot \left[ \nabla (\bar{\rho}_1 + \delta_1 e^{\alpha t} e^{i\vec{k}\cdot\vec{v}}) + a (\bar{\rho}_1 + \delta_1 e^{\alpha t} e^{i\vec{k}\cdot\vec{v}}) \nabla (\bar{\rho}_N + \delta_N e^{\alpha t} e^{i\vec{k}\cdot\vec{v}}) \right] \\ &\quad + (\bar{\rho}_1 + \delta_1 e^{\alpha t} e^{i\vec{k}\cdot\vec{v}}) \left( b (\bar{\rho}_4 + \delta_4 e^{\alpha t} e^{i\vec{k}\cdot\vec{v}}) - (\bar{\rho}_N + \delta_N e^{\alpha t} e^{i\vec{k}\cdot\vec{v}}) \right). \end{aligned}$$

Note that since  $\frac{\delta \bar{\rho}_1}{\delta t} = 0$ , we know that  $\frac{1}{4} \nabla \cdot [\nabla \bar{\rho}_1 + a \bar{\rho}_1 \nabla \bar{\rho}_N] + \bar{\rho}_1 (b \bar{\rho}_4 - \bar{\rho}_N) = 0$ . Using this and working out the derivations to time and space, we obtain

$$\begin{aligned} \alpha \delta_1 e^{\alpha t} e^{i\vec{k}\cdot\vec{v}} &= \frac{1}{4} \nabla \cdot \left[ i |\vec{k}| \delta_1 e^{\alpha t} e^{i\vec{k}\cdot\vec{v}} + a (\bar{\rho}_1 + \delta_1 e^{\alpha t} e^{i\vec{k}\cdot\vec{v}}) (i |\vec{k}| \delta_N e^{\alpha t} e^{i\vec{k}\cdot\vec{v}}) \right] + \delta_1 e^{\alpha t} e^{i\vec{k}\cdot\vec{v}} (b \bar{\rho}_4 \\ &\quad + \delta_4 e^{\alpha t} e^{i\vec{k}\cdot\vec{v}} - (\bar{\rho}_N + \delta_N e^{\alpha t} e^{i\vec{k}\cdot\vec{v}})) + \bar{\rho}_1 (b \delta_4 e^{\alpha t} e^{i\vec{k}\cdot\vec{v}} - \delta_N e^{\alpha t} e^{i\vec{k}\cdot\vec{v}}) \\ &= \frac{1}{4} \left( -|\vec{k}|^2 \delta_1 e^{\alpha t} e^{i\vec{k}\cdot\vec{v}} - a |\vec{k}|^2 \bar{\rho}_1 \delta_N e^{\alpha t} e^{i\vec{k}\cdot\vec{v}} \right) + \delta_1 e^{\alpha t} e^{i\vec{k}\cdot\vec{v}} (b \bar{\rho}_4 - \bar{\rho}_N) \\ &\quad + \bar{\rho}_1 (b \delta_4 e^{\alpha t} e^{i\vec{k}\cdot\vec{v}} - \delta_N e^{\alpha t} e^{i\vec{k}\cdot\vec{v}}) + O(\delta_j^2) \\ &= e^{\alpha t} e^{i\vec{k}\cdot\vec{v}} \left( \frac{-|\vec{k}|^2}{4} (\delta_1 + a \bar{\rho}_1 \delta_N) + \delta_1 (b \bar{\rho}_4 - \bar{\rho}_N) + \bar{\rho}_1 (b \delta_4 - \delta_N) \right) + O(\delta_j^2). \end{aligned}$$

This is possible because the  $\delta_j$  are very small. Dividing both sides by  $e^{\alpha t} e^{i\vec{k}\cdot\vec{v}}$ , we find

$$\alpha \delta_1 = \frac{-|\vec{k}|^2}{4} (\delta_1 + a \bar{\rho}_1 \delta_N) + \delta_1 (b \bar{\rho}_4 - \bar{\rho}_N) + \bar{\rho}_1 (b \delta_4 - \delta_N) + O(\delta_j^2).$$

So when  $\delta_j$  goes to zero,  $\alpha \delta_1$  goes to

$$\begin{aligned} \alpha \delta_1 &= \delta_1 \left( \frac{-|\vec{k}|^2}{4} (1 + a \bar{\rho}_1) - \bar{\rho}_1 + b \bar{\rho}_4 - \bar{\rho}_N \right) \\ &\quad + \delta_2 \left( -\bar{\rho}_1 \left( 1 + \frac{a |\vec{k}|^2}{4} \right) \right) \\ &\quad + \delta_3 \left( -\bar{\rho}_1 \left( 1 + \frac{a |\vec{k}|^2}{4} \right) \right) \\ &\quad + \delta_4 (b \bar{\rho}_1). \end{aligned} \tag{5.3}$$

Note that we can do exactly the same for the  $T^P$  cells, giving:

$$\begin{aligned}
\alpha\delta_2 &= \delta_1 \left( -\bar{\rho}_2 \left( 1 + \frac{a|\vec{k}^2|}{4} \right) \right) \\
&+ \delta_2 \left( \frac{-|\vec{k}|^2}{4} (1 + a\bar{\rho}_2) - \bar{\rho}_2 + b\bar{\rho}_4 - \bar{\rho}_N \right) \\
&+ \delta_3 \left( -\bar{\rho}_2 \left( 1 + \frac{a|\vec{k}^2|}{4} \right) \right) \\
&+ \delta_4 (b\bar{\rho}_2). \tag{5.4}
\end{aligned}$$

Since the  $T^-$  cells are independent of testosterone, we have to consider its density separately:

$$\begin{aligned}
\frac{\delta}{\delta t} (\bar{\rho}_3 + \delta_3 e^{\alpha t} e^{i\vec{k}\cdot\vec{v}}) &= \frac{1}{4} \nabla \cdot \left[ \nabla (\bar{\rho}_3 + \delta_3 e^{\alpha t} e^{i\vec{k}\cdot\vec{v}}) + a (\bar{\rho}_3 + \delta_3 e^{\alpha t} e^{i\vec{k}\cdot\vec{v}}) \nabla (\bar{\rho}_N + \delta_N e^{\alpha t} e^{i\vec{k}\cdot\vec{v}}) \right] \\
&+ (\bar{\rho}_3 + \delta_3 e^{\alpha t} e^{i\vec{k}\cdot\vec{v}}) \left( 1 - (\bar{\rho}_N + \delta_N e^{\alpha t} e^{i\vec{k}\cdot\vec{v}}) \right).
\end{aligned}$$

Note that since  $\frac{\delta \bar{\rho}_3}{\delta t} = 0$  we know that  $\frac{1}{4} \nabla \cdot [\nabla \bar{\rho}_3 + a\bar{\rho}_3 \nabla \bar{\rho}_N] + \bar{\rho}_3 (1 - \bar{\rho}_N) = 0$ . Using this and working out the derivations to time and space, we obtain

$$\begin{aligned}
\alpha\delta_3 e^{\alpha t} e^{i\vec{k}\cdot\vec{v}} &= \frac{1}{4} \nabla \cdot \left[ i|\vec{k}| \delta_3 e^{\alpha t} e^{i\vec{k}\cdot\vec{v}} + a (\bar{\rho}_3 + \delta_3 e^{\alpha t} e^{i\vec{k}\cdot\vec{v}}) (i|\vec{k}| \delta_N e^{\alpha t} e^{i\vec{k}\cdot\vec{v}}) \right] + \delta_3 e^{\alpha t} e^{i\vec{k}\cdot\vec{v}} (1 \\
&- (\bar{\rho}_N + \delta_N e^{\alpha t} e^{i\vec{k}\cdot\vec{v}})) + \bar{\rho}_3 (-\delta_N e^{\alpha t} e^{i\vec{k}\cdot\vec{v}}) \\
&= \frac{1}{4} \left( -|\vec{k}|^2 \delta_3 e^{\alpha t} e^{i\vec{k}\cdot\vec{v}} - a|\vec{k}|^2 \bar{\rho}_3 \delta_N e^{\alpha t} e^{i\vec{k}\cdot\vec{v}} \right) + \delta_3 e^{\alpha t} e^{i\vec{k}\cdot\vec{v}} (1 - \bar{\rho}_N) \\
&+ \bar{\rho}_3 (-\delta_N e^{\alpha t} e^{i\vec{k}\cdot\vec{v}}) + O(\delta_j^2).
\end{aligned}$$

This is possible because the  $\delta_j$  are very small. Dividing both sides by  $e^{\alpha t} e^{i\vec{k}\cdot\vec{v}}$ :

$$\alpha\delta_3 = \frac{1}{4} \left( -|\vec{k}|^2 \delta_3 - a|\vec{k}|^2 \bar{\rho}_3 \delta_N \right) + \delta_3 (1 - \bar{\rho}_N) + \bar{\rho}_3 (-\delta_N) + O(\delta_j^2).$$

So when  $\delta_j$  is very small,  $\alpha\delta_3$  goes to

$$\begin{aligned}
\alpha\delta_3 &= \delta_1 \left( -\bar{\rho}_3 \left( 1 + \frac{a|\vec{k}^2|}{4} \right) \right) \\
&+ \delta_2 \left( -\bar{\rho}_3 \left( 1 + \frac{a|\vec{k}^2|}{4} \right) \right) \\
&+ \delta_3 \left( \frac{-|\vec{k}|^2}{4} (1 + a\bar{\rho}_3) - \bar{\rho}_3 + 1 - \bar{\rho}_N \right) \\
&+ \delta_4 \cdot 0. \tag{5.5}
\end{aligned}$$

Lastly, we will analyze the testosterone derivative by adding the perturbation.

$$\begin{aligned} \frac{\delta}{\delta t} \left( \bar{\rho}_4 + \delta_4 e^{\alpha t} e^{i\vec{k}\cdot\vec{v}} \right) &= f \Delta \left( \bar{\rho}_4 + \delta_4 e^{\alpha t} e^{i\vec{k}\cdot\vec{v}} \right) + g \left( \bar{\rho}_2 + \delta_2 e^{\alpha t} e^{i\vec{k}\cdot\vec{v}} \right) - h(\bar{\rho}_1 + \bar{\rho}_2) \\ &\quad + (\delta_1 + \delta_2) e^{\alpha t} e^{i\vec{k}\cdot\vec{v}} \left( \bar{\rho}_4 + \delta_4 e^{\alpha t} e^{i\vec{k}\cdot\vec{v}} \right) + l. \end{aligned}$$

Note that since  $\frac{\delta \bar{\rho}_4}{\delta t} = 0$ , we know that  $f \Delta \bar{\rho}_4 + g \bar{\rho}_2 - h(\bar{\rho}_1 + \bar{\rho}_2) \bar{\rho}_4 + l = 0$ . Using this and working out the derivations to time and space, we obtain

$$\begin{aligned} \alpha \delta_4 e^{\alpha t} e^{i\vec{k}\cdot\vec{v}} &= -f \left| \vec{k}^2 \right| \delta_4 e^{\alpha t} e^{i\vec{k}\cdot\vec{v}} + g \delta_2 e^{\alpha t} e^{i\vec{k}\cdot\vec{v}} - h(\delta_1 + \delta_2) e^{\alpha t} e^{i\vec{k}\cdot\vec{v}} \bar{\rho}_4 \\ &\quad - h \delta_4 e^{\alpha t} e^{i\vec{k}\cdot\vec{v}} \left( \bar{\rho}_1 + \bar{\rho}_2 + (\delta_1 + \delta_2) e^{\alpha t} e^{i\vec{k}\cdot\vec{v}} \right) \\ &= -f \left| \vec{k}^2 \right| \delta_4 e^{\alpha t} e^{i\vec{k}\cdot\vec{v}} + g \delta_2 e^{\alpha t} e^{i\vec{k}\cdot\vec{v}} - h(\delta_1 + \delta_2) e^{\alpha t} e^{i\vec{k}\cdot\vec{v}} \bar{\rho}_4 \\ &\quad - h \delta_4 e^{\alpha t} e^{i\vec{k}\cdot\vec{v}} (\bar{\rho}_1 + \bar{\rho}_2) + O(\delta_j^2). \end{aligned}$$

This is possible because the  $\delta_j$  are very small. Dividing both sides by  $e^{\alpha t} e^{i\vec{k}\cdot\vec{v}}$ :

$$\alpha \delta_4 = -f \left| \vec{k}^2 \right| \delta_4 + g \delta_2 - h(\delta_1 + \delta_2) \bar{\rho}_4 - h \delta_4 (\bar{\rho}_1 + \bar{\rho}_2) + O(\delta_j^2).$$

So when  $\delta_j$  goes to zero,  $\alpha \delta_4$  goes to

$$\begin{aligned} \alpha \delta_4 &= \delta_1 (-h \bar{\rho}_4) \\ &\quad + \delta_2 (g - h \bar{\rho}_4) \\ &\quad + \delta_3 \cdot 0 \\ &\quad + \delta_4 \left( - \left| \vec{k}^2 \right| f - h(\bar{\rho}_1 + \bar{\rho}_2) \right). \end{aligned} \tag{5.6}$$

Combining Equations (5.3), (5.4), (5.5) and (5.6), gives us an equation with a 4 by 4 matrix, which we will denote by  $A$ :

$$\alpha \cdot \begin{pmatrix} \delta_1 \\ \delta_2 \\ \delta_3 \\ \delta_4 \end{pmatrix} = A \cdot \begin{pmatrix} \delta_1 \\ \delta_2 \\ \delta_3 \\ \delta_4 \end{pmatrix}, \tag{5.7}$$

with the matrix  $A$  being equal to:

$$\begin{pmatrix} \frac{-|\vec{k}|^2}{4} (1 + a\bar{\rho}_1) - \bar{\rho}_1 + b\bar{\rho}_4 - \bar{\rho}_N & -\bar{\rho}_1 \left( 1 + \frac{a|\vec{k}|^2}{4} \right) & -\bar{\rho}_1 \left( 1 + \frac{a|\vec{k}|^2}{4} \right) & b\bar{\rho}_1 \\ -\bar{\rho}_2 \left( 1 + \frac{a|\vec{k}|^2}{4} \right) & \frac{-|\vec{k}|^2}{4} (1 + a\bar{\rho}_2) - \bar{\rho}_2 + b\bar{\rho}_4 - \bar{\rho}_N & -\bar{\rho}_2 \left( 1 + \frac{a|\vec{k}|^2}{4} \right) & b\bar{\rho}_2 \\ -\bar{\rho}_3 \left( 1 + \frac{a|\vec{k}|^2}{4} \right) & -\bar{\rho}_3 \left( 1 + \frac{a|\vec{k}|^2}{4} \right) & \frac{-|\vec{k}|^2}{4} (1 + a\bar{\rho}_3) - \bar{\rho}_3 + 1 - \bar{\rho}_N & 0 \\ -h\bar{\rho}_4 & g - h\bar{\rho}_4 & 0 & -|\vec{k}|^2 f - h(\bar{\rho}_1 + \bar{\rho}_2) \end{pmatrix}. \tag{5.7 \frac{1}{2}}$$

Equation (5.7) is an eigenvalue equation with eigenvalue  $\alpha$ , and can be rewritten as:

$$(A - \alpha I_4) \begin{pmatrix} \delta_1 \\ \delta_2 \\ \delta_3 \\ \delta_4 \end{pmatrix} = 0.$$

First, we substitute an equilibrium solution from Section 5.2.5, and then use Maple to calculate the corresponding eigenvalues. These eigenvalues indicate whether and when the equilibrium is stable. We will consider equilibrium solutions 1 and 2. At equilibrium 3, the only non-zero populations are the testosterone dependent  $T^+$  tumor cells and the testosterone densities. This equilibrium state is less relevant for further analysis because  $T^+$  cells can be effectively eliminated by treatment, as explained in Chapter 6.

### 5.3.1. Equilibrium 1

The first equilibrium point is given by  $\left(\frac{-bh\bar{\rho}_4^2 + bg\bar{\rho}_4 + l}{g}, \frac{bh\bar{\rho}_4^2 - l}{g}, 0, \bar{\rho}_4\right)$ , which corresponds to a state with no  $T^-$  tumor cells and where the testosterone density remains a free variable. The matrix  $A$ , evaluated at this equilibrium, has four distinct eigenvalues. If we can identify parameter values such that all four eigenvalues have negative real parts for all  $\vec{k} \in \mathbb{R}_{\geq 0}^2$ , then equilibrium 1 will be stable for those parameter values. Additionally, note that there are extra constraints on the parameter values due to the requirement that densities are non-negative. In this case, this gives the conditions  $-bh\bar{\rho}_4^2 + bg\bar{\rho}_4 + l \geq 0$ ,  $bh\bar{\rho}_4^2 \geq l$  and  $\bar{\rho}_4 \geq 0$ .

The first eigenvalue, of the matrix given in (5.7  $\frac{1}{2}$ ), is  $-\frac{|\vec{k}|^2}{4}$ , which is real and negative for all  $|\vec{k}| \neq 0$ . However, for  $|\vec{k}| = 0$  it is equal to zero, which makes the stability of the equilibrium point uncertain.

The second eigenvalue is  $-\frac{|\vec{k}|^2}{4} + 1 - b\bar{\rho}_4$ , which is negative for all  $\vec{k}$  when  $b\bar{\rho}_4 > 1$ . The last two eigenvalues are of the form  $-P + \frac{\sqrt{Q}}{8}$  and  $-P - \frac{\sqrt{Q}}{8}$ , with  $P = \frac{ab|\vec{k}|^2\bar{\rho}_4}{8} + \frac{b\bar{\rho}_4h}{2} + \frac{|\vec{k}|^2f}{2} + \frac{b\bar{\rho}_4}{2} + \frac{|\vec{k}|^2}{8}$  and  $Q = a^2b^2|\vec{k}|^4\bar{\rho}_4^2 - 8ab^2h|\vec{k}|^2\bar{\rho}_4^2 - 8abf|\vec{k}|^4\bar{\rho}_4 + 8b^2\bar{\rho}_4^2a|\vec{k}|^2 + 2|\vec{k}|^4ab\bar{\rho}_4 + 16b^2h^2\bar{\rho}_4^2 + 32b\bar{\rho}_4h|\vec{k}|^2f + 16|\vec{k}|^4f^2 - 32b^2h\bar{\rho}_4^2 - 32bf|\vec{k}|^2\bar{\rho}_4 - 8bh|\vec{k}|^2\bar{\rho}_4 - 8f|\vec{k}|^4 + 16b^2\bar{\rho}_4^2 + 8b|\vec{k}|^2\bar{\rho}_4 + |\vec{k}|^4 - 64bl$ .

We want to see if there exist parameter values for which  $P > \text{Re}\left(\frac{\sqrt{Q}}{8}\right)$  for all  $\vec{k}$ . Assume the following:

$$ab\bar{\rho}_4(1 - 4f) \leq 4f, \quad (5.8)$$

and

$$ab\bar{\rho}_4(1 - h) \leq (1 - h)(4f - 1). \quad (5.9)$$

Note that if  $f = \frac{1}{4}$  and  $h = 1$ , these assumptions give no restrictions on the testosterone density. In the dimensional system this means that  $f = \frac{C}{4D} = \frac{1}{4}$ , which is equivalent to  $C_4 = C$ , and  $h = \frac{\eta}{\gamma_c} = 1$ .

Now, rearrange  $Q$  by grouping terms with the same power of  $|\vec{k}|$  together:

$$\begin{aligned} Q &= |\vec{k}|^4 (a^2b^2\bar{\rho}_4^2 - 8abf\bar{\rho}_4 + 2ab\bar{\rho}_4 + 16f^2 - 8f + 1) \\ &\quad + |\vec{k}|^2 (-8ab^2h\bar{\rho}_4^2 + 8b^2\bar{\rho}_4^2a + 32b\bar{\rho}_4hf - 32bf\bar{\rho}_4 - 8bh\bar{\rho}_4 + 8b\bar{\rho}_4) \\ &\quad + 16b^2h^2\bar{\rho}_4^2 + 16b^2\bar{\rho}_4^2 - 32b^2h\bar{\rho}_4^2 - 64bl. \end{aligned}$$

By letting go of the last two negative terms (since  $h, b, l > 0$ ), we know  $Q$  is strictly smaller than

$$\begin{aligned} Q &< |\vec{k}|^4 (a^2b^2\bar{\rho}_4^2 + 2ab\bar{\rho}_4(-4f + 1) + 16f^2 - 8f + 1) \\ &\quad + |\vec{k}|^2 (-8ab^2h\bar{\rho}_4^2 + 8ab^2\bar{\rho}_4^2 + 32b\bar{\rho}_4hf - 32bf\bar{\rho}_4 - 8bh\bar{\rho}_4 + 8b\bar{\rho}_4) \\ &\quad + 16b^2h^2\bar{\rho}_4^2 + 16b^2\bar{\rho}_4^2 \\ &\leq |\vec{k}|^4 (a^2b^2\bar{\rho}_4^2 + 2 \cdot 4f + 16f^2 - 8f + 1) \\ &\quad + |\vec{k}|^2 \cdot 8b\bar{\rho}_4 (ab\bar{\rho}_4(1 - h) - 4f(1 - h) + (1 - h)) \\ &\quad + 16b^2h^2\bar{\rho}_4^2 + 16b^2\bar{\rho}_4^2. \end{aligned} \quad (5.10)$$

In the last inequality we used the first assumption (5.8) in the  $|\vec{k}|^4$  terms.

Next, use the second assumption (5.9) in the  $|\vec{k}|^2$  terms, which makes the last equation (5.10) smaller or equal then

$$\begin{aligned} &\leq |\vec{k}|^4 (a^2 b^2 \bar{\rho}_4^2 + 16f^2 + 1) \\ &+ |\vec{k}|^2 \cdot 8b(1-h)\bar{\rho}_4(4f-1-4f+1) \\ &+ 16b^2 h^2 \bar{\rho}_4^2 + 16b^2 \bar{\rho}_4^2 \\ &= |\vec{k}|^4 (a^2 b^2 \bar{\rho}_4^2 + 16f^2 + 1) + 16b^2 h^2 \bar{\rho}_4^2 + 16b^2 \bar{\rho}_4^2. \end{aligned}$$

So the third eigenvalue is smaller than

$$\begin{aligned} &-P + \frac{1}{8}\sqrt{Q} < \\ &-P + \frac{1}{8}\sqrt{|\vec{k}|^4 (a^2 b^2 \bar{\rho}_4^2 + 16f^2 + 1) + 16b^2 h^2 \bar{\rho}_4^2 + 16b^2 \bar{\rho}_4^2} \leq \\ &-P + \frac{1}{8}\left(\sqrt{|\vec{k}|^4} \left(\sqrt{a^2 b^2 \bar{\rho}_4^2} + \sqrt{16f^2} + \sqrt{1}\right) + \sqrt{16b^2 h^2 \bar{\rho}_4^2} + \sqrt{16b^2 \bar{\rho}_4^2}\right), \end{aligned}$$

by the triangle inequality  $\sqrt{x+y} \leq \sqrt{x} + \sqrt{y}$ . We can use this since all terms are non-negative. Filling in  $P$  gives us for eigenvalue 3:

$$\begin{aligned} \lambda_3 &< -\frac{ab|\vec{k}|^2 \bar{\rho}_4}{8} - \frac{b\bar{\rho}_4 h}{2} - \frac{|\vec{k}|^2 f}{2} - \frac{b\bar{\rho}_4}{2} - \frac{|\vec{k}|^2}{8} + \frac{1}{8}\left(|\vec{k}|^2 (ab\bar{\rho}_4 + 4f + 1) + 4bh\bar{\rho}_4 + 4b\bar{\rho}_4\right) \\ &= 0. \end{aligned}$$

The square  $\sqrt{Q}$  can be negative though, which would make the eigenvalues imaginary. However, this proves that the real parts of eigenvalues 3 and 4 are negative for all  $\vec{k}$  if (but not only if) the parameters satisfy the assumptions given by Equations (5.8) and (5.9).

To check these conclusions, we run simulations starting from this first equilibrium point. For the simulations, we use the parameter values provided in Table 5.2 with  $\chi = 0.3$  and the following initial values for the non-boundary lattice points of the non-dimensional system:

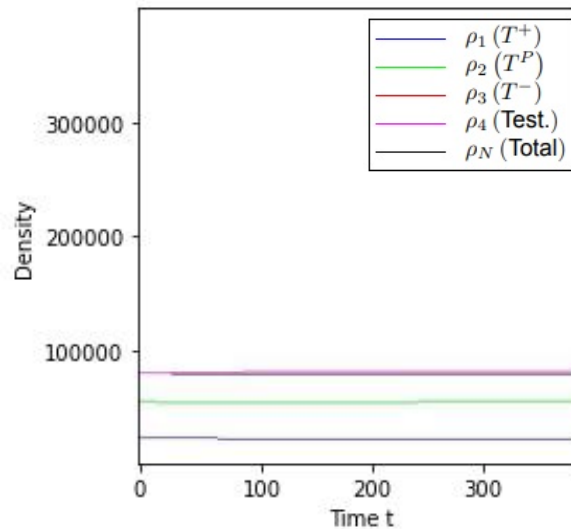
$$\begin{cases} \bar{\rho}_1 = 11.1, \\ \bar{\rho}_2 = 24.9, \\ \bar{\rho}_3 = 0, \\ \bar{\rho}_4 = 36. \end{cases} \quad (5.11)$$

Parameter	Description	Value
$L$	$L \times L$ is the lattice size	50
$l$	Spatial-step	0.02
$\delta t$	Time-step	1
$C_i$	Movement probability	0.1 for all $i$
$\beta$	The rate at which the cells are pushed	$1.0 \cdot 10^{-5}$
$\alpha_i$	Birth-rates	$\alpha_1 = \alpha_2 = 0.001, \alpha_3 = 0.2$
$\gamma_i$	Death-rates	$\gamma_1 = \gamma_2 = \gamma_3 = 0.001$
$\mu$	Production-rate testosterone	0.04
$\eta$	Consumption-rate testosterone	0.001

**Table 5.2:** The parameter values which are used in the simulations of the equilibrium solutions.

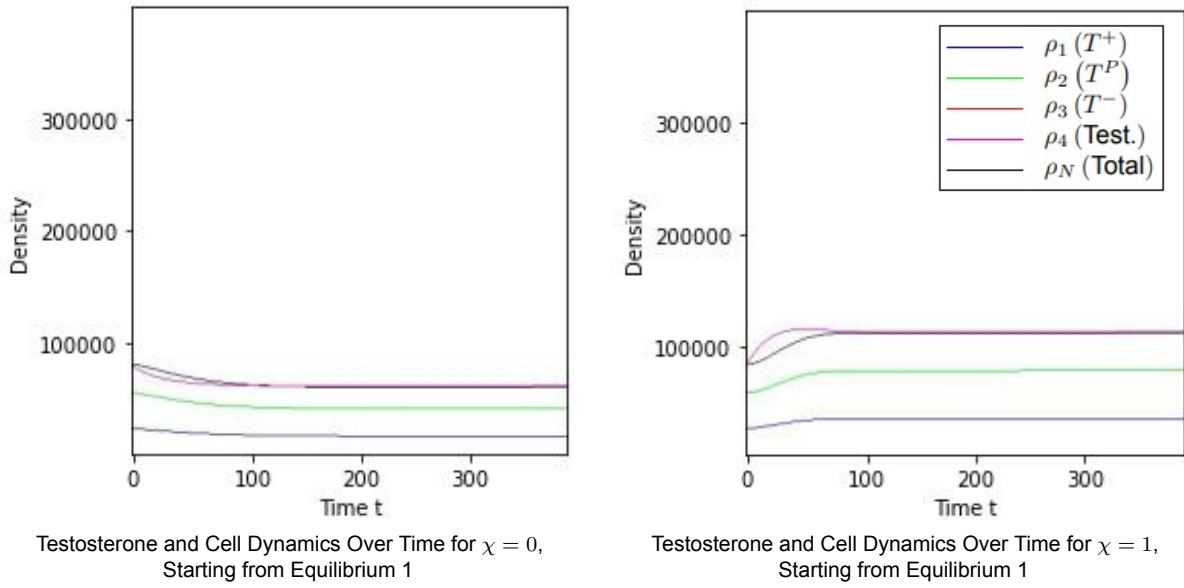
When running the simulation implemented in C++ with the SFML library, Figure 5.1 shows that the total cell densities remain constant over time. This indicates that, for the given parameter values and initial conditions, the system has reached a stable equilibrium, since it is resilient to small perturbations. At each lattice point, a small perturbation introduced by the movement terms is quickly counteracted, letting the system to return to its equilibrium state.

**Testosterone and Cell Dynamics Over Time for  $\chi = 0.3$ , Starting from Equilibrium 1**



**Figure 5.1:** The total number of cells (black),  $T^P$  cells (green),  $T^+$  cells (blue) and the testosterone levels (purple) are plotted against time from  $t = 0$  to  $t = 390$ . With these parameter values the first equilibrium is stable.

Following this equilibrium state, we explored the effects of testosterone manipulation on the tumor cell populations in Figure 5.2. In the first scenario, testosterone is removed from the system ( $\chi = 0$ ), causing a reduction in cell densities as the system adapts to the absence of testosterone, eventually reaching a new, lower equilibrium. This is possible since the  $T^-$  population is absent in equilibrium 1. In contrast, when testosterone is added to the system in equilibrium 1 ( $\chi = 1$ ), the cell populations respond by increasing in density. The system stabilizes at a new equilibrium with higher overall densities, demonstrating the direct influence of testosterone on tumor cell dynamics. This highlights how varying testosterone levels can drive changes in tumor behavior.

The Impact of the Testosterone Level in the Blood  $\chi$  on Equilibrium 1

**Figure 5.2:** Two scenarios showing the impact of testosterone levels on tumor cell populations starting from an initial equilibrium. In the first case (left), testosterone is removed from the system ( $\chi = 0$ ), leading to a decrease in the total cell densities as the populations settle into a new equilibrium. In the second case (right), testosterone is added to the blood ( $\chi = 1$ ), resulting in an increase in cell densities until they stabilize at a new equilibrium. The total number of cells (black),  $T^P$  cells (green),  $T^+$  cells (blue) and the testosterone levels (purple) are plotted against time from  $t = 0$  to  $t = 390$ . There is no  $T^-$  population.

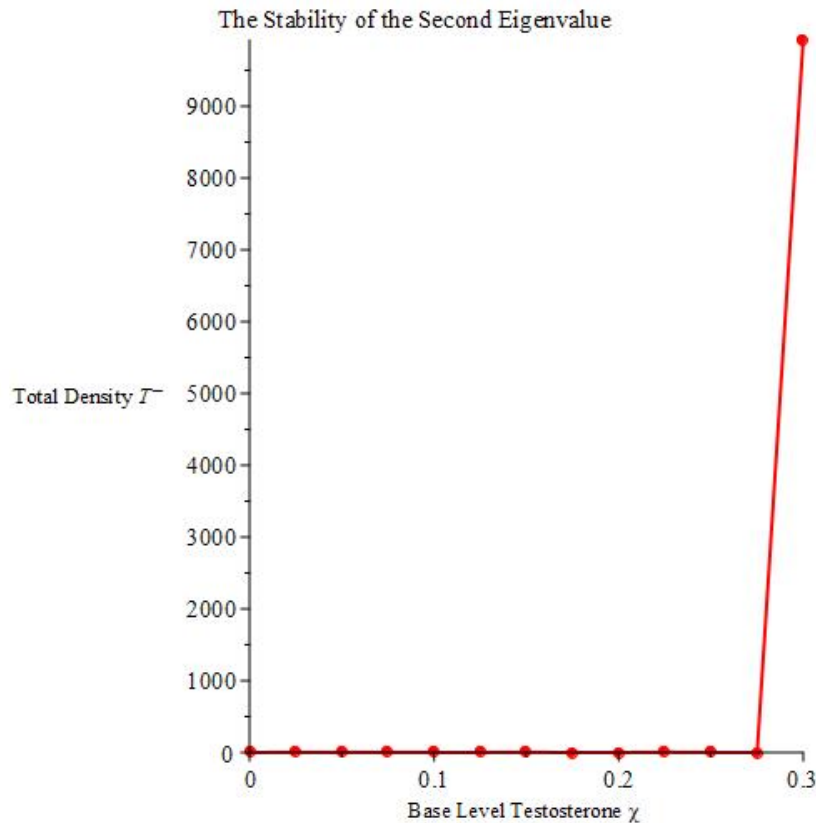
### 5.3.2. Equilibrium 2

The second equilibrium point is given by  $\left( -\frac{\bar{\rho}_3 bg - bg - lb - h\bar{\rho}_3 + h}{bg}, -\frac{lb + h\bar{\rho}_3 - h}{bg}, \bar{\rho}_3, \frac{1}{b} \right)$ , which corresponds to a state where all three tumor cell types are present, and the  $T^-$  cell density is a free variable. The matrix  $A$  given in (5.7  $\frac{1}{2}$ ), evaluated at this equilibrium, has very large eigenvalues, making their analysis beyond the scope of this thesis. Therefore, we perform a numerical exploration of stability and rely on simulations to identify parameter values that are likely to lead to instability in this equilibrium. It is important to note that the parameter values are constrained by the requirement of non-negative densities. This leads to the conditions  $-\bar{\rho}_3 bg + bg + lb + h\bar{\rho}_3 - h \geq 0$ ,  $-lb - h\bar{\rho}_3 + h \geq 0$  and  $\bar{\rho}_3 \geq 0$ .

For the simulations, we use the parameter values provided in Table 5.2 and the following initial values for the non-boundary lattice points of the non-dimensional system:

$$\begin{cases} \bar{\rho}_1 = 7.5 + 25\chi, \\ \bar{\rho}_2 = -25\chi + 7.5, \\ \bar{\rho}_3 = 5, \\ \bar{\rho}_4 = 20. \end{cases} \quad (5.12)$$

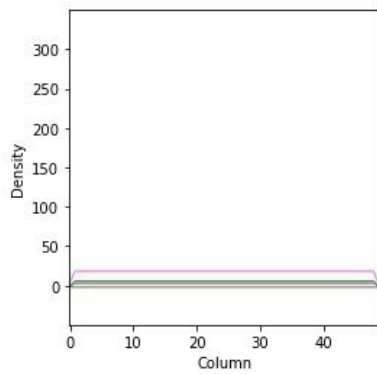
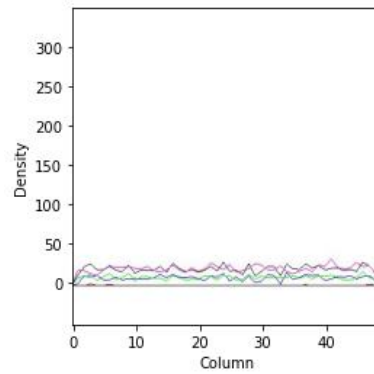
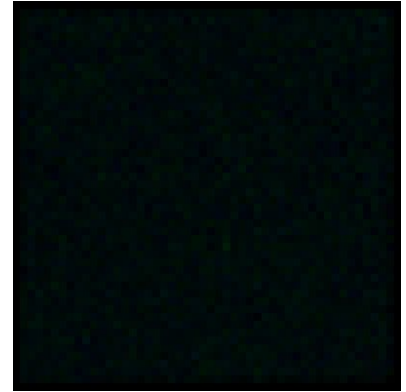
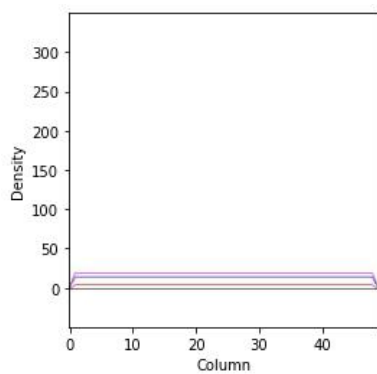
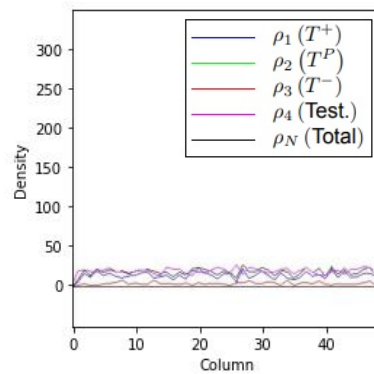
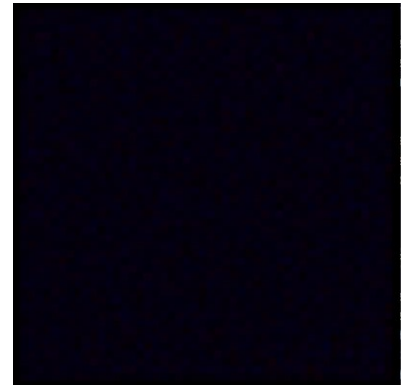
We vary the base level testosterone  $\chi$  between 0 and 0.3, as the initial density of  $T^P$ ,  $\rho_2$ , becomes negative for  $\chi > 0.3$ . The simulations start from the second equilibrium and run until the total density  $T^-$  reaches an equilibrium. This is determined by stopping the calculations when the absolute difference in total density over the past 100 time steps is less than 0.01. The resulting equilibrium value of  $T^-$  for each  $\chi$  is shown in Figure 5.3, made with Maple.



**Figure 5.3:** Plot of the total density  $T^-$  after each simulation has run until  $T^-$  reached a new equilibrium, starting from the second equilibrium for different values of the base level testosterone  $\chi$ , the testosterone coming from the blood. The results show that for  $0 \leq \chi < 0.3$ , the total density declines to zero, indicating instability. At  $\chi = 0.3$ ,  $T^-$  decreases initially but stabilizes just above 9000, suggesting that the equilibrium is unstable under the given conditions.

In Figure 5.3, we observe that the total density of the  $T^-$  cells decreases to 0 for every  $0 \leq \chi < 0.3$ . For  $\chi = 0.3$ , the density initially decreases from the initial value of 11520 but then stabilizes above 9000. This suggests that, for the given parameter values and initial conditions, the equilibrium is unstable for all  $0 \leq \chi < 0.3$ , and in most cases, the  $T^-$  cells eventually die out.

We see this further portrayed in Figure 5.4, where we observe two distinct cases based on different values of the base level testosterone  $\chi$ , and their impact on equilibrium 2. Note that the initial values change when  $\chi$  is adjusted. The upper part of Figure 5.4 shows the results for  $\chi = 0.04$ , presenting a cross-section at  $t = 0$ , at  $t = 2000$ , and the tumor lattice at  $t = 2000$ . For this value of  $\chi$ , the  $T^-$  cells die out over time, leaving the  $T^+$  and  $T^P$  populations. When we look closely at the picture of the lattice of Figure 5.4, we can see  $T^P$  and  $T^+$  populations. By contrast, the bottom row of the figure shows the results for  $\chi = 0.3$ . Here, while the  $T^-$  density remains, the  $T^P$  population vanishes, and both the  $T^+$  and the  $T^-$  populations persist. When we look closely at the picture of the lattice, we can mostly see small  $T^+$  populations. For this Figure we again used the parameter values from Table 5.2.

Comparison of the Behavior of Equilibrium 2 for Different Values of  $\chi$ .Cross-Section at  $t = 0$ ,  $\chi = 0.04$ Cross-Section at  $t = 2000$ ,  $\chi = 0.04$ The tumor lattice at  $t = 2000$ ,  $\chi = 0.04$ Cross-Section at  $t = 0$ ,  $\chi = 0.3$ Cross-Section at  $t = 2000$ ,  $\chi = 0.3$ The tumor lattice at  $t = 2000$ ,  $\chi = 0.3$ 

**Figure 5.4:** At the top, for  $\chi = 0.04$ , the cross-sections at  $t = 0$ ,  $t = 2000$ , and the tumor lattice at  $t = 2000$  show that the  $T^-$  population (in red) dies out, leaving only the  $T^+$  (in blue) and  $T^P$  (in green) populations. At the bottom, for  $\chi = 0.3$ , the same time points and lattice reveal the absence of the  $T^P$  population, while the  $T^+$  and  $T^-$  populations persist. The colors represent: total number of cells (black),  $T^-$  cells (red),  $T^P$  cells (green),  $T^+$  cells (blue), and testosterone levels (purple).

At equilibrium 3, the only non-zero populations are the testosterone dependent  $T^+$  tumor cells and the testosterone densities. This equilibrium state is less relevant for further analysis because  $T^+$  cells can be effectively eliminated by treatment, as explained in Chapter 6.

Having analyzed the dynamics of our prostate cancer model, we can now explore the effects of different treatment strategies on a prostate tumor in the following chapter.

# 6

## Treatment Strategies for Prostate Cancer

This chapter explores three different treatment strategies for prostate cancer, each designed at manipulating testosterone levels, which play a crucial role in prostate tumor growth. This is done for our model given in Section 5.1. In Section 6.1, we outline the parameters and initial values we used in this chapter and examine its progression in the absence of treatment. Section 6.2 discusses a standard first line-treatment, the so-called androgen deprivation, which removes all testosterone from the bloodstream. The second strategy, presented in Section 6.3, uses Lupron with Abiraterone, a medication targeting testosterone-producing cancer cells. Finally, in Section 6.4, we introduce an approach that integrates the use of Lupron and Abiraterone with high-dose testosterone injections, testing whether we can model extinction therapy. We simulate each treatment in the model outlined in Section 5.1.

### 6.1. Parameter Values and Initial Conditions

In this section, we outline the parameters used to model the initial tumor and examine its progression without treatment. We begin with the following initial conditions: each non-boundary cell is assigned a baseline testosterone level,  $\rho_4 = \chi$ . Additionally, 100  $T^-$  cells, 100  $T^+$  cells, and 100  $T^P$  cells ( $\rho_i = 1$ ) are uniformly distributed within a  $10 \times 10$  square in the center of the lattice. The parameter values are provided in Table 6.1.

Parameter	Description	Value
$L$	$L \times L$ is the lattice size	50
$l$	Spatial-step	0.02
$\delta t$	Time-step	1
$C_i$	Movement probability	0.1 for all $i$
$\beta$	The rate at which the cells are pushed	$1.0 \cdot 10^{-5}$
$\alpha_i$	Birth-rates	$\alpha_1 = \alpha_2 = 0.007, \alpha_3 = 0.08$
$\gamma_i$	Death-rates	$\gamma_1 = \gamma_2 = \gamma_3 = 0.001$
$\mu$	Production-rate testosterone	0.03
$\eta$	Consumption-rate testosterone	0.0015
$\chi$	Base-level testosterone	0.15

**Table 6.1:** The parameter values which are used in the simulations showing the model behavior in response to treatment strategies.

Using the model described in System (5.1), we ran the simulations, which were implemented in C++ with the SFML library. Figure 6.1 presents the dynamics of testosterone and tumor cells over time. Initially, we observe a sharp increase in  $T^P$  cells. However, because of the limited space, the  $\rho_N$  in the death-terms of Equation (5.1), the growth rate of all tumor cells slows down, stabilizing the tumor burden.

**Testosterone and Cell Dynamics Over Time, with no treatment**

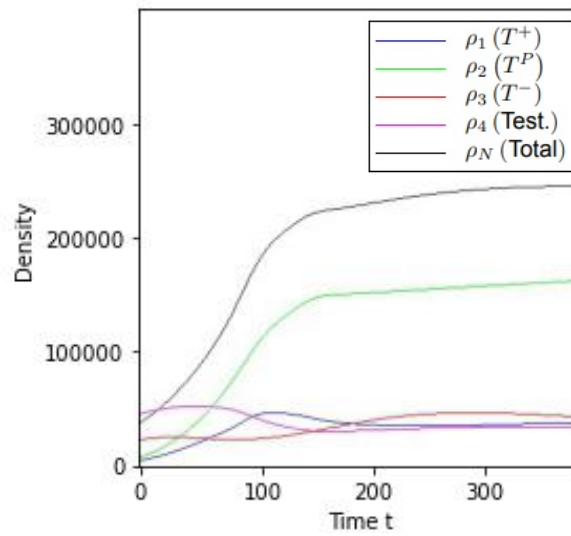


**Figure 6.1:** The total number of cells (black),  $T^-$  cells (red),  $T^P$  cells (green),  $T^+$  cells (blue), and testosterone levels (purple) are plotted against time from  $t = 0$  to  $t = 390$ . In the beginning, we see a big increase of the testosterone-dependent tumor cells, especially  $T^P$ , after which the growth of all the tumor cells slows down.

Figure 6.2 displays the lattice and cross-sections of the middle row of the lattice at different time points. The  $T^P$  cells dominate the upper half of the lattice, the  $T^+$  cells are less prominent, and the  $T^-$  cells mostly occupy the lower half of the lattice. Over time, it looks like that the system stabilizes into an equilibrium.

## Tumor Growth and Cross-Sections, with no treatment

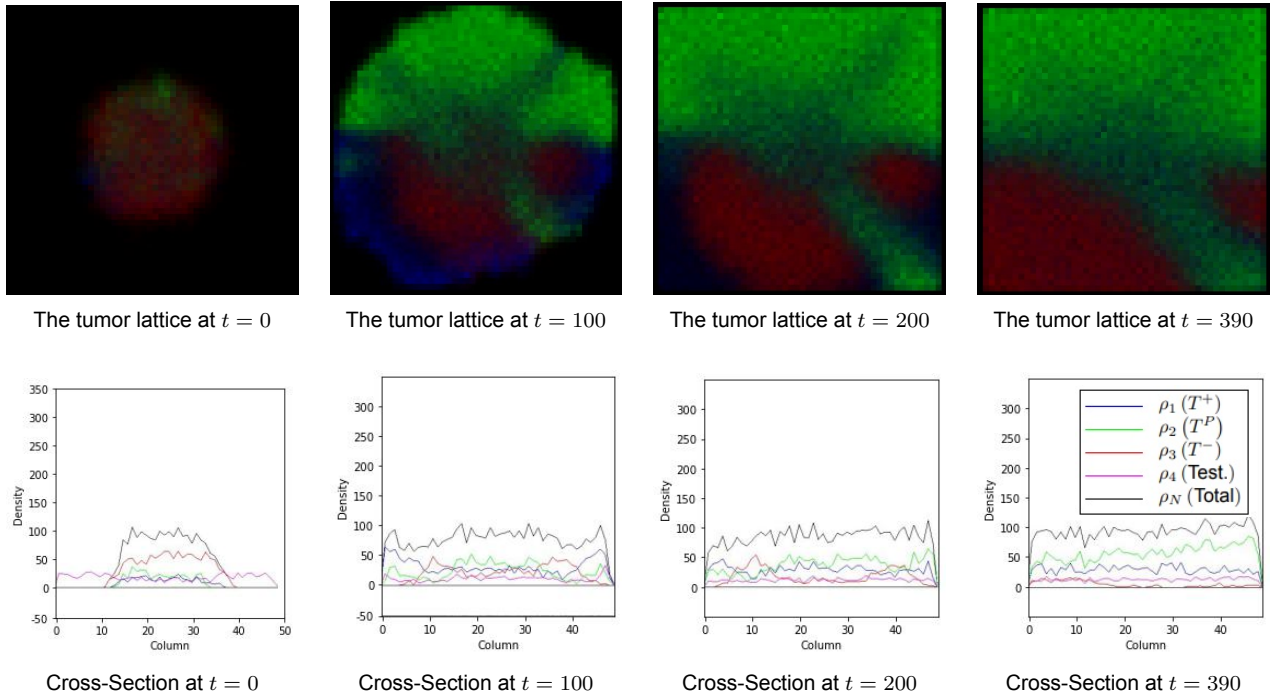


**Figure 6.2:** (a) Lattice representations of the tumor at  $t = 0$ ,  $t = 100$ ,  $t = 200$  and  $t = 390$ , showing the evolution of the spatial distribution of the tumor cells, with  $T^-$  cells (red),  $T^P$  cells (green),  $T^+$  cells (blue), without treatment. (b) Cross-sectional views of the middle row of the lattice at the same time points, illustrating changes in the total number of cells (black),  $T^-$  cells (red),  $T^P$  cells (green),  $T^+$  cells (blue) and testosterone levels (purple).

## 6.2. Effect of Testosterone Removal

Administering the medication Lupron is a common treatment that works by eliminating testosterone from the bloodstream, effectively starving the testosterone-dependent cells [53]. We simulate the removal of testosterone corresponding to this treatment by setting  $\chi = 0$  and setting the total movement probability of testosterone in the blood to zero ( $C_4 = 0$ ), since once the testosterone moves into the bloodstream it is removed. The expected outcome is a decrease in the  $T^+$  and  $T^P$  densities, leaving  $T^-$  cells as the dominant population.

In the simulation, we apply this treatment using the initial conditions from Section 6.1 and track the decline in testosterone-dependent cells over time as they adjust to the new hormone-deprived environment. The tumor state at  $t = 140$  of Section 6.1 is taken as the initial condition for applying the treatments discussed in the following sections. Figure 6.3 presents the testosterone and tumor cells over time. Starting at  $t = 0$ , Lupron is administered, removing the testosterone from the blood. This results in a slower growth of the testosterone-dependent tumor cells, especially  $T^+$  cells, since those cells cannot produce testosterone themselves. On the other hand, the  $T^-$  cells grow faster than when compared to no treatment. A reason for this could be that there is more space available.

Testosterone and Cell Dynamics Over Time, with Lupron

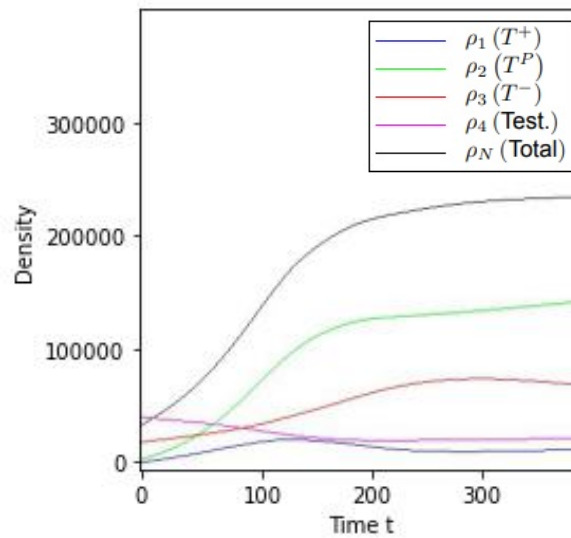


**Figure 6.3:** The total number of cells (black),  $T^-$  cells (red),  $T^P$  cells (green),  $T^+$  cells (blue), and testosterone levels (purple) are plotted against time from  $t = 0$  to  $t = 390$ . Starting at  $t = 0$  Lupron is administered, removing the testosterone from the blood. This results in a slower growth of the testosterone-dependent tumor cells, especially  $T^P$ , since those cells cannot produce testosterone themselves. On the other hand, the  $T^-$  cells grow faster than compared to no treatment, since there is more space left.

Figure 6.4 shows the lattice and cross-sections of the middle row at different time points, giving a detailed perspective on the tumor dynamics. The  $T^P$  cells dominate the upper half of the lattice. The  $T^-$  cells primarily occupy the lower half of the lattice. A key observation is that the effectiveness of this treatment depends largely on the composition of tumor cells within the tumor micro environment. If no testosterone-independent ( $T^-$ ) cells are present, administering Lupron could be more effective in reducing the tumor burden, as the growth of both testosterone-dependent  $T^+$  and  $T^P$  cells rely on testosterone levels. However, since  $T^P$  cells can produce their own testosterone, their presence allow the tumor to persist, even in the absence of external testosterone. On the other hand, if a population of  $T^-$  cells is present, they could benefit from the reduction of testosterone-dependent cells, gaining more space and resources to grow.

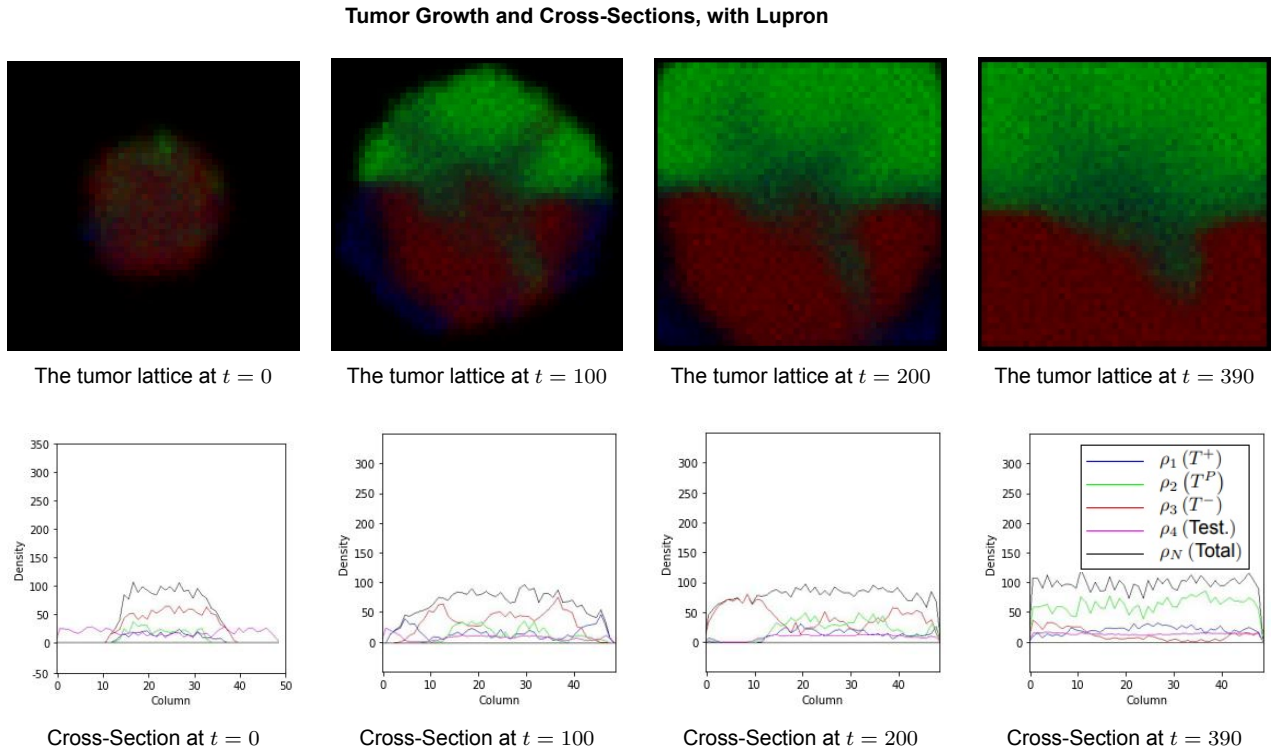


**Figure 6.4:** The tumor dynamics after administering Lupron starting at  $t = 0$ . (a) Lattice representations of the tumor at  $t = 0$ ,  $t = 100$ ,  $t = 200$  and  $t = 390$ , showing the evolution of the spatial distribution of the tumor cells, with  $T^-$  cells (red),  $T^P$  cells (green),  $T^+$  cells (blue). (b) Cross-sectional views of the middle row of the lattice at the same time points, illustrating changes in the total number of cells (black),  $T^-$  cells (red),  $T^P$  cells (green),  $T^+$  cells (blue) and testosterone levels (purple).

### 6.3. Testosterone Removal and Targeting $T^P$

In this strategy, we integrate the use of Lupron with Abiraterone, which targets the testosterone-producing prostate cells ( $T^P$ ). Another example of such a drug is Enzalutamide. We simulate this by setting the growth rate of  $T^P$  cells to zero ( $\alpha_2 = 0$ ). The two drugs slow down the testosterone-related tumor growth, suppressing the tumor more effectively than Lupron alone. Cunningham et al. found in [10] that ongoing Abiraterone therapy typically results in a decrease in tumor burden by targeting and reducing both the  $T^P$  and  $T^+$  tumor cells. We expect a rapid decline in  $T^P$  cells. With no testosterone in the bloodstream due to Lupron and the decline of testosterone-producing cells, the  $T^+$  population will also diminish, as they rely on testosterone for survival but cannot produce it themselves. In contrast,  $T^-$  cells grow faster as they have more space.

While the strategy of treating a patient with Lupron and Abiraterone is expected to slow tumor progression compared to Lupron alone, its effectiveness depends on the presence of  $T^-$  cells. If they are present, the increase in space and resource availability for  $T^-$  cells may allow their numbers to rapidly grow, potentially undermining the benefits of the treatment.

In the simulation, the tumor state at  $t = 140$  of Section 6.1 is taken as the initial condition for applying the treatment. Figure 6.5 presents the testosterone and tumor cell dynamics over time. Starting at  $t = 0$ , Lupron and Abiraterone are administered, removing the testosterone from the blood and targeting  $T^P$ . This results in an extinction of the  $T^P$  cells and later on the  $T^+$  cells. This is because  $\alpha_2$  is set to zero, so the  $T^P$  cells cannot grow anymore and slowly die out. At that moment, no new testosterone can be produced anymore, resulting in the extinction of the  $T^+$  population. On the other hand,  $T^-$  cells grow faster than without treatment if  $T^P$  and  $T^+$  were present, since there is more space left. The tumor burden at  $t = 390$  is lower compared to Figures 6.1 and 6.3 which show the tumor dynamics over time when administering no treatment or only Lupron.

## Testosterone and Cell Dynamics Over Time, with Lupron and Abiraterone

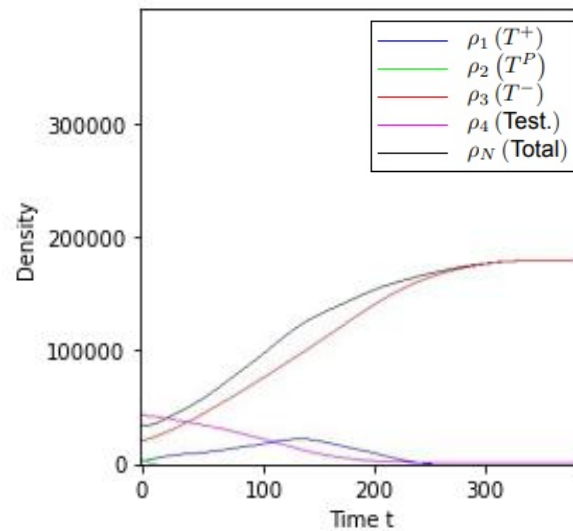


**Figure 6.5:** The total number of cells (black),  $T^-$  cells (red),  $T^P$  cells (green),  $T^+$  cells (blue), and testosterone levels (purple) are plotted against time from  $t = 0$  to  $t = 390$ . Starting at  $t = 0$  the medicines Lupron and Abiraterone are administered, removing the testosterone from the blood and targeting  $T^P$ . This results in an extinction of the  $T^P$  cells and later on the  $T^+$  cells. On the other hand, the  $T^-$  cells grow faster then compared to no treatment, since there is more space left. The tumor burden at  $t = 390$  is lower compared to Figures 6.1 and 6.3.

Figure 6.6 shows the lattice and cross-sections of the middle row of the lattice at different time points. The  $T^P$  and  $T^+$  populations die out due to the lack of testosterone and  $\alpha_2 = 0$ . On the other hand, we see the  $T^-$  cells filling the whole lattice. A key observation is that the effectiveness of this treatment depends largely on the composition of the tumor. If no testosterone-independent ( $T^-$ ) cells are present, administering Lupron and Abiraterone will be effective and remove the whole tumor. However, as can be seen in Figure 6.6, if a population of  $T^-$  cells is present initially, these cells will multiply quickly and fill the lattice.

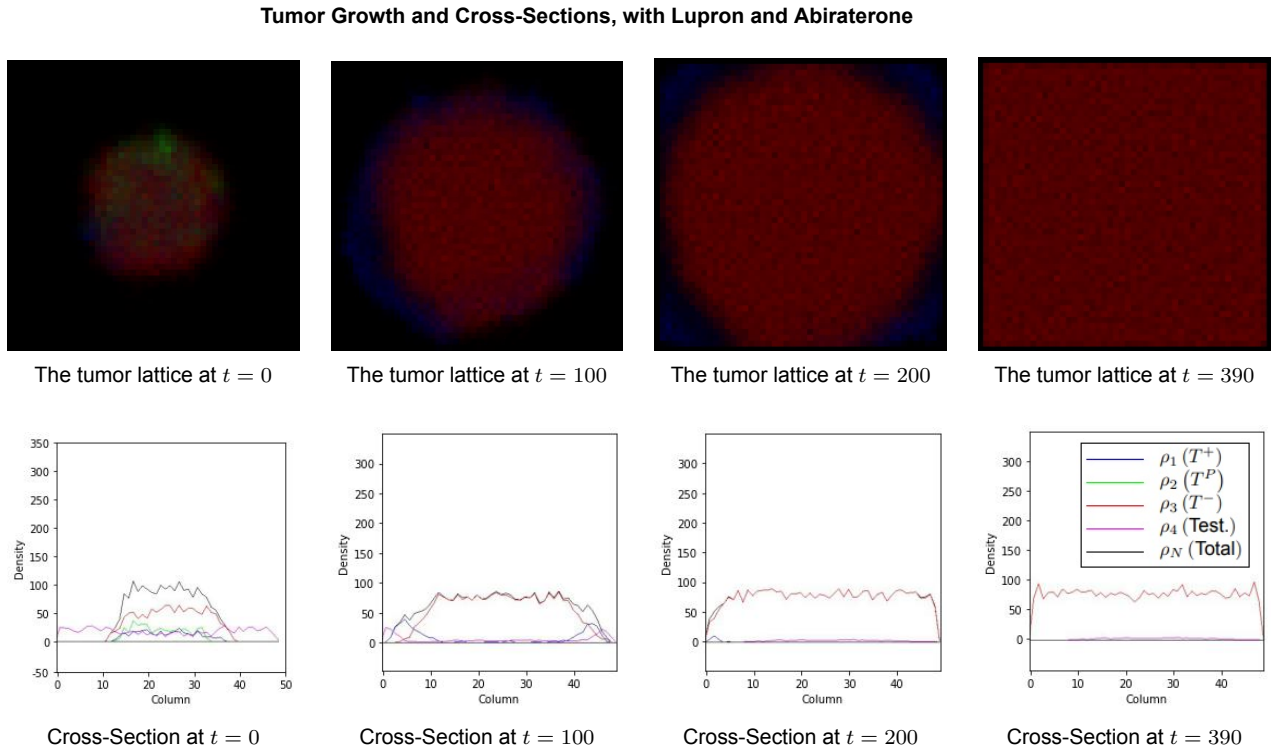


**Figure 6.6:** The tumor dynamics after administering Lupron and Abiraterone starting at  $t = 0$ , removing the testosterone from the blood and targeting the testosterone producing cells  $T^P$ . (a) Lattice representations of the tumor at  $t = 0$ ,  $t = 100$ ,  $t = 200$  and  $t = 390$ , showing the evolution of the spatial distribution of the tumor cells, with  $T^-$  cells (red),  $T^P$  cells (green),  $T^+$  cells (blue). (b) Cross-sectional views of the middle row of the lattice at the same time-points, illustrating changes in the total number of cells (black),  $T^-$  cells (red),  $T^P$  cells (green),  $T^+$  cells (blue) and testosterone levels (purple).

## 6.4. Innovative Treatment for Prostate Cancer

The third strategy involves the use of Lupron, Abiraterone, and testosterone injections. Unlike the previous strategies, this approach reintroduces testosterone into the body, allowing periods of high testosterone levels in the bloodstream (modeled as increasing  $\chi$ ). Although this idea is relatively new, discussions with experts (private communication) [6] suggest it could induce a different tumor response. The hypothesis is that high testosterone exposure might prevent the testosterone-independent cells  $T^-$  to dominate.

This strategy is a form of adaptive therapy, a treatment designed to control the competitive interactions between drug-sensitive and drug-resistant cells. By allowing the testosterone-dependent cells to thrive temporarily, it could suppress the growth of testosterone-independent cells due to resource and space competition. This can help control the overall tumor burden, potentially leading to alternating phases of cell growth and suppression. By carefully adjusting testosterone injection doses, it may be possible to maintain this balance between the different tumor populations.

Alternatively, this strategy could be applied as extinction therapy, as discussed in the introduction, where the goal is complete annihilation of all cancer cells. This is what we will try to simulate in this section, by firstly giving high testosterone injections to aggressively promote the growth of testosterone-dependent populations ( $T^+$  and  $T^P$ ), out competing the testosterone-independent  $T^-$  cells until they are eradicated. Once this is achieved, Lupron and Abiraterone can be administered to target the remaining testosterone-dependent cells, aiming for complete tumor removal.

In the simulation, the tumor state at  $t = 140$  of Section 6.1 is taken as the initial condition for applying the treatments. Figure 6.7 presents the testosterone and tumor cell dynamics over time. Starting at  $t = 0$  testosterone is injected in the blood, by increasing  $\chi$  by 2, making the testosterone-dependent cells

grow a lot, crushing the testosterone-independent  $T^-$  cells. At  $t = 187$  the  $T^-$  cells are extinct, and both Lupron and Abiraterone are administered, removing the testosterone from the blood and targeting  $T^P$ . This results in an extinction of the  $T^P$  cells and later on the  $T^+$  cells. In this way the complete tumor is removed.

**Testosterone and Cell Dynamics Over Time, with Testosterone Injections, Lupron and Abiraterone**

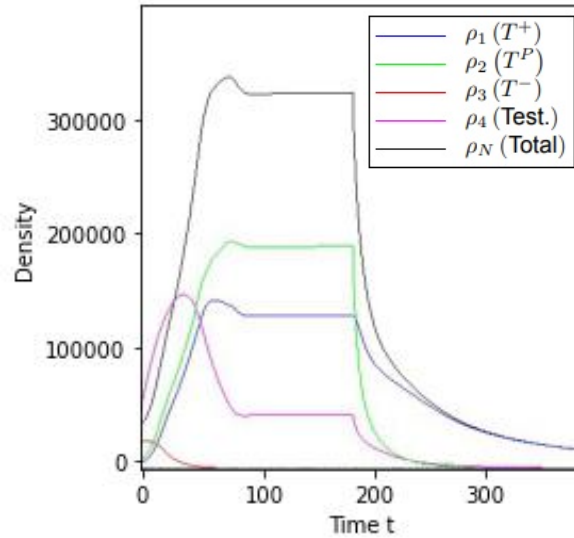


**Figure 6.7:** The total number of cells (black),  $T^-$  cells (red),  $T^P$  cells (green),  $T^+$  cells (blue), and testosterone levels (purple) are plotted against time from  $t = 0$  to  $t = 390$ . Starting at  $t = 0$  testosterone is injected in the blood, by increasing  $\chi$  by 2, making the testosterone-dependent cells grow a lot, crushing the testosterone-independent  $T^-$  cells. At  $t = 187$  the  $T^-$  cells are extinct, and both Lupron and Abiraterone are administered, removing the testosterone from the blood and targeting  $T^P$ . This results in an extinction of the  $T^P$  cells and later on the  $T^+$  cells. In this way the complete tumor is removed.

Figure 6.8 shows the lattice and cross-sections of the middle row at various time points, providing a clearer view of the tumor dynamics throughout treatment. Initially, the testosterone-dependent cells,  $T^P$  and  $T^+$ , experience growth due to the high testosterone levels provided, quickly occupying the entire lattice. On the other hand, the testosterone-independent cells,  $T^-$ , are unable to compete for space and resources, leading to their extinction at time  $t = 187$ .

At this point, Lupron and Abiraterone are administered, and by  $t = 200$ , we observe a reduction in the densities of  $T^P$  and  $T^+$  cells. By  $t = 390$ , these populations are nearly extinct. The  $T^P$  population (green) reaches zero by  $t = 434$ , and finally, the  $T^+$  population (blue) is eradicated at  $t = 3015$ .

## Tumor Growth and Cross-Sections, with Testosterone Injections, Lupron and Abiraterone

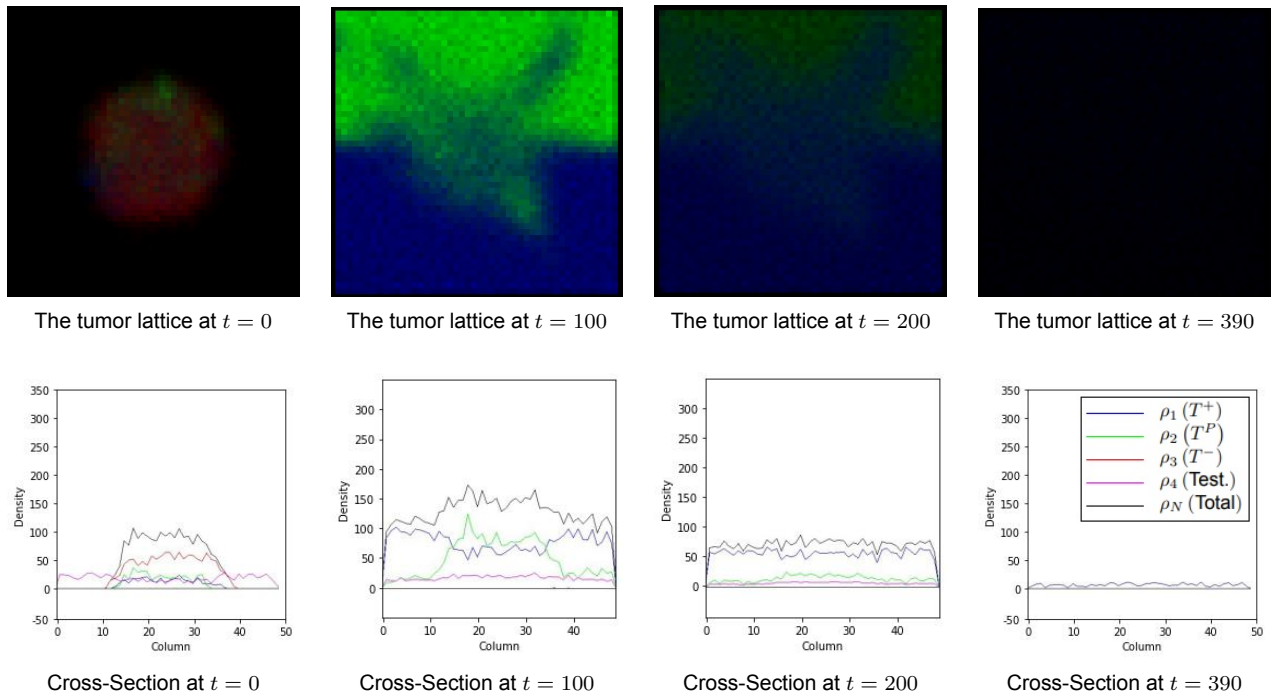


**Figure 6.8:** The tumor dynamics after administering testosterone injections starting at  $t = 0$ . At  $t = 327$  the  $T^-$  cells are extinct, and both Lupron and Abiraterone are administered, removing the testosterone from the blood and targeting  $T^P$ . (a) Lattice representations of the tumor at  $t = 0$ ,  $t = 100$ ,  $t = 200$  and  $t = 390$ , showing the evolution of the spatial distribution of the tumor cells, with  $T^-$  cells (red),  $T^P$  cells (green),  $T^+$  cells (blue). (b) Cross-sectional views of the middle row of the lattice at the same time-points, illustrating changes in the total number of cells (black),  $T^-$  cells (red),  $T^P$  cells (green),  $T^+$  cells (blue) and testosterone levels (purple).

# 7

## Discussion and Conclusions

In this thesis, we used spatiotemporal modeling to better understand hormonal cancer. In Chapter 2, we first explored two common non-spatial population models: replicator dynamics and Lotka-Volterra dynamics. We found an equivalence between the two under certain conditions, especially with an additional variable  $y_0$ , tracking the population size, and getting rid of  $y_0$  affects the speed that solutions travel along the trajectories. After that we switched to spatial models.

Next, in Chapter 3, we designed an agent-based model on a discrete lattice to describe prostate cancer with three different cell types. By changing the testosterone level in the blood ( $\chi$ ), we could control which tumor cells, testosterone-dependent or independent, dominated the lattice, suggesting a phase transition in  $\chi$ . We also simulated tumor growth starting from a few mutated cells.

In Chapter 4, we derived the partial differential equations of the continuum system by taking the continuum limit of the discrete model. Since this system was challenging to analyze, we proposed an alternative continuum spatial model in Chapter 5 and analyzed this, through non-dimensionalization and linear stability analysis. Finally, in Chapter 6, we explored three different treatment strategies for prostate cancer, manipulating testosterone levels to affect tumor dynamics. Lupron removes all testosterone from the bloodstream, Abiraterone stops the testosterone-producing cancer cells ( $T^P$ ) from dividing and high-dose testosterone injections could be applied as extinction therapy.

Our spatiotemporal model is not limited to prostate cancer but has the potential to be applied to other hormonal cancers. By adjusting parameters related to hormone levels, such as testosterone for prostate cancer or estrogen for breast cancer, the same framework can provide insights into how these cancers behave under different treatment strategies. This flexibility in application enhances the model's utility across various cancer types, making it a valuable tool for broader cancer research.

One of the most recurring and striking findings is the role that testosterone levels in the blood play in influencing tumor cell dynamics. Our model clearly shows that adjusting testosterone in the bloodstream can often control which type of tumor cells dominate, highlighting a phase transition in  $\chi$ . This is exciting because it suggests the possibility of using hormonal manipulation as a means of controlling tumor composition as treatment.

While there exist many models in mathematical oncology, including spatial and agent-based approaches, focusing on simulating biological systems to observe behavior, this work is special because we incorporated a mathematical analysis. Our model not only simulates tumor dynamics but also provides a formal understanding through non-dimensionalization and linear stability analysis. This added mathematical layer offers deeper insights into the underlying mechanisms and potential stability of various cell populations, which is not often a focus in purely spatial models.

The results of our simulations, particularly those in Section 6.4, demonstrate that extinction therapy is not only feasible but should be strongly considered as a therapeutic strategy, given its ability to elimi-

nate both testosterone-independent and testosterone-dependent tumor populations.

In this thesis, we have made several simplifying assumptions to allow for a mathematical analysis of the system. However, these assumptions also open the door to many interesting directions for future research. First and foremost, we relied on assumptions regarding parameter values, initial values and biological processes that could be revisited. For example, in our final system we assumed that testosterone levels influence cell division but not cell death. It would be fascinating to explore how the tumor reacts to treatments if testosterone controls cell death instead, like the system we proposed in Chapter 3. Furthermore, we treated several parameters as equal for simplicity such that we could mathematically analyze the system. Future work could benefit from exploring what happens if one lets go of these assumptions.

Another promising direction would be to extend the model to include negative values of  $\chi$ , representing assumptions where testosterone levels in the blood are so low that they extract the testosterone from the whole body. Furthermore, when simulating extinction therapy, it looked like the tumor burden became too high under certain conditions. It would be interesting to optimize the outcomes by minimizing the tumor burden by adjusting the dosage and timing of testosterone injections. By fine-tuning these parameters, especially starting with a smaller initial tumor or altering the treatment's dosage, we may be able to achieve better control over tumor populations and minimize their size throughout the treatment period.

Exploring adaptive treatment strategies is another exciting opportunity to study. In our current research, we showed that extinction therapy is promising, but a different approach could involve alternating phases of dominance between different tumor cell populations. For example, testosterone-dependent and testosterone-independent cells could take turns dominating the lattice. By optimizing doses and timing, one could maybe maintain a balance between these populations, potentially delaying the progression of the disease significantly. Using our model together with this adaptive strategy could lead to more controlled tumor growth, with alternating phases of growth and suppression across different cell types, prolonging survival.

From a mathematical standpoint, the exploration of parameter fields could be extended further. One could search for precise conditions under which the eigenvalues of the system's equilibrium points are stable or unstable. Furthermore, it would be interesting to look if an exact formulation for  $\chi$  which ensures the extinction of the  $T^-$  cells exists and what it would be. If that is the case it means that, not taking the tumor burden and side effects into consideration, extinction therapy could always work. Investigating more complex models where survival probabilities for individual cells are stochastic could also bring a new dimension to the analysis.

Moreover, one area that remains unexplored in this thesis is the inclusion of patient data. It would be useful to fit the parameter values of the model using clinical data and to simulate treatment strategies tailored to specific tumor compositions. This would not only provide a validation of the model but also allow for a more individualized approach to cancer treatment.

Another extension would be the development of a three dimensional version of the model. While we currently simulate the tumor in two dimensions with allowance for multiple cells in a single lattice point (giving a pseudo three dimensional effect), a full three dimensional framework could reveal interactions between different layers of cells that are not captured in our current framework. Adding a third dimension could provide insights into how tumor cells interact vertically with neighboring layers, which could maybe change the tumor's response to treatments. Although this would complicate the mathematical analysis, it could bring the model closer to representing real biological systems.

In addition, adjusting how testosterone levels are handled within the model could lead to more accurate simulations. In the current setup, testosterone levels are not bounded, leading to potential unrealistic scenarios where testosterone levels can rise sharply. Normalizing testosterone levels at each lattice point to a biologically realistic range could combat this issue and provide more accurate results, especially when considering the model of Chapter 5.

Finally, while this model assumes that all cells are updated synchronously, future work could explore the implementation of a Gillespie algorithm, which updates individual cells one at a time with waiting periods between updates [41]. This method would introduce stochasticity in cell behavior, making the model more realistic.

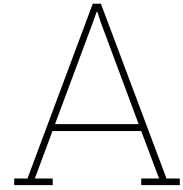
In summary, this work has not only deepened our understanding of prostate cancer but has also laid the foundation for future research across other hormonal cancers. The spatiotemporal model we developed is adaptable, making it a powerful tool in exploring treatment strategies for a range of cancer types. The integration of mathematical analysis with simulation provides unique insights into tumor dynamics, opening exciting possibilities for treatment approaches. With further extensions and real patient data, this model could contribute to personalized cancer treatment, potentially improving patient outcomes in the future.

# References

- [1] A. Alsenafi and A.B.T. Barbaro. “A convection–diffusion model for gang territoriality”. In: *Physica A: Statistical Mechanics and its Applications* 510 (2018), pp. 765–786.
- [2] A.S. Alsenafi. “Segregation Dynamics Motivated By Territorial Markings: The Transition From A Particle To A Continuum Model”. PhD thesis. Case Western Reserve University, 2016.
- [3] A. Barbaro et al. “Modelling and simulations of the migration of pelagic fish”. In: *ICES Journal of Marine Science* 66.5 (2009), pp. 826–838.
- [4] P. Bayer et al. “Coordination games in cancer”. In: *PLoS One* 17.1 (2022), e0261578. DOI: 10.1371/journal.pone.0261578.
- [5] W.E. Boyce and R.C. DiPrima. *Elementary differential equations and boundary value problems*. John Wiley & Sons, 2001.
- [6] J. S. Brown and Moffitt Evolutionary Tumor Board. *Communication with J. S. Brown*. Private communication. 2024.
- [7] J. Chmielecki et al. “Optimization of dosing for EGFR-mutant non–small cell lung cancer with evolutionary cancer modeling”. In: *Science translational medicine* 3.90 (2011), 90ra59–90ra59.
- [8] H. Coggan and K.M. Page. “The role of evolutionary game theory in spatial and non-spatial models of the survival of cooperation in cancer: a review”. In: *J. R. Soc. Interface* 19 (2022), p. 20220346. DOI: <https://doi.org/10.1098/rsif.2022.0346>.
- [9] E.D. Crawford et al. “Treating patients with metastatic castration resistant prostate cancer: a comprehensive review of available therapies”. In: *The Journal of urology* 194.6 (2015), pp. 1537–1547.
- [10] J.J. Cunningham et al. “Optimal control to develop therapeutic strategies for metastatic castrate resistant prostate cancer”. In: *Journal of theoretical biology* 459 (2018), pp. 67–78.
- [11] A. M. Dujon et al. “Identifying key questions in the ecology and evolution of cancer”. In: *Evolutionary Applications* 14.4 (2021), pp. 877–892.
- [12] N. Farrokhan et al. “Measuring competitive exclusion in non–small cell lung cancer”. In: *Science Advances* 8.26 (2022), eabm7212. DOI: 10.1126/sciadv.abm7212.
- [13] R. Gallasch et al. “Mathematical models for translational and clinical oncology”. In: *Journal of clinical bioinformatics* 3 (2013), pp. 1–8.
- [14] R.A. Gatenby, J. Zhang, and J.S. Brown. “First strike–second strike strategies in metastatic cancer: lessons from the evolutionary dynamics of extinction”. In: *Cancer research* 79.13 (2019), pp. 3174–3177.
- [15] R.A. Gatenby et al. “Adaptive therapy”. In: *Cancer research* 69.11 (2009), pp. 4894–4903.
- [16] M. Gluzman, J.G. Scott, and A. Vladimirov. “Optimizing adaptive cancer therapy: dynamic programming and evolutionary game theory”. In: *Proceedings of the Royal Society B* 287.1925 (2020), p. 20192454. DOI: 10.1098/rspb.2019.2454.
- [17] N.L. Grigorenko et al. “Lotka–Volterra Competition Model with a Nonmonotone Therapy Function for Finding Optimal Strategies in the Treatment of Blood Cancers”. In: *Proceedings of the Steklov Institute of Mathematics* 317.Suppl 1 (2022), S71–S89. DOI: 10.1134/S0081543822030063.
- [18] M. Hagedoorn, U.Kreicbergs, and C.Appel. “Coping with cancer: The perspective of patients’ relatives”. In: *Acta Oncologica* 50.2 (2011), pp. 205–211.
- [19] D. Hanahan. “Hallmarks of cancer: new dimensions”. In: *Cancer discovery* 12.1 (2022), pp. 31–46.
- [20] D. Hanahan and R.A. Weinberg. “Hallmarks of cancer: the next generation”. In: *cell* 144.5 (2011), pp. 646–674.

- [21] J. Hofbauer. "On the occurrence of limit cycles in the Volterra-Lotka equation". In: *Nonlinear Analysis: Theory, Methods & Applications* 5.9 (1981), pp. 1003–1007.
- [22] J. Hofbauer and K. Sigmund. *Evolutionary Games and Population Dynamics*. Cambridge University Press, 1998.
- [23] Integraal Kankercentrum Nederland. *Kans op kanker toegenomen naar 1 op de 2 Nederlanders*. 2024. URL: <https://iknl.nl/nieuws/2023/kansopkanker> (visited on 09/30/2024).
- [24] A. Jemal et al. "Annual report to the nation on the status of cancer, 1975–2014, featuring survival". In: *JNCI: Journal of the National Cancer Institute* 109.9 (2017), djx030.
- [25] Kanker.nl. *Hoe ontstaat kanker?* 2024. URL: <https://www.kanker.nl/algemene-onderwerpen/wat-is-kanker/algemeen/ho-ontstaat-kanker> (visited on 09/04/2024).
- [26] A. Kaznatcheev et al. "Cancer treatment scheduling and dynamic heterogeneity in social dilemmas of tumour acidity and vasculature". In: *British journal of cancer* 116.6 (2017), pp. 785–792. DOI: 10.1038/bjc.2017.5.
- [27] A. Kaznatcheev et al. "Fibroblasts and alectinib switch the evolutionary games played by non-small cell lung cancer". In: *Nature ecology & evolution* 3.3 (2019), pp. 450–456.
- [28] T. J. A. Key. "Hormones and cancer in humans". In: *Mutation Research/Fundamental and Molecular Mechanisms of Mutagenesis* 333.1-2 (1995), pp. 59–67.
- [29] A.J. Lotka. "Elements of physical biology". In: *Science Progress in the Twentieth Century (1919–1933)* 21.82 (1926), pp. 341–343.
- [30] M.A. Masud and E. Kim. "Theoretical understanding of evolutionary dosing following tumor dynamics". In: *Chaos, Solitons & Fractals* 179 (2024), p. 114451. DOI: 10.1016/j.chaos.2024.114451.
- [31] J. Maynard Smith and G.R. Price. "The logic of animal conflict". In: *Nature* 246.5427 (1973), pp. 15–18.
- [32] E.E. McConnell. "The maximum tolerated dose: the debate". In: *Journal of the American College of Toxicology* 8.6 (1989), pp. 1115–1120.
- [33] S. Mendoza-Palacios and O. Hernández-Lerma. *Evolutionary games and the replicator dynamics*. Cambridge University Press, 2024.
- [34] Y. Miki. *Hormone-Dependent Cancers: New Aspects on Biochemistry and Molecular Pathology*. 2023.
- [35] H. Moore. "How to mathematically optimize drug regimens using optimal control". In: *Journal of pharmacokinetics and pharmacodynamics* 45.1 (2018), pp. 127–137.
- [36] National Cancer Institute. *What Is Cancer?* 2024. URL: <https://www.cancer.gov/about-cancer/understanding/what-is-cancer> (visited on 09/04/2024).
- [37] D. Okuonghae and A. Omame. "Analysis of a mathematical model for COVID-19 population dynamics in Lagos, Nigeria". In: *Chaos, Solitons & Fractals* 139 (2020), p. 110032.
- [38] F. Ovidi et al. "Agent-based model and simulation of mitigated domino scenarios in chemical tank farms". In: *Reliability Engineering & System Safety* 209 (2021), p. 107476.
- [39] K.J. Pienta et al. "Convergent evolution, evolving evolvability, and the origins of lethal cancer". In: *Molecular Cancer Research* 18.6 (2020), pp. 801–810.
- [40] G.G. Powathil, D.J.A. Adamson, and M.A.J. Chaplain. "Towards predicting the response of a solid tumour to chemotherapy and radiotherapy treatments: clinical insights from a computational model". In: *PLoS computational biology* 9.7 (2013), e1003120.
- [41] C.V. Rao and A.P. Arkin. "Stochastic chemical kinetics and the quasi-steady-state assumption: Application to the Gillespie algorithm". In: *The Journal of chemical physics* 118.11 (2003), pp. 4999–5010.
- [42] P. Rawla. "Epidemiology of Prostate Cancer". In: *World Journal of Oncology* 10.2 (2019), p. 63.
- [43] K.A. Rejniak and L.J. McCawley. "Current trends in mathematical modeling of tumor–microenvironment interactions: a survey of tools and applications". In: *Experimental Biology and Medicine* 235.4 (2010), pp. 411–423.

- [44] M. Sang et al. "The genomic physics of tumor–microenvironment crosstalk". In: *Physics Reports* 1029 (2023), pp. 1–51. DOI: 10.1016/j.physrep.2023.07.006.
- [45] SFML. *Simple and Fast Multimedia Library*. 2024. URL: <https://example.com> (visited on 03/08/2024).
- [46] A. Soboleva et al. "Validation of polymorphic Gompertzian model of cancer through in vitro and in vivo data". In: *bioRxiv* (2023), pp. 2023–04.
- [47] K. Staňková et al. "Optimizing cancer treatment using game theory". In: *JAMA oncology* 5.1 (2019), pp. 96–103.
- [48] F. Taillandier et al. "An agent-based model to simulate inhabitants' behavior during a flood event". In: *International Journal of Disaster Risk Reduction* 64 (2021), p. 102503.
- [49] P.D. Taylor and L.B. Jonker. "Evolutionary stable strategies and game dynamics". In: *Mathematical biosciences* 40.1-2 (1978), pp. 145–156. DOI: 10.1016/0025-5564(78)90077-9.
- [50] L.C. Vieira, R.S. Costa, and D. Valério. "An overview of mathematical modelling in cancer research: fractional calculus as modelling tool". In: *Fractal and Fractional* 7.8 (2023), p. 595.
- [51] V. Volterra. *Variazioni e fluttuazioni del numero d'individui in specie animali conviventi*. Accademia dei Lincei, 1927.
- [52] J. West, M. Robertson-Tessi, and A.R.A. Anderson. "Agent-based methods facilitate integrative science in cancer". In: *Trends in cell biology* 33.4 (2023), pp. 300–311.
- [53] J. West et al. "Towards multi-drug adaptive therapy". In: *Cancer Research* 80.7 (2020), pp. 1578–1589.
- [54] K.A.J. White, M.A. Lewis, and J.D. Murray. "A model for wolf-pack territory formation and maintenance". In: *Journal of Theoretical Biology* 178.1 (1996), pp. 29–43.
- [55] B. Wöfl et al. "The contribution of evolutionary game theory to understanding and treating cancer". In: *Dynamic Games and Applications* 12.2 (2022), pp. 313–342. DOI: 10.1007/s13235-021-00397-w.
- [56] World Health Organization. *Cancer*. 2024. URL: <https://www.who.int/news-room/fact-sheets/detail/cancer> (visited on 09/04/2024).
- [57] L. You et al. "Spatial vs. non-spatial eco-evolutionary dynamics in a tumor growth model". In: *Journal of theoretical biology* 435 (2017), pp. 78–97.
- [58] S. Zegers. "Cross diffusion in singlestep enzymatic reactions". Bachelor's thesis. Delft University of Technology.
- [59] J. Zhang et al. "Evolution-based mathematical models significantly prolong response to abiraterone in metastatic castrate-resistant prostate cancer and identify strategies to further improve outcomes". In: *Elife* 11 (2022), e76284.
- [60] J. Zhang et al. "Integrating evolutionary dynamics into treatment of metastatic castrate-resistant prostate cancer". In: *Nature Communications* 8 (2017), p. 1816. DOI: 10.1038/s41467-017-01968-5.



## The C++ Code

```
1 // This code is made to simulate prostate cancer (or other hormonal cancers).
2 // For it to work you need to install SFML, and link it to the project.
3 #include <SFML/Graphics.hpp> // For the plots
4 #include <iostream>
5 #include <string> // For legend plot
6 #include <vector>
7 #include <cstdlib> // For rand() and srand()
8 #include <ctime> // For time()
9 #include <cmath> // For floor()
10
11 class GridSquare {
12 public:
13     sf::Color color; // Color of the square
14
15     double test; // Testosterone
16     double test_new;
17     double test_new2;
18     double healthy_cells; // Healthy cells
19     double healthy_cells_new;
20     double healthy_cells_new2;
21     double blue; // Tumor cells needing testosterone, T+
22     double red; // Tumor cells independent of testosterone, T-
23     double green; // Tumor cells producing testosterone, TP
24     double blue_new;
25     double red_new;
26     double green_new;
27     double blue_new2;
28     double red_new2;
29     double green_new2;
30
31     // Constructor
32     GridSquare(int x, int y, int size) :
33         x(x), y(y), size(size),
34         blue(0.0), red(0.0), green(0.0),
35         blue_new(0.0), red_new(0.0), green_new(0.0),
36         blue_new2(0.0), red_new2(0.0), green_new2(0.0),
37         color(sf::Color(0, 0, 0, 255)),
38         test(0.0), test_new(0.0), test_new2(0.0),
39         healthy_cells(0.0), healthy_cells_new(0.0), healthy_cells_new2(0.0) {}
40
41     // Default constructor
42     GridSquare() : x(0), y(0), size(0) {}
43
```

```

44     // Function to set the color of the square
45     void setColor(sf::Color newColor) {
46         color = newColor;
47     }
48
49     // Function which returns the total number of cells at a site
50     double total_cells() {
51         return red + blue + green + healthy_cells;
52     }
53
54     double next_total_cells() {
55         return red_new + blue_new + green_new + healthy_cells_new;
56     }
57
58     // Function to draw the square
59     void draw(sf::RenderWindow& window) {
60         sf::RectangleShape square(sf::Vector2f(size, size));
61         square.setPosition(x, y);
62         square.setFillColor(color);
63         window.draw(square);
64     }
65
66 private:
67     int x; // x-coordinate of the square in the grid
68     int y; // y-coordinate of the square in the grid
69     int size; // Size of the square
70 };
71
72 int main() {
73     // Set random seed
74     std::srand(625);
75
76     // Create windows
77     int windowHeight = 400; // Be careful with changing this (change the plots as
78                             // well)
79     int windowWidth = 400;
80     double time = 0;
81     sf::RenderWindow windowtumor(sf::VideoMode(windowWidth, windowHeight), "Grid
82         all tumor cells", sf::Style::Close | sf::Style::Titlebar | sf::Style::
83         Resize);
84     sf::RenderWindow windowgreen(sf::VideoMode(windowWidth, windowHeight), "Grid
85         green tumor cells", sf::Style::Close | sf::Style::Titlebar | sf::Style::
86         Resize);
87     sf::RenderWindow windowred(sf::VideoMode(windowWidth, windowHeight), "Grid red
88         tumor cells", sf::Style::Close | sf::Style::Titlebar | sf::Style::Resize);
89     sf::RenderWindow windowblue(sf::VideoMode(windowWidth, windowHeight), "Grid
90         blue tumor cells", sf::Style::Close | sf::Style::Titlebar | sf::Style::
91         Resize);
92     sf::RenderWindow windowtest(sf::VideoMode(windowWidth, windowHeight), "Grid
93         testosterone", sf::Style::Close | sf::Style::Titlebar | sf::Style::Resize);
94     sf::RenderWindow windowhealthy(sf::VideoMode(windowWidth, windowHeight), "Grid
95         healthy cells", sf::Style::Close | sf::Style::Titlebar | sf::Style::Resize
96         );
97     sf::RenderWindow windowplot(sf::VideoMode(windowWidth, windowHeight), "Plot
98         middle row", sf::Style::Close | sf::Style::Titlebar | sf::Style::Resize);
99     sf::RenderWindow windowtotal(sf::VideoMode(windowWidth, windowHeight), "Total
100         cell density vs time", sf::Style::Close | sf::Style::Titlebar | sf::Style::
101         Resize);
102     sf::RenderWindow windowlegend(sf::VideoMode(2 * windowHeight / 3, windowHeight)
103         , "Legend", sf::Style::Close | sf::Style::Titlebar | sf::Style::Resize);

```

```

90 // Make sure the windows are positined next to each other
91 windowtumor.setPosition(sf::Vector2i(windowWidth / 2 - 180, windowHeight / 2 -
    100));
92 windowgreen.setPosition(sf::Vector2i(windowtumor.getPosition().x + windowWidth
    + 5, windowtumor.getPosition().y));
93 windowred.setPosition(sf::Vector2i(windowgreen.getPosition().x + windowWidth +
    5, windowtumor.getPosition().y));
94 windowblue.setPosition(sf::Vector2i(windowred.getPosition().x + windowWidth +
    5, windowtumor.getPosition().y));
95 windowtest.setPosition(sf::Vector2i(windowtumor.getPosition().x, windowtumor.
    getPosition().y + windowHeight + 45));
96 windowhealthy.setPosition(sf::Vector2i(windowgreen.getPosition().x, windowtest
    .getPosition().y));
97 windowplot.setPosition(sf::Vector2i(windowred.getPosition().x, windowtest.
    getPosition().y));
98 windowtotal.setPosition(sf::Vector2i(windowblue.getPosition().x, windowtest.
    getPosition().y));
99 windowlegend.setPosition(sf::Vector2i(windowblue.getPosition().x + windowWidth
    + 5, windowtest.getPosition().y));
100
101 // Define grid properties
102 int numRows = 50; // Make sure this is a divider of WindowWidth
103 int numCols = 50;
104 int cellSize = windowHeight / numRows;
105
106 // Model parameters
107 // Cell division
108 double prod_b = 0.007; // For alterate system: prod_b=prod_g
109 double prod_g = 0.007;
110 double prod_r = 0.08;
111 double prod_h = 0; // Cancer cells grow faster than healthy cells
112 // Testosterone
113 double prod = 0.03; // Testosterone creation rate by green tumor cells
114 double consumption_rate = 0.0015; // Testosterone consumption rate
115 double test_stay = 0.9; // Probability of testosterone staying at its lattice
    point
116 double base = 0.15; // Standard testosterone level, coming from the blood
117 // Cell death
118 double death_b = 0.001;
119 double death_g = 0.001;
120 double death_r = 0.001;
121 double death_h = 0;
122 double starve = 0.08; // Death due to lack of testosterone -> not used in
    alternat system
123 // Cell movement
124 double beta = 0.00001;
125 double C_h = 0.1; // Probability healthy cells move
126 double C_b = 0.1; // For alternat system C_h=C_b=C_g=C_r
127 double C_g = 0.1;
128 double C_r = 0.1;
129 // Needed for treatment
130 int answer;
131 double addtobaseleveltest = 0;
132
133 // Create a grid of grid squares
134 std::vector<std::vector<GridSquare>> grid(numRows, std::vector<GridSquare>(
    numCols));
135 std::vector<std::vector<GridSquare>> greengrid(numRows, std::vector<GridSquare
    >(numCols));
136 std::vector<std::vector<GridSquare>> redgrid(numRows, std::vector<GridSquare>(
    numCols));

```

```

137     std::vector<std::vector<GridSquare>> bluegrid(numRows, std::vector<GridSquare
138         >(numCols));
139     std::vector<std::vector<GridSquare>> testgrid(numRows, std::vector<GridSquare
140         >(numCols));
141     std::vector<std::vector<GridSquare>> healthygrid(numRows, std::vector<
142         GridSquare>(numCols));
143
144     // Add initial coordinates
145     for (int i = 0; i < numRows; ++i) {
146         for (int j = 0; j < numCols; ++j) {
147             // Calculate the position of the current grid square
148             int posX = j * cellSize; // Column index * cell size
149             int posY = i * cellSize; // Row index * cell size
150             // Initialize the grid square at the current position
151             grid[i][j] = GridSquare(posX, posY, cellSize);
152         }
153     }
154
155     // Initial conditions
156     // Uniformly distribute 100 red, 100 blue, and 100 green cells in a 10x10
157     // square in the middle
158     int centerX = numCols / 2;
159     int centerY = numRows / 2;
160     int startX = centerX - 5;
161     int startY = centerY - 5;
162     int endX = centerX + 5;
163     int endY = centerY + 5;
164     for (int i = 0; i < 100; ++i) {
165         int xRed = std::rand() % 10 + startX;
166         int yRed = std::rand() % 10 + startY;
167         int xBlue = std::rand() % 10 + startX;
168         int yBlue = std::rand() % 10 + startY;
169         int xGreen = std::rand() % 10 + startX;
170         int yGreen = std::rand() % 10 + startY;
171
172         grid[yRed][xRed].red += 1;
173         grid[yBlue][xBlue].blue += 1;
174         grid[yGreen][xGreen].green += 1;
175     }
176
177     // Set initial value testosterone to base level
178     for (int i = 1; i < numRows - 1; ++i) {
179         for (int j = 1; j < numCols - 1; ++j) {
180             grid[i][j].test = base;
181         }
182     }
183
184     // Set initial values for equilibrium 1
185     /*for (int i = 1; i < numRows - 1; ++i) {
186         for (int j = 1; j < numCols-1; ++j) {
187             grid[i][j].blue = 11.1;
188             grid[i][j].green = 24.9;
189             grid[i][j].red = 0;
190             grid[i][j].healthy_cells = 0;
191             grid[i][j].test = 36;
192         }
193     }*/
194
195     // Set initial values for equilibrium 2
196     /*for (int i = 1; i < numRows-1; ++i) {
197         for (int j = 1; j < numCols-1; ++j) {
198             grid[i][j].blue = 7.5 + 25 * base;

```

```
194         grid[i][j].green = -(25 * base) + 7.5;
195         grid[i][j].red = 5;
196         grid[i][j].healthy_cells = 0;
197         grid[i][j].test = 20;
198     }
199 }*/
200
201 // Empty boundaries
202 for (int j = 0; j < numCols; ++j) {
203     grid[0][j].test = 0;
204     grid[0][j].healthy_cells = 0;
205     grid[0][j].blue = 0;
206     grid[0][j].green = 0;
207     grid[0][j].red = 0;
208     grid[numRows - 1][j].test = 0;
209     grid[numRows - 1][j].healthy_cells = 0;
210     grid[numRows - 1][j].blue = 0;
211     grid[numRows - 1][j].green = 0;
212     grid[numRows - 1][j].red = 0;
213 }
214 for (int i = 0; i < numRows; ++i) {
215     grid[i][0].test = 0;
216     grid[i][0].healthy_cells = 0;
217     grid[i][0].blue = 0;
218     grid[i][0].green = 0;
219     grid[i][0].red = 0;
220     grid[i][numCols - 1].test = 0;
221     grid[i][numCols - 1].healthy_cells = 0;
222     grid[i][numCols - 1].blue = 0;
223     grid[i][numCols - 1].green = 0;
224     grid[i][numCols - 1].red = 0;
225 }
226
227 // Needed for total number of cells plot
228 std::vector<sf::Vertex> allLines;
229 std::vector<sf::Vertex> allLinestest;
230 std::vector<sf::Vertex> allLinesgreen;
231 std::vector<sf::Vertex> allLinesred;
232 std::vector<sf::Vertex> allLinesblue;
233 std::vector<sf::Vertex> allLineshealthy;
234 double oldtotal = 0;
235 double newtotal = 0;
236 double oldtotaltest = 0;
237 double newtotaltest = 0;
238 double oldtotalblue = 0;
239 double newtotalblue = 0;
240 double oldtotalgreen = 0;
241 double newtotalgreen = 0;
242 double oldtotalred = 0;
243 double newtotalred = 0;
244 double oldtotalhealthy = 0;
245 double newtotalhealthy = 0;
246
247 for (int i = 0; i < numRows; ++i) {
248     for (int j = 0; j < numCols; ++j) {
249         oldtotal += grid[i][j].total_cells();
250         oldtotaltest += grid[i][j].test;
251         oldtotalblue += grid[i][j].blue;
252         oldtotalgreen += grid[i][j].green;
253         oldtotalred += grid[i][j].red;
254         oldtotalhealthy += grid[i][j].healthy_cells;
```

```

255     }
256 }
257
258 // Legend
259 sf::Font font;
260 if (!font.loadFromFile("C:/Users/jrral/Documents/TU/Thesis/C++ thesis/Roboto/
    Roboto-Thin.ttf")) { // Change it to the position of a font you like
261     // Handle error
262 }
263 sf::Text legend;
264 legend.setFont(font);
265 legend.setCharacterSize(20);
266 legend.setFill-color(sf::Color::Black);
267 legend.setPosition(10, 10); // Position the text in the window
268
269 // Needed for plot showing all the different types of cells of the middle row
270 sf::VertexArray rline(sf::LinesStrip, numCols);
271 sf::VertexArray bline(sf::LinesStrip, numCols);
272 sf::VertexArray gline(sf::LinesStrip, numCols);
273 sf::VertexArray testline(sf::LinesStrip, numCols);
274 sf::VertexArray topline(sf::LinesStrip, numCols);
275 sf::VertexArray hline(sf::LinesStrip, numCols);
276 sf::VertexArray nullline(sf::LinesStrip, numCols);
277 sf::VertexArray maxline(sf::LinesStrip, numCols);
278
279 // Fix the colors for the plot t=0
280 for (int i = 1; i < numRows - 1; ++i) {
281     for (int j = 1; j < numCols - 1; ++j) {
282         grid[i][j].setColor(sf::Color(std::max(std::min(grid[i][j].red, (
                double)255), (double)0), std::max(std::min(grid[i][j].green, (
                double)255), (double)0), std::max(std::min(grid[i][j].blue, (double)
                )255), (double)0), 255));
283         greengrid[i][j].setColor(sf::Color(0, std::max(std::min(grid[i][j].
                green, (double)255), (double)0), 0, 255));
284         redgrid[i][j].setColor(sf::Color(std::max(std::min(grid[i][j].red, (
                double)255), (double)0), 0, 0, 255));
285         bluegrid[i][j].setColor(sf::Color(0, 0, std::max(std::min(grid[i][j].
                blue, (double)255), (double)0), 255));
286         testgrid[i][j].setColor(sf::Color(0, std::max(std::min(grid[i][j].test
                , (double)255), (double)0), 0, 255));
287         healthygrid[i][j].setColor(sf::Color(std::max(std::min(grid[i][j].
                healthy_cells, (double)255), (double)0), 0, 0, 255));
288     }
289 }
290
291 bool paused = false; // Pause button
292
293 // Main loop
294 while (windowtumor.isOpen()) {
295     sf::Event evnt;
296     while (windowtumor.pollEvent(evnt)) {
297         if (evnt.type == sf::Event::Closed) {
298             windowtumor.close();
299             windowgreen.close();
300             windowblue.close();
301             windowred.close();
302             windowtest.close();
303             windowhealthy.close();
304             windowplot.close();
305             windowtotal.close();
306             windowlegend.close();

```

```

307     }
308     else if (evnt.type == sf::Event::KeyPressed && evnt.key.code == sf::
           Keyboard::Space)
309         paused = !paused; // Pause when spacebar is pressed (does not
                           always work yet)
310     }
311
312     if (!paused) {
313         // Needed for total cells vs time plot
314         for (int i = 0; i < numRows; ++i) {
315             for (int j = 0; j < numCols; ++j) {
316                 newtotal += grid[i][j].total_cells();
317                 newtotaltest += grid[i][j].test;
318                 newtotalblue += grid[i][j].blue;
319                 newtotalgreen += grid[i][j].green;
320                 newtotalred += grid[i][j].red;
321                 newtotalhealthy += grid[i][j].healthy_cells;
322             }
323         }
324
325         // If you want to start with a more grown tumor to try out treatment
           strategies, set this to the preferred time != 0
326         int t_0 = 0;
327
328         // Start the densities vs time plot again if the window is full
329         if ((int)(time - t_0) % windowWidth == 0) {
330             allLines.clear();
331             allLinestest.clear();
332             allLinesgreen.clear();
333             allLinesred.clear();
334             allLinesblue.clear();
335             allLineshealthy.clear();
336         }
337
338         if ((int)time >= t_0) {
339             allLines.push_back(sf::Vertex(sf::Vector2f((int)(time-t_0) %
           windowWidth, 400 - oldtotal / 1000), sf::Color::Black));
340             allLines.push_back(sf::Vertex(sf::Vector2f((int)(time-t_0 + 1) %
           windowWidth, 400 - newtotal / 1000), sf::Color::Black));
341
342             allLinestest.push_back(sf::Vertex(sf::Vector2f((int)(time - t_0) %
           windowWidth, 400 - oldtotaltest / 1000), sf::Color::Magenta));
343             allLinestest.push_back(sf::Vertex(sf::Vector2f((int)(time-t_0 + 1)
           % windowWidth, 400 - newtotaltest / 1000), sf::Color::Magenta)
           );
344
345             allLinesblue.push_back(sf::Vertex(sf::Vector2f((int)(time - t_0) %
           windowWidth, 400 - oldtotalblue / 1000), sf::Color::Blue));
346             allLinesblue.push_back(sf::Vertex(sf::Vector2f((int)(time - t_0 +
           1) % windowWidth, 400 - newtotalblue / 1000), sf::Color::Blue)
           );
347
348             allLinesgreen.push_back(sf::Vertex(sf::Vector2f((int)(time - t_0)
           % windowWidth, 400 - oldtotalgreen / 1000), sf::Color::Green));
349             allLinesgreen.push_back(sf::Vertex(sf::Vector2f((int)(time-t_0 +
           1) % windowWidth, 400 - newtotalgreen / 1000), sf::Color::Green)
           ));
350
351             allLinesred.push_back(sf::Vertex(sf::Vector2f((int)(time - t_0) %
           windowWidth, 400 - oldtotalred / 1000), sf::Color::Red));
352             allLinesred.push_back(sf::Vertex(sf::Vector2f((int)(time-t_0 + 1)

```

```

    % windowHeight, 400 - newtotalred / 1000), sf::Color::Red));
353
354     allLineshealthy.push_back(sf::Vertex(sf::Vector2f((int)(time - t_0
        ) % windowHeight, 400 - oldtotalhealthy / 1000), sf::Color::Cyan
        ));
355     allLineshealthy.push_back(sf::Vertex(sf::Vector2f((int)(time-t_0 +
        1) % windowHeight, 400 - newtotalhealthy / 1000), sf::Color::
        Cyan));
356 }
357
358     oldtotal = newtotal;
359     newtotal = 0;
360     oldtotaltest = newtotaltest;
361     newtotaltest = 0;
362     oldtotalblue = newtotalblue;
363     newtotalblue = 0;
364     oldtotalgreen = newtotalgreen;
365     newtotalgreen = 0;
366     oldtotalred = newtotalred;
367     newtotalred = 0;
368     oldtotalhealthy = newtotalhealthy;
369     newtotalhealthy = 0;
370
371     // Only make the plots every 30 timesteps
372     if ((int)time % 30 == 0 and time >= t_0) {
373         // Clear window
374         windowtumor.clear(sf::Color::Black);
375         windowgreen.clear(sf::Color::Black);
376         windowblue.clear(sf::Color::Black);
377         windowred.clear(sf::Color::Black);
378         windowtest.clear(sf::Color::Black);
379         windowhealthy.clear(sf::Color::Black);
380         windowplot.clear(sf::Color::White);
381         windowtotal.clear(sf::Color::White);
382         windowlegend.clear(sf::Color::White);
383
384         // Draw grid squares
385         for (int i = 0; i < numRows; ++i) {
386             for (int j = 0; j < numCols; ++j) {
387                 grid[i][j].draw(windowtumor);
388                 greengrid[i][j].draw(windowgreen);
389                 redgrid[i][j].draw(windowred);
390                 bluegrid[i][j].draw(windowblue);
391                 testgrid[i][j].draw(windowtest);
392                 healthygrid[i][j].draw(windowhealthy);
393             }
394         }
395
396         // Make plot showing all the different types of cells of the
397         // middle row
398         for (int j = 0; j < numCols; ++j) {
399             int x = j * cellSize;
400             // Change these numbers if you change the window size:
401             rline[j] = sf::Vertex(sf::Vector2f(x, 350 - grid[numRows / 2][
402                 j].red), sf::Color::Red); //
403             bline[j] = sf::Vertex(sf::Vector2f(x, 350 - grid[numRows / 2][
404                 j].blue), sf::Color::Blue);
405             gline[j] = sf::Vertex(sf::Vector2f(x, 350 - grid[numRows / 2][
406                 j].green), sf::Color::Green);
407             testline[j] = sf::Vertex(sf::Vector2f(x, 350 - grid[numRows /
408                 2][j].test), sf::Color::Magenta);

```

```

404         totline[j] = sf::Vertex(sf::Vector2f(x, 350 - grid[numRows /
405             2][j].total_cells()), sf::Color::Black); // Total number of
                cells - black
406         hline[j] = sf::Vertex(sf::Vector2f(x, 350 - grid[numRows / 2][
407             j].healthy_cells), sf::Color::Cyan); // Healthy cells -
                light blue
408         nullline[j] = sf::Vertex(sf::Vector2f(x, 350), sf::Color::Black
409             ); // To show if things go below zero
410         maxline[j] = sf::Vertex(sf::Vector2f(x, 95), sf::Color::Black)
411             ; // To show if things go higher than max color
412     }
413     windowplot.draw(totline);
414     windowplot.draw(rline);
415     windowplot.draw(blline);
416     windowplot.draw(gline);
417     windowplot.draw(testline);
418     windowplot.draw(hline);
419     windowplot.draw(nullline);
420     //windowplot.draw(maxline);
421
422     // Make a total cells vs time plot
423     windowtotal.draw(&allLines[0], allLines.size(), sf::Lines);
424     windowtotal.draw(&allLinestest[0], allLinestest.size(), sf::Lines)
425         ;
426     windowtotal.draw(&allLinesblue[0], allLinesblue.size(), sf::Lines)
427         ;
428     windowtotal.draw(&allLinesgreen[0], allLinesgreen.size(), sf::
429         Lines);
430     windowtotal.draw(&allLinesred[0], allLinesred.size(), sf::Lines);
431     windowtotal.draw(&allLineshealthy[0], allLineshealthy.size(), sf::
432         Lines);
433
434     // Making the legend plot
435     std::string result = "Legend: \n \nBlack: all cells \nLight blue:
436         Healthy cells\nPurple: Testosterone\nTime: " + std::to_string(
437         time);
438     legend.setString(result);
439     windowlegend.draw(legend);
440
441     // Display the windows
442     windowtumor.display();
443     windowgreen.display();
444     windowblue.display();
445     windowred.display();
446     windowtest.display();
447     windowhealthy.display();
448     windowplot.display();
449     windowtotal.display();
450     windowlegend.display();
451     //int k = 0;
452     //std::cout << "Enter a number if you are ready to go on with the
453         simulations." << std::endl;
454     //std::cin >> k; // Pauses the simulation such that you can make a
455         snapshot of the pictures
456 }
457
458 // Set a maximum on the tumor burden
459 /*if (oldtotal >= 180000) {
460     std::cout << "Total = " << oldtotal << " at time " << time << std
461         ::endl;
462     std::cout << "Patient died..." << std::endl;

```

```

450         int k;
451         std::cin >> k;
452     }*/
453
454     std::cout << "Time = " << time << std::endl; // Print the time to
         check
455
456     // Treatment
457     if ((int)time % 30 == 0 and time >= t_0){
458         std::cout << "What treatment do you want to give: Lupron (base=0
         and test_stay=0)(1), Abiraterone (prod_g=0)(2), inject
         testosterone (increase base)(3) or both 1&2 (4) do nothing(5)?"
         ;
459         std::cin >> answer;
460         if (answer == 1) {
461             std::cout << "All testosterone in the blood will be removed.";
462             base = 0;
463             test_stay = 1;
464         }
465         else if (answer == 2) {
466             std::cout << "The green cells will be targeted.";
467             prod_g = 0;
468         }
469         else if (answer == 3) {
470             std::cout << "Enter a number testosterone to add each timestep
         to each cell: ";
471             std::cin >> addtobaseleveltest;
472             std::cout << "You entered: " << addtobaseleveltest << std::
         endl;
473             base += addtobaseleveltest;
474         }
475         else if (answer == 4) {
476             std::cout << "All testosterone in the blood will be removed
         and the green cells will be targeted.";
477             base = 0;
478             test_stay = 1;
479             prod_g = 0;
480         }
481     }
482     std::cout << "Base = " << base << std::endl; // Print values to check
483     std::cout << "C_{test} = " << 1-test_stay << std::endl;
484     std::cout << "Alpha_g = " << prod_g << std::endl;
485     time += 1; // Update the time
486
487
488     // Update the cells (with empty boundaries)
489     for (int i = 1; i < numRows - 1; ++i) {
490         for (int j = 1; j < numCols - 1; ++j) {
491             grid[i][j].red_new = grid[i][j].red; // Red cells are
         independent of test, T^-
492             grid[i][j].blue_new = grid[i][j].blue; // Blue cells need test
         , T^+
493             grid[i][j].green_new = grid[i][j].green; // Green cells
         produce test, T^P
494             grid[i][j].test_new = grid[i][j].test;
495             grid[i][j].healthy_cells_new = grid[i][j].healthy_cells;
496
497             // Testosterone production by green T^p cells
498             grid[i][j].test_new += prod * grid[i][j].green + base;
499             // Testosterone consumption by blue T^+, green T^P and healthy
         cells

```

```

500     grid[i][j].test_new -= consumption_rate * grid[i][j].test * (
        grid[i][j].blue + grid[i][j].healthy_cells + grid[i][j].
        green);
501
502     // Cell death (natural)
503     grid[i][j].green_new -= death_g * grid[i][j].total_cells() *
        grid[i][j].green;
504     grid[i][j].red_new -= death_r * grid[i][j].total_cells() *
        grid[i][j].red;
505     grid[i][j].blue_new -= death_b * grid[i][j].total_cells() *
        grid[i][j].blue;
506     grid[i][j].healthy_cells_new -= death_h * grid[i][j].
        total_cells() * grid[i][j].healthy_cells;
507
508     /// Cell death due to lack of testosterone
509     //grid[i][j].green_new -= starve * grid[i][j].green / ( (
        double)1 + grid[i][j].test);
510     //grid[i][j].blue_new -= starve * grid[i][j].blue / ((double)1
        + grid[i][j].test);
511     //grid[i][j].healthy_cells_new -= starve * grid[i][j].
        healthy_cells / ((double)1 + grid[i][j].test);
512
513     /// Cell birth
514     //grid[i][j].green_new += prod_g * grid[i][j].green;
515     //grid[i][j].red_new += prod_r * grid[i][j].red;
516     //grid[i][j].blue_new += prod_b * grid[i][j].blue;
517     //grid[i][j].healthy_cells_new += prod_h * grid[i][j].
        healthy_cells;
518
519     // Cell birth influenced by grid.test - alternate system
520     grid[i][j].green_new += prod_g * grid[i][j].green * grid[i][j]
        ].test;
521     grid[i][j].red_new += prod_r * grid[i][j].red;
522     grid[i][j].blue_new += prod_b * grid[i][j].blue * grid[i][j].
        test;
523     grid[i][j].healthy_cells_new += prod_h * grid[i][j].
        healthy_cells * grid[i][j].test;
524
525     // Cell movement
526     //double z_0 = exp(-zeta * grid[i][j].total_cells() / Max_pop)
        ; -> use for more complex model
527     double z_1 = exp( - beta * grid[i + 1][j].total_cells());
528     if (i == numRows - 2)
529         z_1 = 0;
530     double z_2 = exp( -beta * grid[i - 1][j].total_cells());
531     if (i == 1)
532         z_2 = 0;
533     double z_3 = exp(-beta * grid[i][j + 1].total_cells());
534     if (j == numCols - 2)
535         z_3 = 0;
536     double z_4 = exp(-beta * grid[i][j - 1].total_cells());
537     if (j == 1)
538         z_4 = 0;
539     double z = z_1 + z_2 + z_3 + z_4; // Summing the terms over
        the neighboring gridpoints
540     grid[i][j].green_new2 += grid[i][j].green_new;
541     grid[i][j].blue_new2 += grid[i][j].blue_new;
542     grid[i][j].red_new2 += grid[i][j].red_new;
543     grid[i][j].healthy_cells_new2 += grid[i][j].healthy_cells_new;
544
545     // Moving the green T^P tumor cells

```

```

546         if (grid[i][j].green_new >= 1) { // Only moving cells if there
547             are cells to move
548             for (int k = 1; k <= grid[i][j].green_new; ++k) {
549                 double move_g = static_cast<double>(std::rand()) /
550                     RAND_MAX; // Create random number between 0 and 1
551                 if (move_g <= (C_g * z_1 / z) and z_1 !=0) {
552                     grid[i + 1][j].green_new2 += 1;
553                     grid[i][j].green_new2 -= 1;
554                 }
555                 else if (move_g <= (C_g * (z_1 + z_2) / z)) {
556                     grid[i - 1][j].green_new2 += 1;
557                     grid[i][j].green_new2 -= 1;
558                 }
559                 else if (move_g <= (C_g * (z_1 + z_2 + z_3) / z)) {
560                     grid[i][j + 1].green_new2 += 1;
561                     grid[i][j].green_new2 -= 1;
562                 }
563                 else if (move_g <= C_g) {
564                     grid[i][j-1].green_new2 += 1;
565                     grid[i][j].green_new2 -= 1;
566                 }
567             }
568         }
569     }
570
571     // Moving the blue T+ tumor cells
572     if (grid[i][j].blue_new >= 1) { // Only moving cells if there
573         are cells to move
574         for (int k = 1; k <= grid[i][j].blue_new; ++k) {
575             double move_b = static_cast<double>(std::rand()) /
576                 RAND_MAX; // Create random number between 0 and 1
577             if (move_b <= (C_b * z_1 / z) and z_1 != 0) {
578                 grid[i + 1][j].blue_new2 += 1;
579                 grid[i][j].blue_new2 -= 1;
580             }
581             else if (move_b <= (C_b * (z_1 + z_2) / z)) {
582                 grid[i - 1][j].blue_new2 += 1;
583                 grid[i][j].blue_new2 -= 1;
584             }
585             else if (move_b <= (C_b * (z_1 + z_2 + z_3) / z)) {
586                 grid[i][j + 1].blue_new2 += 1;
587                 grid[i][j].blue_new2 -= 1;
588             }
589             else if (move_b <= C_b) {
590                 grid[i][j - 1].blue_new2 += 1;
591                 grid[i][j].blue_new2 -= 1;
592             }
593         }
594     }
595
596     // Moving the red T- tumor cells
597     if (grid[i][j].red_new >= 1) { // Only moving cells if there
598         are cells to move
599         for (int k = 1; k <= grid[i][j].red_new; ++k) {
600             double move_r = static_cast<double>(std::rand()) /

```

```

601         grid[i][j].red_new2 -= 1;
602     }
603     else if (move_r <= (C_r * (z_1 + z_2 + z_3) / z)) {
604         grid[i][j + 1].red_new2 += 1;
605         grid[i][j].red_new2 -= 1;
606     }
607     else if (move_r <= C_r) {
608         grid[i][j - 1].red_new2 += 1;
609         grid[i][j].red_new2 -= 1;
610     }
611     }
612 }
613
614 // Moving the healthy cells
615 if (grid[i][j].healthy_cells_new >= 1) { // Only moving cells
        if there are cells to move
616     for (int k = 1; k <= grid[i][j].healthy_cells_new; ++k) {
617         double move_h = static_cast<double>(std::rand()) /
        RAND_MAX; // Create random number between 0 and 1
618         if (move_h <= (C_h * z_1 / z) and z_1 !=0) {
619             grid[i + 1][j].healthy_cells_new2 += 1;
620             grid[i][j].healthy_cells_new2 -= 1;
621         }
622         else if (move_h <= (C_h * (z_1 + z_2) / z)) {
623             grid[i - 1][j].healthy_cells_new2 += 1;
624             grid[i][j].healthy_cells_new2 -= 1;
625         }
626         else if (move_h <= (C_h * (z_1 + z_2 + z_3) / z)) {
627             grid[i][j + 1].healthy_cells_new2 += 1;
628             grid[i][j].healthy_cells_new2 -= 1;
629         }
630         else if (move_h <= C_h) {
631             grid[i][j - 1].healthy_cells += 1;
632             grid[i][j].healthy_cells -= 1;
633         }
634     }
635 }
636
637 // Testosterone diffusion
638 grid[i][j].test_new2 += grid[i][j].test_new;
639 if (grid[i][j].test_new >= 1) { // Only moving cells if there
        is testosterone to move
640     for (int k = 1; k <= grid[i][j].test_new; ++k) {
641         double move_t = static_cast<double>(std::rand()) /
        RAND_MAX; // Create random number between 0 and 1
642         if (test_stay == 1) {
643         }
644     }
645     else if (move_t <= (1 - test_stay) / 4 and (i <
        numRows - 2)) {
646         grid[i + 1][j].test_new2 += 1;
647         grid[i][j].test_new2 -= 1;
648     }
649     else if (move_t <= 2 * (1 - test_stay) / 4 and (i > 1)
        ) {
650         grid[i - 1][j].test_new2 += 1;
651         grid[i][j].test_new2 -= 1;
652     }
653     else if (move_t <= 3 * (1 - test_stay) / 4 and (j <
        numCols - 2)) {
654         grid[i][j + 1].test_new2 += 1;

```

```

655         grid[i][j].test_new2 -= 1;
656     }
657     else if (move_t <= 4 * (1 - test_stay) / 4 and (j > 1)
658         ) {
659         grid[i][j - 1].test_new2 += 1;
660         grid[i][j].test_new2 -= 1;
661     }
662 }
663 }
664 }
665
666 // Set the next colour to be the current color and update the colors
667 // for the plots
668 for (int i = 0; i < numRows; ++i) {
669     for (int j = 0; j < numCols; ++j) {
670         grid[i][j].red = grid[i][j].red_new2;
671         grid[i][j].blue = grid[i][j].blue_new2;
672         grid[i][j].green = grid[i][j].green_new2;
673         grid[i][j].healthy_cells = grid[i][j].healthy_cells_new2;
674         grid[i][j].test = grid[i][j].test_new2;
675
676         grid[i][j].setColor(sf::Color(std::max(std::min(grid[i][j].red
677             , (double)255), (double)0), std::max(std::min(grid[i][j].
678             green, (double)255), (double)0), std::max(std::min(grid[i][
679             j].blue, (double)255), (double)0), 255));
680
681         if (grid[i][j].blue < 0.5) // If there are not many left they
682             will die
683             grid[i][j].blue = 0;
684         if (grid[i][j].green < 0.5)
685             grid[i][j].green = 0;
686         if (grid[i][j].red < 0.5)
687             grid[i][j].red = 0;
688
689         // Fix the green T^P cells grid
690         greengrid[i][j] = grid[i][j];
691         greengrid[i][j].setColor(sf::Color(0, std::max(std::min(grid[i
692             ][j].green, (double)255), (double)0), 0, 255));
693
694         // Fix the red T^- cells grid
695         redgrid[i][j] = grid[i][j];
696         redgrid[i][j].setColor(sf::Color(std::max(std::min(grid[i][j].
697             red, (double)255), (double)0), 0, 0, 255));
698
699         // Fix the blue T^+ cells grid
700         bluegrid[i][j] = grid[i][j];
701         bluegrid[i][j].setColor(sf::Color(0, 0, std::max(std::min(grid
702             [i][j].blue, (double)255), (double)0), 255));
703
704         // Fix the testosterone grid
705         testgrid[i][j] = grid[i][j];
706         testgrid[i][j].setColor(sf::Color(0, std::max(std::min(grid[i
707             ][j].test, (double)255), (double)0), 0, 255));
708
709         // Fix the healthy cells grid
710         healthygrid[i][j] = grid[i][j];
711         healthygrid[i][j].setColor(sf::Color(std::max(std::min(grid[i
712             ][j].healthy_cells, (double)255), (double)0), 0, 0, 255));

```

```
705         }
706     }
707
708     for (int i = 1; i < numRows - 1; ++i) {
709         for (int j = 1; j < numCols - 1; ++j) {
710             grid[i][j].red_new2 = 0;
711             grid[i][j].blue_new2 = 0;
712             grid[i][j].green_new2 = 0;
713             grid[i][j].healthy_cells_new2 = 0;
714             grid[i][j].test_new2 = 0;
715         }
716     }
717 }
718 }
719
720 return 0;
721 }
```